# UTILIZATION OF RUTHENIUM AND RUTHENIUM-IRON ALLOYS AS BOSCH PROCESS CATALYSTS


by

CHARTSIRI SOPHONPANICH

B.S., Worcester Polytechnic Institute (1980)

SUBMITTED TO THE DEPARTMENT OF CHEMICAL ENGINEERING
IN PARTIAL FULFILLMENT OF THE REQUIREMENTS
FOR THE DEGREE OF


MASTER OF SCIENCE IN CHEMICAL ENGINEERING

at the

MASSACHUSETTS INSTITUTE OF TECHNOLOGY

December 1982



Signature of Author Chartsiri Sophonpanich
Department of Chemical Engineering
December 27, 1982

Certified by Michael P. Manning
Professor Michael P. Manning
Thesis Supervisor

Robert C. Reid
Professor Robert C. Reid
Thesis Supervisor

Accepted by Glen C. Williams
Professor Glen C. Williams
Chairman, Department Committee

# UTILIZATION OF RUTHENIUM AND RUTHENIUM-IRON ALLOYS AS BOSCH PROCESS CATALYSTS

by

CHARTSIRI SOPHONPANICH

Submitted to the Department of Chemical Engineering on December 27, 1982, in partial fulfillment of the requirements for the Degree of Master of Science in Chemical Engineering at the Massachusetts Institute of Technology

## Abstract

The Bosch process has been considered as a means to recover oxygen from metabolic carbon dioxide through the catalytic production of water. Previous investigations have shown that the oxide formation accounts for the limited activity of the iron catalyst. On the other hand, the maximum water concentrations achievable in the nickel and cobalt systems have been shown to correspond to the carbide formation. This thesis presents the results of an experimental study carried out to determine the effectiveness of ruthenium and its unsupported alloys with iron -- namely, 50Ru50Fe and 33Ru67Fe -- as alternative Bosch catalysts. Carbon deposition boundaries over the unsupported alloys are reported.

Experiments have also been carried out over 50Ru50Fe and 97Ru3Fe catalysts supported on γ-alumina to determine their performance in the synthesis of low molecular weight olefins. High production of ethylene and propylene would be beneficial for an improvement of an overall Bosch process, as a gas phase containing high olefin content would enhance carbon deposition in a Bosch reactor.

THESIS SUPERVISORS: Professor Michael P. Manning
Professor Robert C. Reid

Acknowledgements

I would like to acknowledge the support of the National Aeronautics and Space Administration in sponsoring this research, including the assistance of the NASA officer, Dr. Phillip D. Quattrone. My sincere appreciation is also graciously extended to Professors Michael P. Manning and Robert C. Reid for their valuable guidance and expertise, and most of all, their unfailing patience.

Also acknowledged is the contributions of Doug Borowski, Evan Morris, Brian Moroney, Brad Sackett and James Willard from their participation in the 10.26 Chemical Engineering Laboratory course. Brad Sackett and James Willard further assisted in this thesis through their involvement in a UROP project. Help was also provided by Rhonda Wilson at the initial stage of this research as a UROP student.

Special thanks are due to my colleagues from the Fuels Lab, particularly Cheng-Shiou Chang, Steve Chiu Kin Lai, John Nenniger, Michael A. Serio, Michael Snow, and William Sun. Their freindship, encouragement and support were much needed. Michael Snow and Bhakorn Vanuptikul provided their skills helping me prepare most of the figures presented in this thesis.

Finally, I would like to thank my family for their encouragement and support they have given me throughout my education.

Table of Contents

Table of Contents (Continued)

## List of Figures

List of Figures (Continued)

List of Figures (Continued)

## List of Tables

## 1. Introduction

A reliable regenerative life support system is required for future long-duration space missions. An important step in the life support system is the reduction of metabolic carbon dioxide to oxygen, the carbon dioxide being concentrated from ambient spacecraft atmospheric concentrations with an electrochemical concentration cell. This regeneration of oxygen can be accomplished by several techniques, including the Bosch, the Sabatier and the Solid-Electrolyte process (1). Of interest in this investigation is the Bosch process, in which carbon dioxide reacts catalytically with hydrogen to form carbon and water, with the carbon depositing on the catalyst. The water produced is electrolyzed to oxygen and hydrogen, the latter being recycled to the Bosch reactor. The overall process can be summarized by the following reactions.

$$\text{Bosch Reaction: } CO_2 + 2H_2 \rightarrow C + 2H_2O \qquad (1.1)$$

$$\text{Electrolysis: } 2H_2O \rightarrow 2H_2 + O_2 \qquad (1.2)$$

$$\text{Overall: } CO_2 \rightarrow C + O_2 \qquad (1.3)$$

Several prototype recycle Bosch reactors have been investigated by NASA, utilizing ordinary steel wool as the catalysts (2,3,4). The reactor is typically run in a recycle

mode in a temperature range of 800-1000K, as single pass efficiencies through the reactor are less than 10%. The formation of carbon monoxide and methane also occurs. Water is continuously condensed from the effluent stream, while the remaining effluent gas is recycled and mixed with the inlet $CO_2$ and $H_2$.

A major problem associated with the transition metal iron catalyst was that the effluent water concentration obtained in the reactor had been significantly less than expected from thermodynamic equilibrium considerations. Previous investigations at the Massachusetts Institute of Technology have shown that the low water yield was related to the formation of iron oxides, which were noncatalytic to the carbon deposition (5,6,7,8). The oxidation of the iron catalyst occurs, in addition to the other reactions taking place in the gas mixture consisting of hydrogen, carbon dioxide, carbon monoxide, methane and water.

$$\text{At } T < 860K \quad 3Fe + 4H_2O \rightleftarrows Fe_3O_4 + 4H_2 \qquad (1.4)$$

$$3Fe + 4CO_2 \rightleftarrows Fe_3O_4 + 4CO \qquad (1.5)$$

$$\text{At } T > 860K \quad Fe + H_2O \rightleftarrows FeO + H_2 \qquad (1.6)$$

$$Fe + CO_2 \rightleftarrows FeO + CO \qquad (1.7)$$

Manning and Reid (6) suggested, with further experimental confirmation by Sacco and Reid (8), that the Bosch process

should be operated in the carbon depositing region above the iron-iron oxide-gas equilibrium line in the C-H-O triangular diagram, as shown in Figure 1.1. The iron catalyst would be in a metallic form in this region.

Consequently, in the search for an alternative Bosch catalyst, consideration must be made of the limiting concentrations of water or carbon dioxide in the system before catalyst oxidation occurred. Theoretical calculations for both the nickel and cobalt systems indicated that the interference of oxide formation would not exist under operating Bosch gas compositions (9,10). As shown in Figure 1.2 for the nickel system, the metal-metal oxide-gas equilibrium line was below the graphite-gas equilibria boundary, and thus no limitation on carbon depostion in the form of an oxidized catalyst was to be expected. The experimental investigation by Garmirian et al. (10) confirmed the above postulate for both nickel and cobalt systems. Their results, however, showed strong evidence that carbon deposition occurred via a metal carbide intermediate, with subsequent decomposition to carbon, in region X of Figure 1.2 and ceased upon reaching the metal-metal carbide-gas equilibrium line. In region Y, where the formation of a metal carbide would not be thermodynamically favored, no carbon deposition was observed.

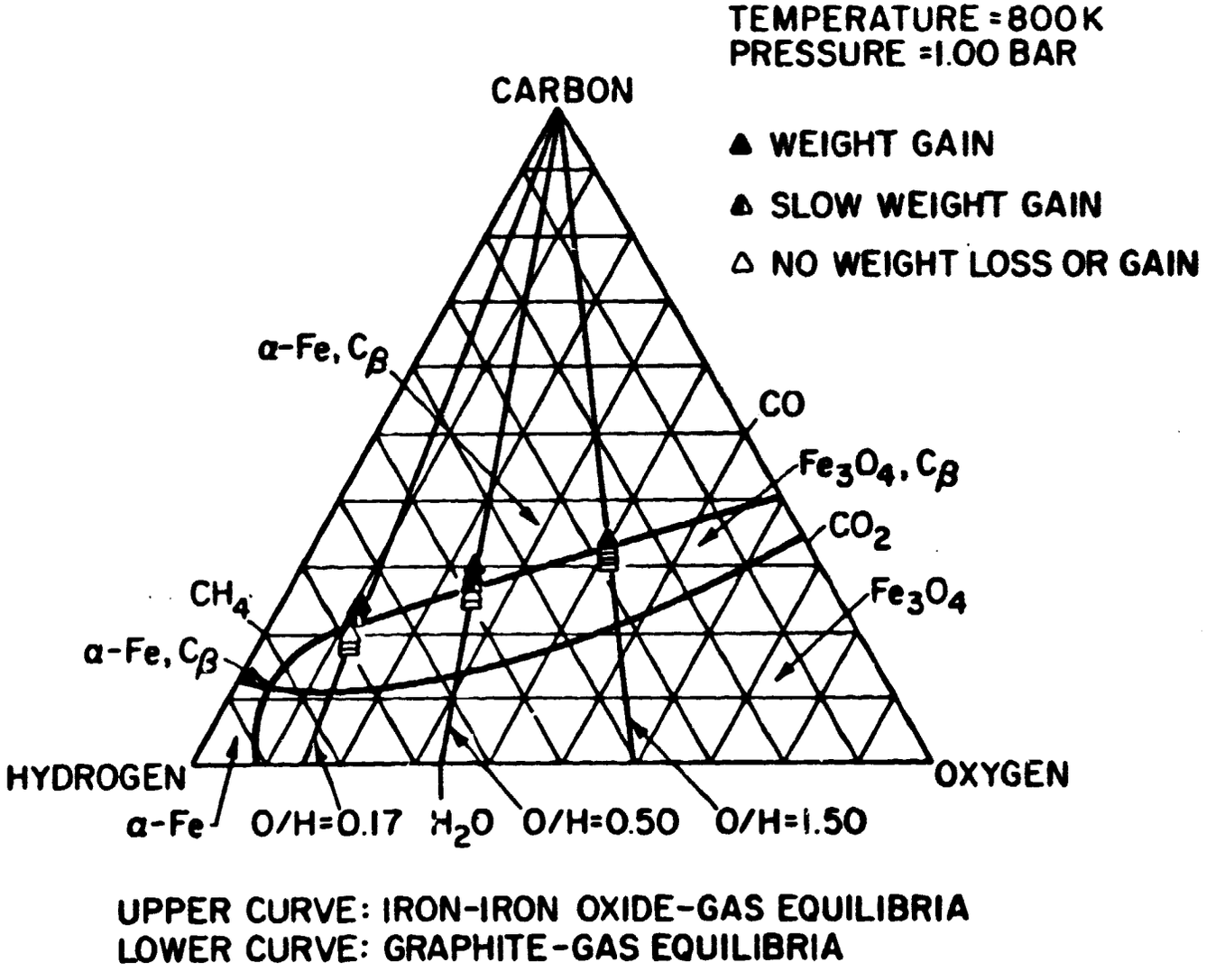


Figure 1.1 Inhibition of Carbon Deposition by $Fe_3O_4$ at Various O/H ratios (8)

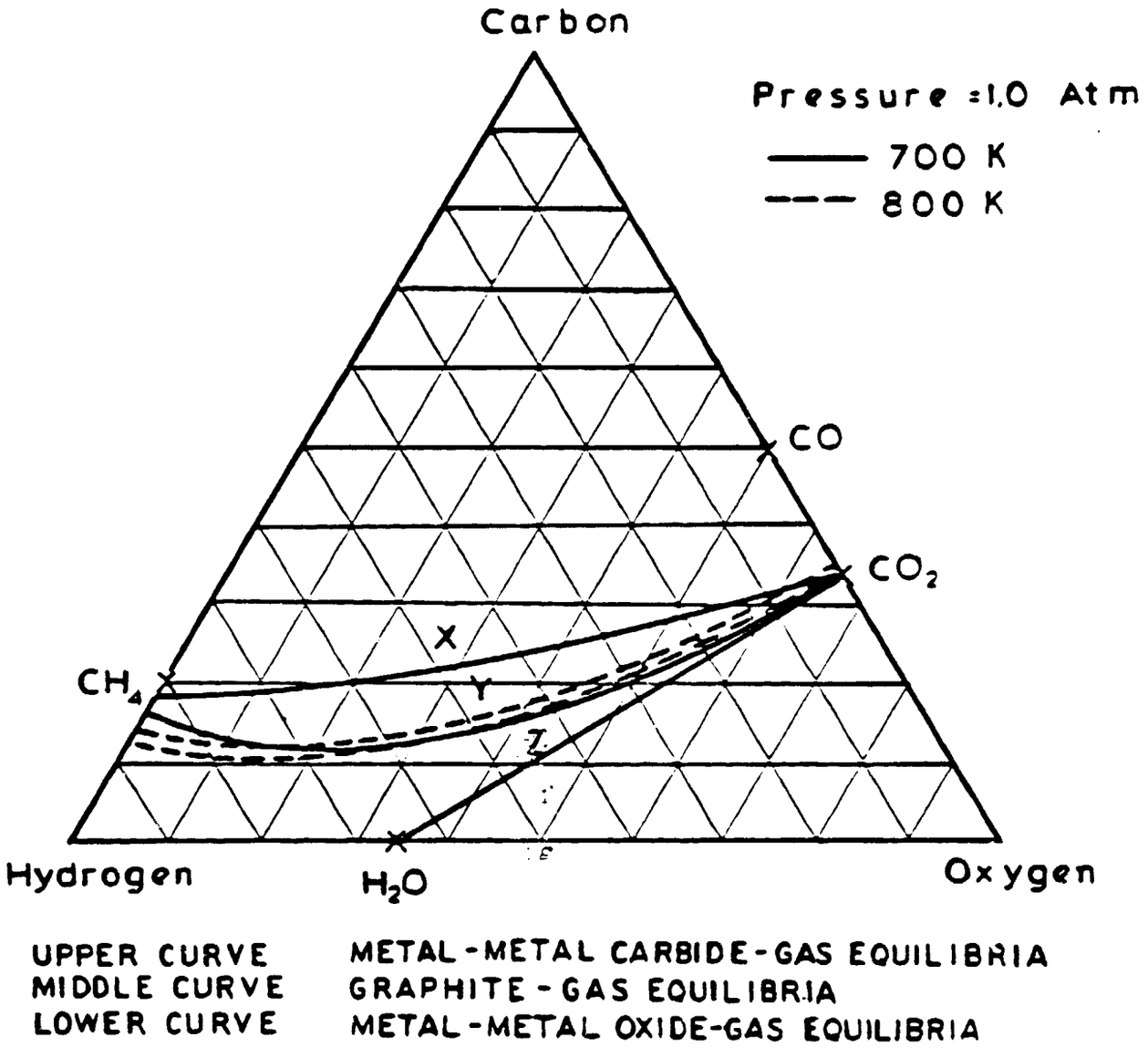


Figure 1.2 Phase Diagram for Nickel-Catalyzed Bosch Process (9)

Studies on iron, nickel and cobalt as catalysts in the Bosch process have led to the conclusion that the catalyst performance is limited by the formation of oxides or carbides. Similar to Fe, Ni and Co, ruthenium (Ru) has been shown to catalyze reactions between carbon monoxide and hydrogen through dissociative adsorption of carbon monoxide at elevated temperatures (11). Although ruthenium does form an oxide, thermodynamic data for the formation of ruthenium oxide ($RuO_2$) (12) are such that the metal-metal oxide-gas boundary is removed from the graphite-gas equilibrium line, as is the case for nickel and cobalt. Consequently, ruthenium oxide is not expected to form under typical conditions of the Bosch process. In addition, the carbides of ruthenium have been reported to be unstable or of very limited stability in comparison to those of iron, nickel and cobalt (13). Thus, as the rate of carbon deposition on nickel and cobalt appears to be limited by the decomposition rate of metal carbides, the carbon deposition rate on ruthenium must be expected to be faster than that on nickel or cobalt.

Interesting results have been reported with the use of unsupported ruthenium-iron alloys in the investigation of Fischer-Tropsch reactions (14). High product ratios of olefinic species to paraffinic compounds have been observed for the alloy catalysts of intermediate composition. The high olefin content is expected to enhance the rate of carbon deposition on the Ru-Fe alloys, as has been observed for

similar systems by Baker (15).

The above evidence seems to indicate ruthenium and Ru-Fe alloys to be superior to the previously investigated Bosch catalysts. Hence, a study on ruthenium and Ru-Fe alloys has been carried out to determine their effectiveness as catalysts for the Bosch process.

## 2. Literature Review

The Bosch process consists of a complex set of reactions occurring in both parallel and series combinations. The overall stoichiometry of the process can be represented by the equation below, where carbon dioxide can be visualized as converted to solid carbon and water by the reaction with hydrogen.

$$CO_2 + 2H_2 \rightarrow C + 2H_2O \qquad (2.1)$$

The process is catalyzed by transition metals in a temperature range of 700-1000K.

Iron, nickel and cobalt have been investigated in the Bosch process by Manning (5), Sacco (7) and Garmirian (9). The results of their studies are summarized below. Following will then be a review of related studies of ruthenium and ruthenium-iron alloys, which possess several prominent features that could lead to promising applications in the Bosch process.

### 2.1 The Iron System

The water concentration significantly below that expected from thermodynamic considerations was observed in the effluent stream of a NASA prototype Bosch recycle reactor utilizing an iron catalyst. A thermodynamic analysis and an experimental study of the iron-catalyzed Bosch process were

carried out by Manning (5) in investigating the behavior of iron. His study has shown good evidence of interference of catalyst oxidation in the Bosch process. In one experiment, $CO/CO_2$ gas mixtures of different compositions were passed over an iron wool catalyst at 823K. While no weight change was observed for a 50:50 $CO:CO_2$ mixture, a rapid rate of carbon deposition was noted for a 66:34 $CO:CO_2$ mixture. The reactions involved in the experiment include the oxidation of iron,

$$3Fe + 4CO \rightleftarrows Fe_3O_4 + 4CO \qquad (2.2)$$

and the disproportionation of carbon monoxide,

$$2CO \rightleftarrows CO_2 + C \qquad (2.3)$$

The CO equilibrium concentrations for the two reactions at 823K are 53 and 13 mole percent, respectively. Based upon thermodynamic considerations, the disproportionation reaction should have proceeded to the right, resulting in carbon deposition. However, with a 50:50 $CO:CO_2$ mixture, the oxidation of iron was favored and thus no carbon deposition was observed. On the other hand, when a $CO:CO_2$ mixture of 66:34 was used, iron oxide was converted to its elemental form, at which point carbon deposition took place.

Further verification of the interference of iron oxides in the Bosch process was made by Sacco (7). In the determination of carbon deposition boundaries, equilibrium studies employing gas mixtures of $H_2$, CO, $CH_4$, $CO_2$ and $H_2O$ were performed over an iron catalyst in a temperature range of

800-900K. At a fixed value of an O/H ratio Baeco started with a gas composition for which carbon deposition was possible, and he then decreased the O/H ratios of the inlet gas mixture. The carbon deposition boundary was determined by the point where no carbon deposition began. A typical example of his experimental results is shown graphically in Figure 1.1, which demonstrates an excellent agreement between the experimentally determined phase boundary and the theoretical iron-iron oxide-gas equilibrium line.

The results of Baeco's investigation are very significant in that they provide further evidence supporting Manning's hypothesis of the inhibitive role of iron oxides in carbon deposition. The catalyst oxidation accounts for the low water concentrations obtained in Bosch recycle reactors. Reactions involved in the iron oxidation include the following.

| | | | | |
|---|---|---|---|---|
| At T < 860K | $3Fe + 4H_2O$ | $\rightleftarrows$ | $Fe_3O_4 + 4H_2$ | (2.4) |
| | $3Fe + 4CO_2$ | $\rightleftarrows$ | $Fe_3O_4 + 4CO$ | (2.5) |
| At T > 860K | $Fe + H_2O$ | $\rightleftarrows$ | $FeO + H_2$ | (2.6) |
| | $Fe + CO_2$ | $\rightleftarrows$ | $FeO + CO$ | (2.7) |

## 2.2 The Nickel and Cobalt Systems

A study of the nickel and cobalt catalyzed Bosch process was subsequently carried out by Garmirian (9) in the search for an alternative Bosch catalyst. Like iron, the

transition metals nickel and cobalt have been known to catalyze all the reaction systems involved in the Bosch process. However, a significant difference of these two metals from iron is that the interference of oxide formation would not exist under operating Bosch gas compositions. A thermodynamic analysis indicates that the metal- metal oxide-gas equilibrium line for either the nickel or cobalt system lies below the graphite-gas equilibrium boundary in a C-H-O triangular diagram, such as the one shown in Figure 1.2 for the nickel catalyzed Bosch process. Although his experimental study indeed verified the noninterference of catalyst oxidation, Garmirian (9) observed that there existed a region where the expected carbon deposition would not occur.

This phenomenon is not unsurprising. For carbon deposition reactions, the solid phase in equilibrium with the gas phase can range from β-graphite to a solid phase having a Gibbs energy significantly greater than β-graphite. Dent et al. (16) and Rostrup-Nielsen (17) carried out equilibrium studies of the decomposition reactions of both methane and carbon monoxide over nickel catalysts in the temperature ranges of 600-1200K and 700-1000K, respectively. Garmirian (9) performed Bosch equilibrium studies on nickel and cobalt catalysts covering temperatures of 700-900K. Below certain temperatures, experimental equilibrium measurements of all three investigations showed deviation from the calculated values of equilibrium constants based upon the solid carbon

phase of β-graphite. The deviation from the β-graphite equilibrium was pronounced at low temperatures. When extrapolated to lower temperatures, these experimental results were in good agreement with equilibrium measurements made by Browning and Emmett (18) in the $Ni_3C$-Ni-$CH_4$-$H_2$ system in the temperature range of 500-600K and in the $Co_2C$-Co-$CH_4$-H2 system at 460-720K.

It should be noted that a number of studies (19,20,21,22) have indicated the metastable existence of both nickel and cobalt carbides at temperatures between 600 and 800K. In explaining the results of his Bosch equilibrium studies, Garmirian (9) attributed the difference in Gibbs energies involving the formation of experimental carbon and β-graphite to the metal carbide intermediates in the carbon deposition process. At low temperatures, the formation of carbide intermediates could occur by reactions such as

$$CH_4 + nMe \rightleftarrows Me_nC + 2H_2 \qquad (2.8)$$

$$H_2 + CO + nMe \rightleftarrows Me_n + H_2O \qquad (2.9)$$

$$2CO + nMe \rightleftarrows Me_nC + CO_2 \qquad (2.10)$$

with a subsequent carbide decomposition to free carbon,

$$Me_nC \rightleftarrows C + nMe \qquad (2.11)$$

X-ray diffraction analyses were performed on the used cobalt catalysts but failed to detect cobalt carbides. It was very likely that the cobalt carbides decomposed during the cooldown period after the experiments had been completed, as the decomposition of $Co_2C$ and $Co_3C$ has been reported to occur at

temperatures in a range of 723-743K and 753-763K, respectively (22).

## 2.3 Ruthenium and Ruthenium-Iron Alloys

The investigations on iron, nickel and cobalt as catalysts in the Bosch process have pointed to two important features: that at high temperatures the maximum water yield achievable is confined to graphite-gas equilibria, and that at low temperatures the catalyst performance is limited by the formation of oxides or carbides. Consequently, a good Bosch catalyst should not be oxidized under operating conditions, nor should carbon deposition reactions be limited by the decomposition of metal carbides. Thermodynamic considerations and other experimental studies for closely related reactions show ruthenium and ruthenium-iron alloys to be of significant promise as effective Bosch catalysts. Positive indications of the performance of ruthenium and its alloys with iron are cited below.

### 2.3.1 Ruthenium

As reviewed by Shunk (23), ruthenium does form an oxide. However, according to thermodynamic data by Bell and Tagami (12), interference of the ruthenium oxide ($RuO_2$) formation under Bosch operating conditions is not expected. In other words, the metal-metal oxide-gas boundary is removed

from the graphite-gas equilibrium line, as is the case for nickel and cobalt. In addition, the standard heats of formation of metal oxides shown in Table 2.1 (13) indicate that the ease of reduction of metal oxides should be in the order of Ru, Co, Ni and Fe, with ruthenium being the easiest to reduce.

Although definite verification of ruthenium carbides is yet to be confirmed (23), the carbides, if they exist, have been reported to be unstable or of very limited stability as compared to those of iron, nickel and cobalt (13). Consequently, if carbon deposition on ruthenium occurs by way of the decomposition of metal carbide intermediates, as has been postulated for the nickel and cobalt systems, carbon deposition on ruthenium in the Bosch process would then be expected to proceed until approaching the graphite-gas equilibrium boundary.

Carbon deposition on ruthenium has been observed in a number of investigations (11,24,25,26). Singh and Grenga (24) studied the catalytic decomposition of carbon monoxide on single crystalline ruthenium at 823K and 760 Torr for times varying from 6 to 96 hours. Reflection high energy electron diffraction (RHEED) was used to identify the solid products of the decomposition reaction. It was found that carbon monoxide had decomposed catalytically to produce graphite, which deposited very slowly at low- index poles of the unsupported ruthenium crystalline surface. Neither oxides nor carbides were observed.

Table 2.1 Standard Heats of Formation of Metal Oxides (13)

**Standard Heats of Formation ($-\Delta H°$)[a] of Select Oxides and Sulfides**

| | | | | | | | | | | | | | | | | |
|---|---|---|---|---|---|---|---|---|---|---|---|---|---|---|---|---|
| Oxides | TiO | 123.9[b] | VO | 103.2[c] | | | MnO | 92.0[c] | FeO | 63.2[c] | CoO | 57.1[c] | NiO | 57.3[c] | CuO | 37.1[c] |
| | $TiO_2$ | 112.4[b] | $V_2O_3$ | 98.7[b] | $Cr_2O_3$ | 90[c] | $Mn_3O_4$ | 82.7[b] | $Fe_2O_3$ | 65.5[b] | $Co_3O_4$ | 51.0[b] | | | $Cu_2O$ | 39.8[b] |
| Sulfides | TiS | 78.8[c] | | | CrS | 46.7[c] | MnS | 66.4[c] | FeS | 39.4[c] | $Co_9S_8$ | 40.8[c] | NiS | 37.9[c] | CuS | 27.9[c] |
| | $TiS_2$ | 64[c] | | | | | $MnS_2$ | 42.1 | $FeS_2$ | 35.9[c] | $CoS_2$ | 33.7[c] | | | | |
| Oxides | $ZrO_2$ | 130.8[c] | NbO | 98[c] | $MoO_2$ | 70.4[c] | | Tc | | | RhO | 22[c] | PdO | 22.9[c] | $Ag_2O$ | 7.2[c] |
| | | | $NbO_2$ | 94.6[b] | $MoO_3$ | 60.1[b] | | | $RuO_2$ | 36[c] | $Rh_2O_3$ | 22.8[b] | | | | |
| Sulfides | | | | | | | | | RuS | 54.5[d] | | | | | | |
| | $ZrS_2$ | 84.4[c] | $NbS_2$ | 51.8[c] | $MoS_2$ | 48.3[c] | | | $RuS_2$ | 40[c] | $Rh_2S_3$ | 36.3[c] | PdS | 32.3[c] | $Ag_2S$ | 23[c] |
| | | | | | | | | | | | | | $PdS_2$ | 24.8[c] | | |
| Oxides | | | | | $WO_2$ | 70.5[c] | $ReO_2$ | 51[c] | | | $Ir_2O_3$ | 22.7[b] | | | $Au_2O_3$ | 0.3[c] |
| | $HfO_2$ | 133[c] | $Ta_2O_5$ | 97.7[c] | $WO_3$ | 66.9[b] | $ReO_3$ | 48.7[b] | $OsO_2$ | 31[b] | $IrO_2$ | 26.5[c] | | | | |
| Sulfides | | | | | | | | | OsS | 40.9[d] | $Ir_2S_3$ | 32.1[c] | PtS | 35.3[c] | | |
| | | | $TaS_2$ | 57.7[c] | $WS_2$ | 46[c] | $ReS_2$ | 36.8[c] | $OsS_2$ | 33.0[c] | $IrS_2$ | 31.3[c] | $PtS_2$ | 28.6[c] | | |
| Oxides | $La_2O_3$ | 143.2[b] | $Al_2O_3$ | 133.4[b] | $SiO_2$ | 54.5[c] | | | | | | | | | | |
| Sulfides | $La_2S_3$ | 112.7[c] | $Al_2S_3$ | 73[c] | | | | | | | | | | | | |
| | $LaS_2$ | 89.9[c] | | | | | | | | | | | | | | |

[a] Δ in kcal (gm atom nonmetal)$^{-1}$ at 298°K.
[b] Samsonov (1973).
[c] Mills (1974).
[d] McDonald (1962).
[e] Searcy (1970).

**Standard Heats of Formation ($-\Delta H°$)[a] of Select Nitrides and Carbides[b]**

| | | | | | | | | | | | | | | | | |
|---|---|---|---|---|---|---|---|---|---|---|---|---|---|---|---|---|
| Nitrides | TiN | 80.4 | VN | 52 | $Cr_2N$ | 27.3 | $Mn_4N$ | 30.5 | $Fe_4N$ | 3 | $Co_3N$ | −2 | $Ni_3N$ | 0 | $Cu_3N$ | −18 |
| Carbides | TiC | 44.1 | $VC_{.88}$ | 24.5 | $Cr_3C_2$ | 2.8 | $Mn_3C$ | 4 | $Fe_3C$ | −5 | $Co_3C$ | −4 | $Ni_3C$ | −9 | Unstable | |
| Nitrides | ZrN | 87.3 | NbN | 57 | $Mo_2N$ | 16.6 | | Tc | | Unstable | | Unstable | | Unstable | | Unstable |
| Carbides | $ZrC_{.93}$ | 47.0 | NbC | 33.6 | MoC | ~3 | | | | Low Stab. | | Unstable | | Unstable | | Unstable |
| Nitrides | HfN | 88.2 | TaN | 59 | Low stab. | | | Unstable | | Unstable | | Unstable | | Unstable | | Unstable |
| Carbides | $HfC_{.956}$ | 50.1 | TaC | 34.1 | WC | 97 | | Unstable | | Unstable | | Unstable | | Unstable | | Unstable |
| Nitrides | LaN | 71 | | | | | | | | | | | | | | |

[a] $\Delta H_f°$ in kcal (gm atom nonmetal)$^{-1}$ at 298°K.
[b] Data from Searcy (1970).

Carbon deposition on silica-supported ruthenium has also been reported by Rabo et al. (11) in their investigation of the reaction mechanism involved in hydrocarbon synthesis. Pulses of carbon monoxide were introduced over the catalyst surface at temperatures ranging from 296K to 573K, followed by hydrogen pulses at various temperatures. Effluent streams were analyzed by gas chromatography. The adsorption of $CO_2$ on ruthenium at 573K was shown to be largely dissociative, resulting in CO disproportionation to CO and surface carbon, the species which was readily hydrogenated even at room temperature. The degree of CO disproportionation increased when the reaction temperature was raised to 673K. At room temperature, however, disproportionation of CO was absent and the adsorbed CO was inert to $H_2$. Ni, Co and Pd supported on silica gel were also used in the study, and the adsorption behavior of the first two supported metals was shown to be very similar to that of Ru. In contrast, the adsorption of carbon monoxide on Pd at 573K was found to be nondissociative, and the chemisorbed CO was less reactive to $H_2$ than the surface carbon species formed on Ni, Co or Ru.

The temperature-programmed desorption (TPD) of CO and temperature- programmed reaction (TPR) of chemisorbed CO in $H_2$ has been studied on a $Ru/Al_2O_3$ catalyst by Low and Bell (25). The investigation was aimed at identifying the forms of CO present on Ru, the conditions under which CO disproportionation takes place, and the reactivity of the surface carbon

formed. Carbon monoxide was shown to be molecularly adsorbed at 303K to produce methane and ethane. The following reaction sequence has been proposed for carbon deposition on the surface of ruthenium (25,26).

$$CO + S \rightleftarrows CO_s \qquad (2.12)$$

$$CO_s + S \rightleftarrows C_s + O_s \qquad (2.13)$$

$$O_s + CO \rightleftarrows CO_2 + S \qquad (2.14)$$

Low and Bell (25) and Ekerdt and Bell (26) have noted the importance of $CO_2$ formation of the last reaction in shifting the balance of the highly endothermic reaction (2.13) toward carbon deposition. When $H_2$ is present in addition to CO, the removal of surface oxygen is further enhanced, as shown by the following reaction.

$$O_s + H_2 \rightarrow H_2O + S \qquad (2.15)$$

In their study of hydrocarbon synthesis from CO and $H_2$ over silica-supported ruthenium, Ekerdt and Bell (26) have reported that the amount of carbon deposited on the ruthenium catalyst at 464K was an order of magnitude higher when both CO and $H_2$ were present together than when CO was used alone. In addition, the amount of carbon deposited was shown to increase with the reaction temperature. Consequently, as the stoichiometric ratio of O/H for the Bosch process is normally kept at 0.5, equivalent to a $H_2/CO$ ratio of 1.0, and since operating temperatures of the Bosch process are in the range of 700-900K, several hundred degrees higher than the Fischer-Tropsch temperatures, the results for a ruthenium

catalyst in the Bosch process are expected to be very interesting.

### 2.3.2 Ruthenium-Iron Alloys

The phase diagram of ruthenium-iron binary alloys is shown in Figure 2.1. As can be seen from the phase diagram, for temperatures below 773K ruthenium and iron form a continuous series of solid solutions in the region ranging from 23.5 to 100 atomic percent of ruthenium, with Fe atoms substituted into the hcp Ru lattice. A two-phase region exists between 4.8 and 23.5% Ru. Below 4.8% Ru, solid solutions are formed, with Ru atoms substituted into the bcc crystal structure of Fe.

Recent Fischer-Tropsch studies of ruthenium-iron alloys by Ott *et al.* (14) and Vannice *et al.* (27) have indicated potential applications of these alloys to the Bosch process. In the investigation of CO hydrogenation, Ott *et al.* (14) used unsupported RuFe powders prepared from the hydrazine reduction of aqueous salt mixtures, the alloy powders having the surface areas of 7-10 $m^2/g$. A gas mixture of 3.3 $H_2/CO$ was applied at 1 atm and 573K over the alloy catalysts having atomic compositions of 97Ru3Fe, 75Ru25Fe and 33Ru67Fe. Differential kinetic measurements were made over the alloy catalysts, and the results were compared with those of unsupported Ru and Fe metals. A spectrum of carbon-containing species ranging from $CO_2$ and methane through $C_4$ hydrocarbons were observed, as

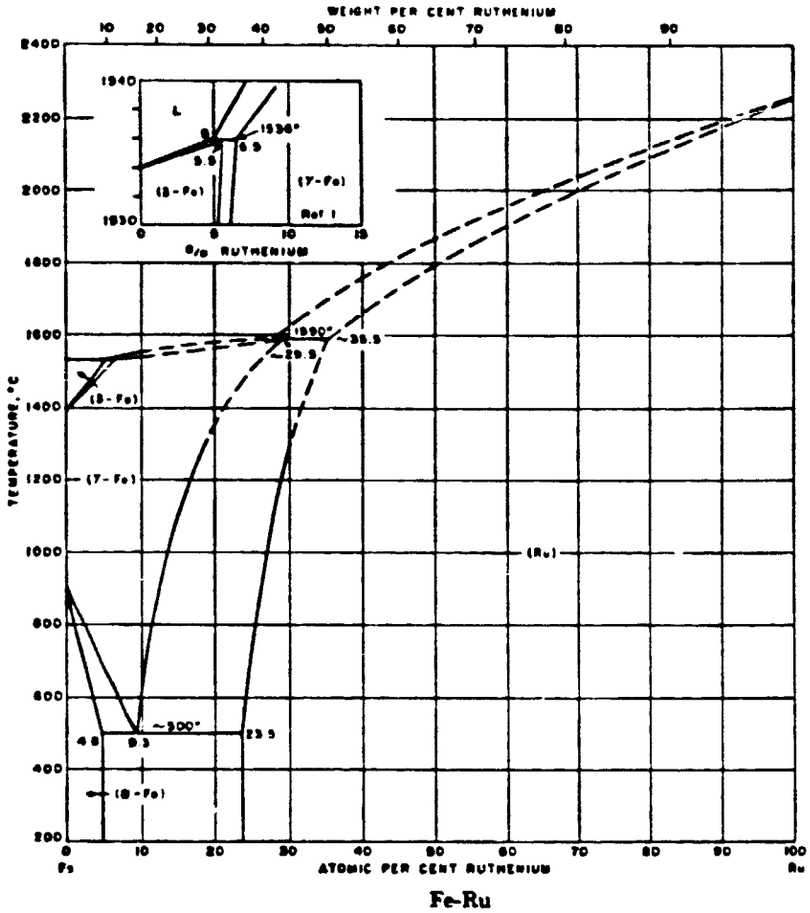


Fe-Ru

Figure 2.1 Iron-Ruthenium Phase Diagram (42)

shown in Figure 2.2 where the product selectivities of freshly reduced powder samples were plotted as a function of bulk composition of the catalysts. As can be seen from the product distribution, selectivity towards methane decreased significantly upon the introduction of iron to ruthenium, thus resulting in increased selectivity towards higher hydrocarbons. The most striking aspect of the study, however, was the dramatic increase in the ratios of unsaturated to saturated products for the $C_2$ and $C_3$ hydrocarbons, as evidenced in Figure 2.3.

Ott et al. (14) also performed surface analyses of fresh catalyst samples, utilizing x-ray photoelectron spectroscopy (XPS) and secondary ion mass spectrometry (SIMS). As has been noted elsewhere, the behavior of the catalytic surface was significantly different from that of the bulk. Strong surface enrichment by iron was observed, particularly in the region where the Fe bulk content was less than 50 atomic percent. Interestingly, the major changes in the surface composition corresponded to the major changes in selectivity of the catalysts. Ott et al. postulated that, analogous to the promotional effect of $K_2O$ on Fe Fischer-Tropsch catalysts, the introduction of iron to the ruthenium system would lower the work function, which could subsequently increase electron donation to CO, thus raising its heat of adsorption and also suppressing the adsorption of $H_{ad}$. The lowered concentration of surface hydrogen and the

Figure 2.2

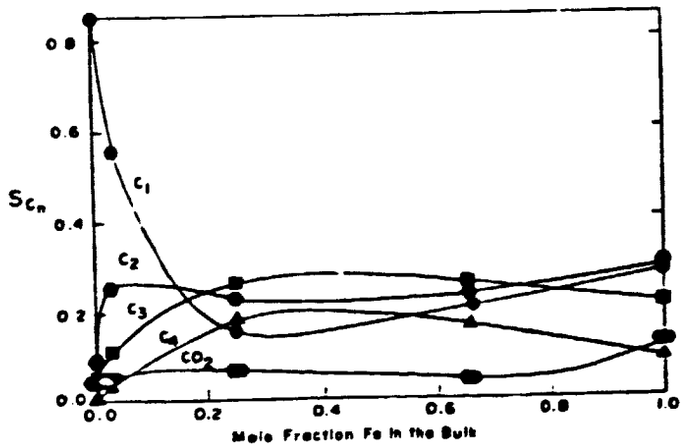


Hydrocarbon selectivity in $3.3H_2/CO$ at 1 atm and 573 K for freshly reduced FeRu catalysts as a function of bulk composition. $C_n$ indicates number of carbon atoms in the product molecule. (14)

Figure 2.3

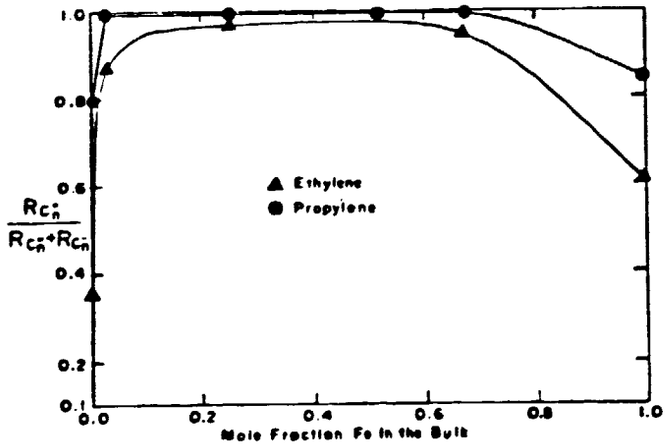


Relative selectivity of FeRu catalysts to unsaturated products in $3.3H_2/CO$ at 1 atm and 573 K. (14)

lengthened residence time of carbon intermediates would thus account for an increase in the production of unsaturated higher hydrocarbons, namely ethylene and propylene.

High olefin yields have also been reported for silica-supported RuFe Fischer-Tropsch catalysts (27). However, selectivities of these catalysts towards olefins are not as high as those of unsupported RuFe alloys, thus suggesting the influence of support interaction and metal particle size on reaction products (14).

The prominently high olefin yields in CO hydrogenation over RuFe alloy catalysts could have several beneficial effects in their applications to the Bosch process. The high production of olefinic compounds indicates that carbon deposition on the alloy would be enhanced when the system is operated at high temperatures. In other words, the appearance of significant amounts of ethylene and propylene in the hydrocarbon synthesis is undoubtedly a kinetic rather than an equilibrium phenomenon. Consequently, in approaching the equilibrium state of the system, the rate of carbon deposition from a gas phase containing olefins, rather than paraffins, would expectedly be enhanced, as has been observed for similar systems by Baker (15). This enhancement of carbon deposition activity coupled with the low temperature synthesis activity of a ruthenium- iron catalyst is expected to lead to an improved catalyst for the Bosch process.

# 3. Apparatus and Procedure

## 3.1 Experimental Apparatus[1]

Figure 3.1 shows a block diagram of the experimental system. It consists of three basic elements: the feed-gas delivery system, the thermogravimetric reactor, and the gas analytical system. Details of each section are described below.

### 3.1.1 Feed-Gas Delivery System

In the feed-gas delivery system, chemically pure gases were individually metered and mixed to give desired dry gas compositions. If required, water was then added to the gas mixture as steam before the feed was sent to the reactor. The requisite rate of steam was produced by metering liquid water and vaporizing it.

The delivery system of dry reactant gases is shown schematically in Figure 3.2. It consisted of a set of gas cylinders, two-stage gas regulators, and flow controlling systems which included mass flow regulators, capillary tubes and U-tube manometers. Table 3.1 lists suppliers and purities of reactant gases used in this experimental study. The

1. The original apparatus was designed and built by Manning(5), with further improvement made by Sacco(7) and Garmirian(9). Minor modifications were also made in this study.

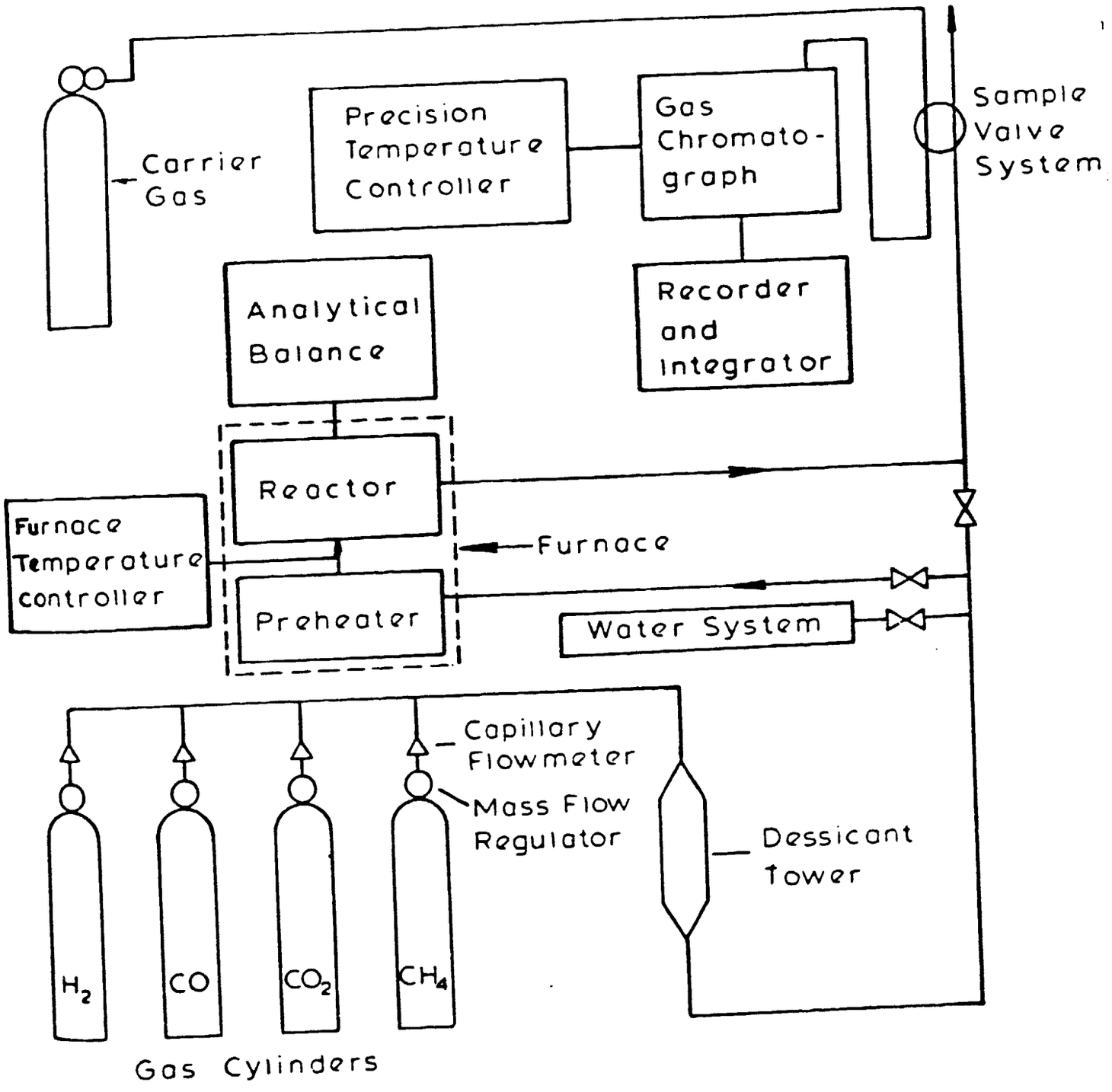


Figure 3.1 Schematic Diagram of Experimental System (9)

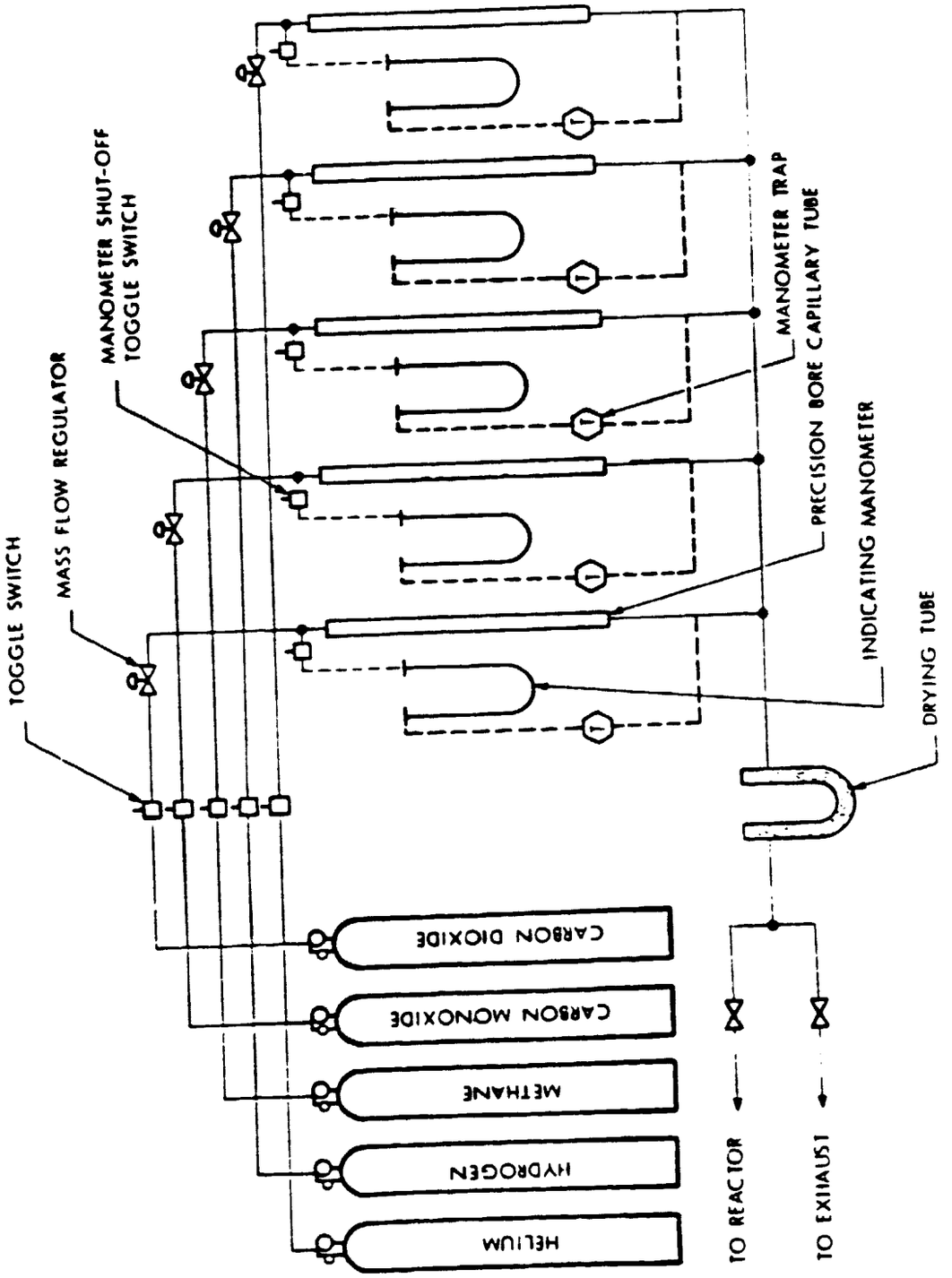


Figure 3.2 Dry Feed Gas Delivery System (7)

Table 3.1 Feed-Gas Analysis

| Gas | Supplier | $CO_2$ | $O_2$ | $N_2$ | Dew Point |
|---|---|---|---|---|---|
| Hydrogen (Prepurified Grade) | Airco | | < 20 ppm | | 213.6K |
| Methane (CP Grade) | Matheson | 0.2 mole % | 0.005 mole % | 0.6 mole % | |
| Carbon Dioxide (Bone Dry Grade) | Matheson | 99.95 mole % | 0.05 mole % | | 238.6K |
| Carbon Monoxide (CP Grade) | Matheson | 50 ppm | 600 ppm | 1500 ppm | |
| Helium (High Purity Grade) | Airco | 1 ppm | 1 ppm | 14 ppm | |

upstream pressure of each gas component was maintained at 3.45 x $10^5$ $N/m^2$ (50 psig) by the two-stage regulators. The gases were individually fed to Brooks Model 8944 mass flow regulators equipped with digital settings and inlet line filters capable of removing entrained particles larger than 2 m. The gases then passed through 91.5-cm precision bore capillary tubes with capillary diameters between 1.0 and 1.4 mm (tolerance of capillary diameter:+ 0.0007 mm). The pressure drops across the tubes were measured by U-tube manometers filled with Meriam high vacuum indicating fluid (density: 1.04 $g/cm^3$). The capillary tubes were calibrated for gas flow rates using soap film flow meters. As would be expected, a linear relationship between flow rate and pressure drop was observed, since the capillary tubes used for each gas were selected so that the flow in the capillary tubes would remain laminar for experimental flow rates anticipated. This phenomenon was in accordance with the Poiseuille's Law, stating that the gas flow rate is directly proportional to the pressure drop for laminar flow, as shown mathematically in the following equation.

$$Q = (\pi d^4 \Delta P)/(128 \mu L) \qquad (3.1)$$

where $Q$ = volumetric flow rate

$d$ = capillary diameter

$\Delta P$ = pressure drop across the capillary tube

$\mu$ = gas viscosity

$L$ = capillary length

The gases exiting the capillary tubes were mixed and dried in a Kimax U-tube packed with indicating silica gel dessicant. At this point the gas mixture could either be fed to the reactor, with or without steam added, or diverted to the vent.

The water vapor delivery system is shown in Figure 3.3. The desired rate of steam flow was produced by metering liquid water and vaporizing it. A 1-liter cylindrical water reservoir was pressurized at 2.07 $N/m^2$ (30 psig). The water flow rate was controlled by a Nupro bellow metering valve. A precision bore capillary tube with an i.d. of 0.2 mm, in combination with a mercury manometer, allowed the calibration of the flow system. A 15-μm filter was installed to prevent the blocking of the capillary tube. The metered water flow was then fed to the vaporizer made from a 0.4-m length of 0.64 cm (1/4 inch) stainless steel tubing. The tube was packed with 0.5-mm borosilicate beads to enhance heat transfer, and Nichrome wire served as the heating element. The wire was wound between two layers of electrically insulating Sauereisen cement, which was coated on the external surface of the tubing. The power input to the Nichrome wire was controlled by a Variac.

The steam exiting the vaporizer was then fed to a 1-m length of 0.64 cm (1/4 inch) stainless steel tubing, which served to eliminate any surges in the water vapor line. The tubing was wrapped with Briskeat heating tapes and insulated

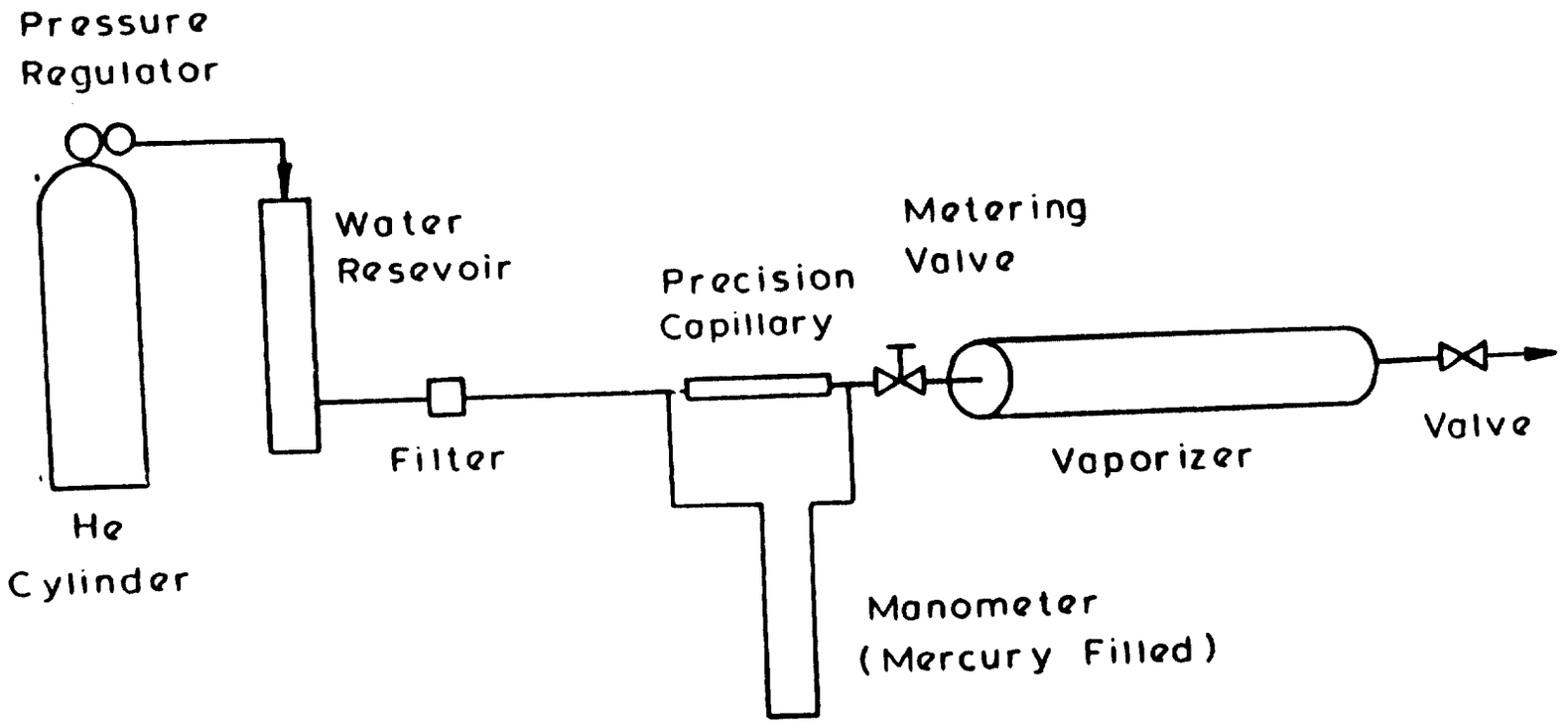


Figure 3.3 Water Vapor Delivery System (9)

with a Kaowool blanket. Like the vaporizer, the heated line was maintained at approximately 400K. Provisions were made at the end of the tubing so that the steam could either be added to the dry gas mixture before delivery to the reactor, or be bypassed to the atmosphere.

### 3.1.2 Thermogravimetric Reactor

The thermogravimetric reactor and its supporting components consisted of the following: lower reactor support tube, the top section of the reactor support tube, the catalyst assembly, and the heating furnace. A basic configuration of the reactor assembly is shown in Figure 3.4. Entering the inlet tube, the gas mixture from the feed preparation section passed through the helical preheating coil to the base of the reactor support tube. The gas mixture then flowed upward over the catalyst, leaving the system by way of either the weighing port or the sample line. Details of each reactor part are provided below.

#### 3.1.2.1 Preheater and Lower Reactor Support Tube

Figure 3.5 features the preheater and both the lower and upper sections of the reactor support tube. The preheater and the lower reactor support tube served as the base of the quartz reactor. The preheater was constructed from a 6-m length of 7-mm o.d. quartz tubing closely wound into a helical coil of 60 mm in diameter. The base of the preheater termina-

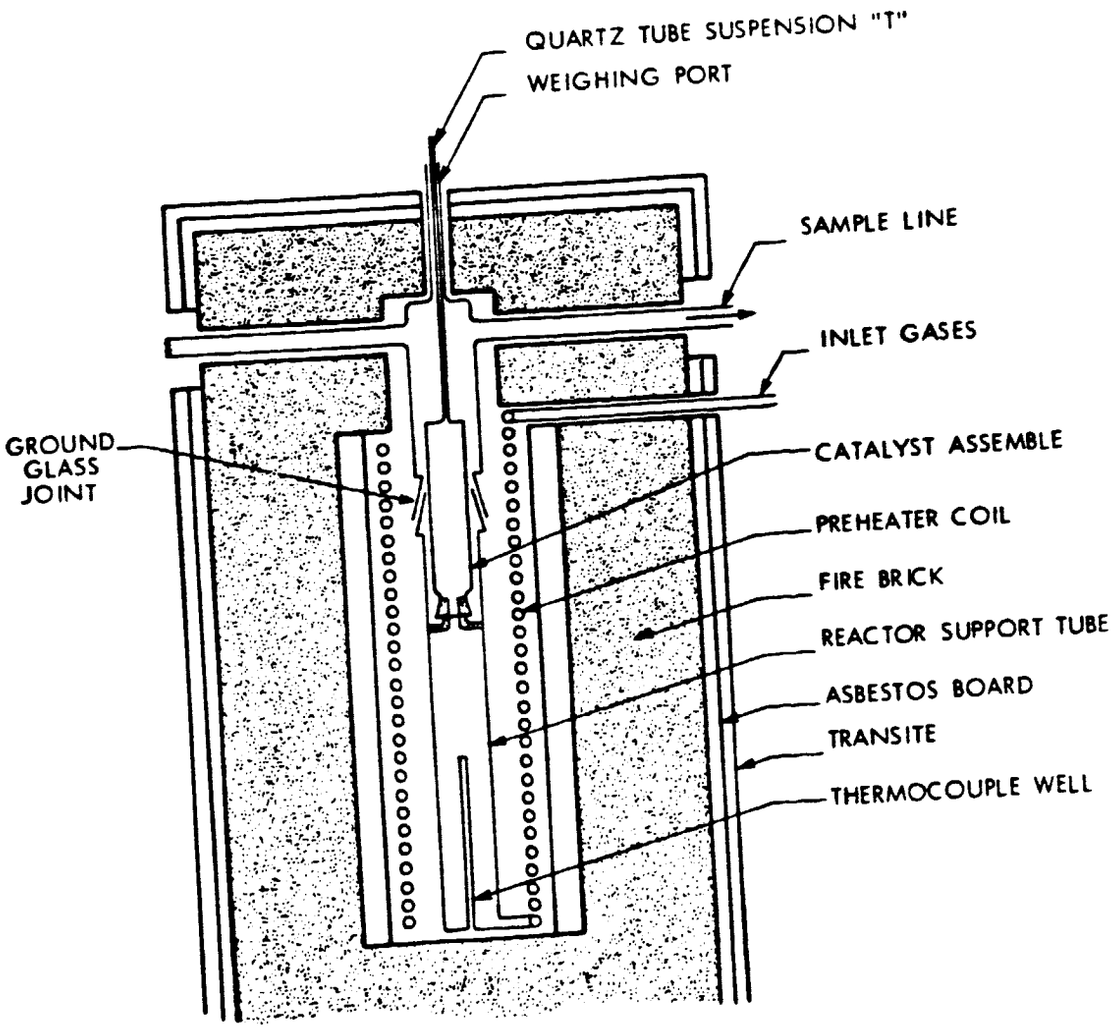


Figure 3.4 Reactor Assembly in Furnace (7)

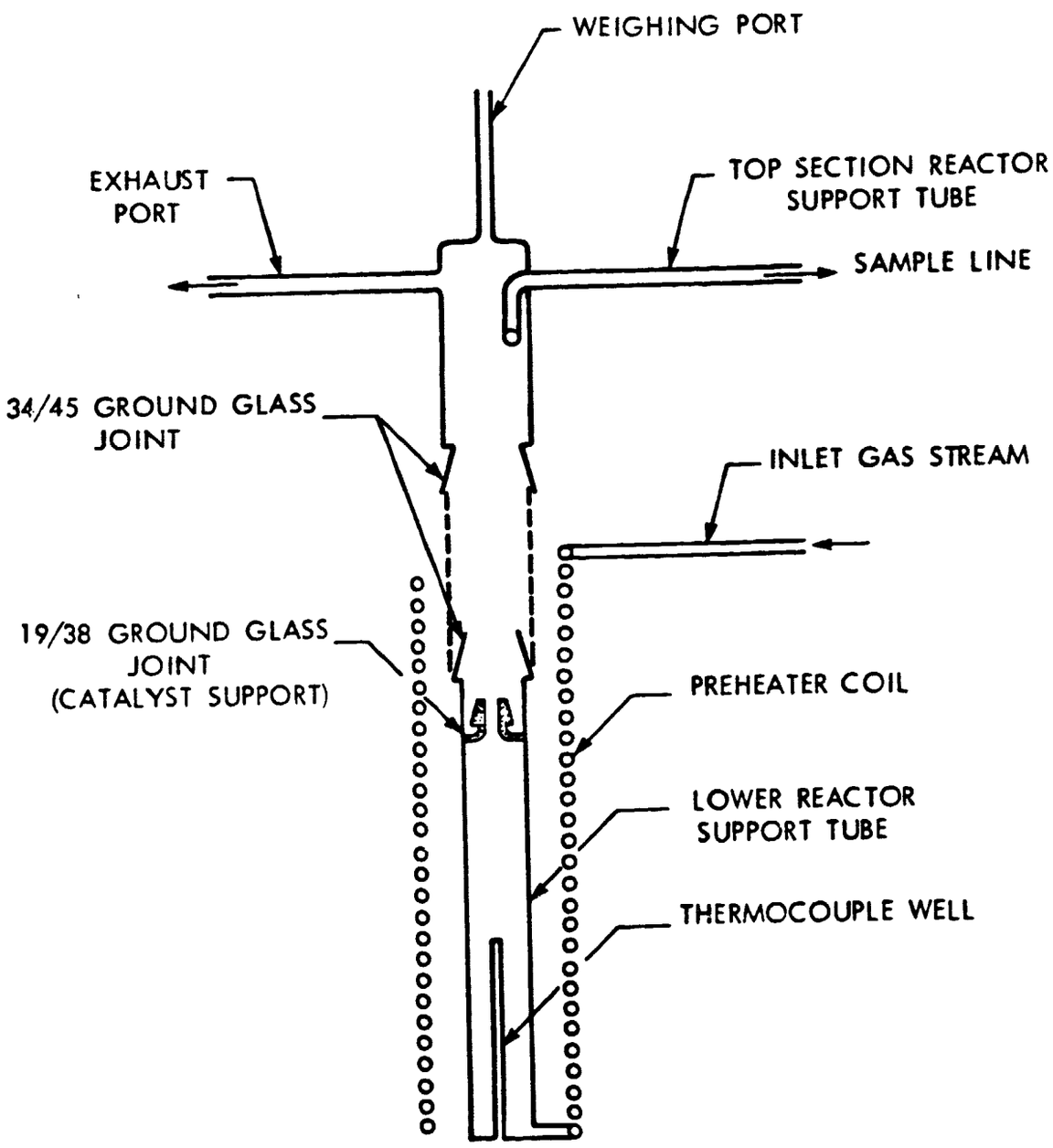


Figure 3.5 Top and Lower Reactor Sections with Preheater (7)

ted in the lower reactor support tube, a 28-mm o.d. quartz tube of 28 cm in height, mounted concentrically with the preheater coil. Also provided at the base of the support tube was a 110-mm quartz thermocouple well, which housed a two-hole Alundum thermocouple sheath holding two chromel-alumel (type K) thermocouples. A 34/45 tapered male ground glass joint was attached to the upper end of the lower reactor support tube. In addition, on the inside wall of the reactor support tube, a 19/38 inner ground glass joint was mounted upward to support the catalyst assembly.

3.1.2.2 Top Section of Reactor Support Tube

In addition to supporting the reactor within the furnace, the top reactor section was designed to allow the sampling and exhausting of outlet gases, and to facilitate the weighing of the catalyst sample. The upper support tube consisted of a 28-mm i.d. quartz tube, 15.2 cm in height, fitted with a female 34/45 ground glass joint on its lower end, which joined with the lower reactor support tube. Connected concentrically on the upper end of this top reactor support tube was a 8-mm i.d. quartz tube, which served as a weighing port. Two additional 8-mm i.d. quartz tubes were mounted perpendicularly to the support tube centerline. One of these extensions was sealed and served only to hold the top reactor section in place; the other was connected to the gas sampling line for the analysis of outlet gases.

3.1.2.3 Catalyst Assembly

Illustrated in Figure 3.6 is the catalyst assembly in the reactor support tube. The catalyst was held in place between plugs of quartz wool inside the catalyst carrier, which was constructed out of a 20-mm i.d. quartz tube, 120 mm in length, with one end fitted with a 19/38 female tapered ground glass joint. This joint allowed the reactor carrier to be connected to the lower reactor support tube, thus permitting the gas mixture from the preheating coil to pass over the catalyst. Attached concentrically to the top of the catalyst carrier was a quartz rod, 3 mm in diameter and approximately 25 cm in length. The quartz rod allowed weight measurements to be taken by periodically suspending it from an overhead Sartorius balance, sensitive to an accuracy of ± 1 mg.

3.1.2.4 Furnace

As shown in Figure 3.4, all the reactor units described above were housed in a heating furnace. The central component of the furnace was the cylindrical heating surface, consisting of two Thermcraft Model RH254 semicylindrical ceramic heating elements which formed a heated cavity 75 mm in diameter and 30.5 cm in length. Capable of delivering a maximum power output of 2300 watts, these heating elements were wired in parallel to a 220-volt electrical line. The reactor temperature was controlled by a Thermolyne Dubuque III solid state

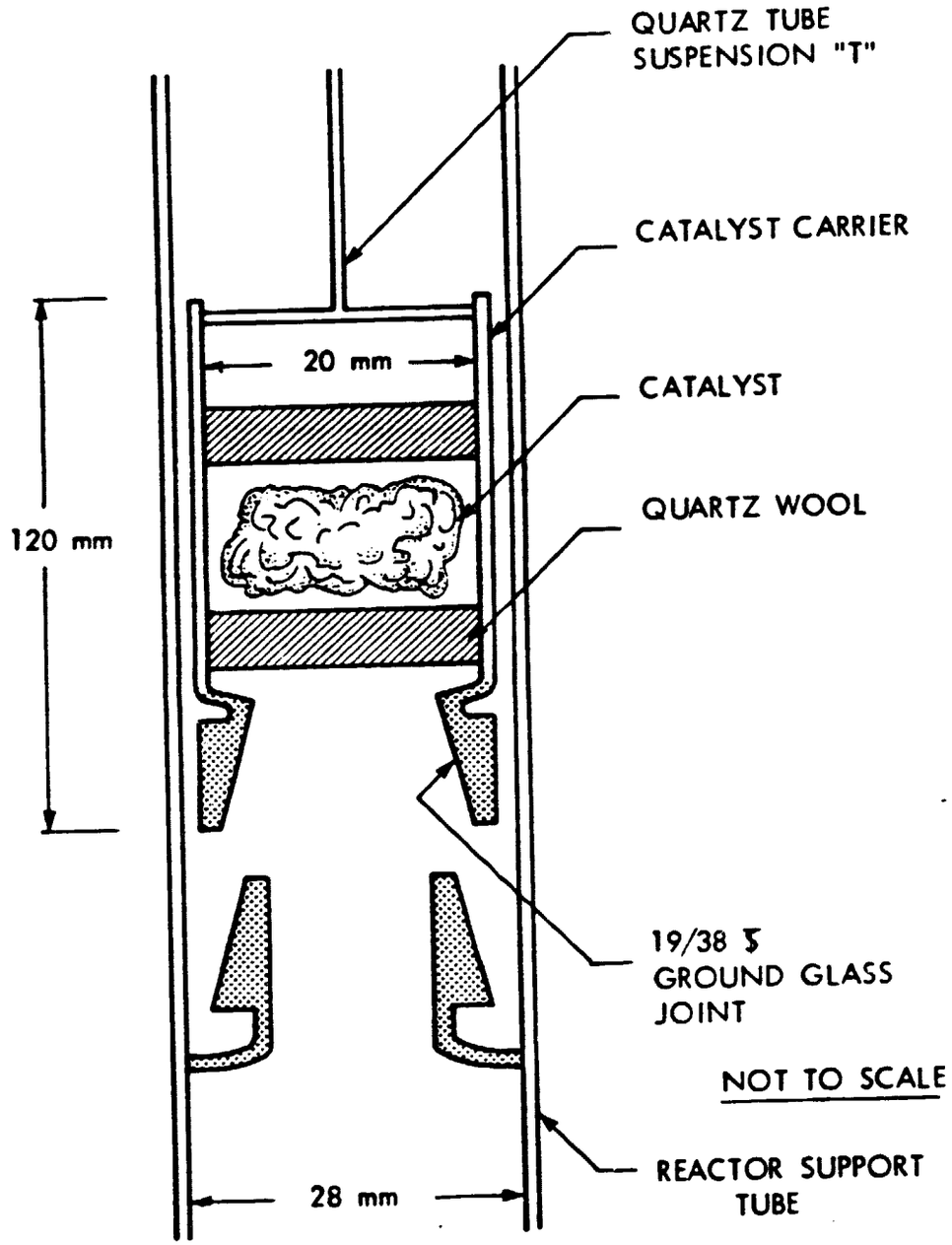


Figure 3.6 Catalyst Carrier in Support Tube (7)

proportional controller. The sensor of the temperature controller was an Omega Inconel sheathed chromel-alumel thermocouple located directly below the catalyst assembly in the quartz thermocouple well. A similar thermocouple, also in the thermocouple well, was connected to an Omega Engineering 200 digital pyrometer, thus allowing a continuous monitor of the reactor temperature.

The ceramic heating elements were enclosed by Babcock and Wilcox Type K-30 insulating firebrick, forming a square structure about the cylindrical heaters. The firebrick was further enclosed by an asbestos board, 6.5 mm thick, and the entire furnace was structurally supported by a layer of 6.5-mm thick Transite, an asbestos-concrete composite.

### 3.1.3 Gas Sampling and Analytical System

Designed to determine the compositions of inlet and outlet gas mixtures, the data acquisition system included two basic components: a gas sampling system and an on-line Hewlett-Packard Model 700 gas chromatograph equipped with a thermal conductivity detector.

Housed in the gas chromatograph oven, the gas sampling system consisted of a Hewlett-Packard Model 19020 sample valve equipped with 0.25-ml sample loops, a series of four toggle shut-off valves for different choices of gas sampling, and a toggle valve connected to a vacuum system allowing for the evacuation of sample loops and the drawing of gas samples. A

representation of the gas sampling system is shown schematically in Figure 3.7.

During normal operation, a vacuum would be drawn on the sample valve system. Consequently, with the desired toggle valve open, the sample loop was flushed with a sample gas. When the vacuum toggle valve was closed, the sample gas continued to flow into the system until the pressure in the sample loop equaled the barometric pressure. The sample injection into the gas chromatograph then followed. The sample loop pressure was determined by using a U-tube mercury manometer, one leg of which was open to the atmosphere.

The analysis of gas samples was accomplished by a series of GC columns packed with Porapak QS (mesh 50/80) and molecular sieve 5A (mesh 50/60). (Refer to Figure 3.7.) A Carle Model 2014 micro-volume valve allowed the gas sample to be directed, for further separation, to either a Porapak QS or a molecular sieve 5A column. In a normal analysis for a gas mixture of $H_2$, CO, $CH_4$, $CO_2$ and $H_2O$, the Carle micro-volume valve was positioned such that the gas mixture would flow through both the 5.0-m and the 2.0-m Porapak QS columns. However, periodic checking for a possible air leak into the thermogravimetric reactor was desirable. As carbon monoxide and air could not be separated by a Porapak QS column at ambient temperature or above, the analysis was carried out by a series of the 5.0-m Porapak QS column and the 2.0-m molecular sieve 5A column. The former separated the gas components

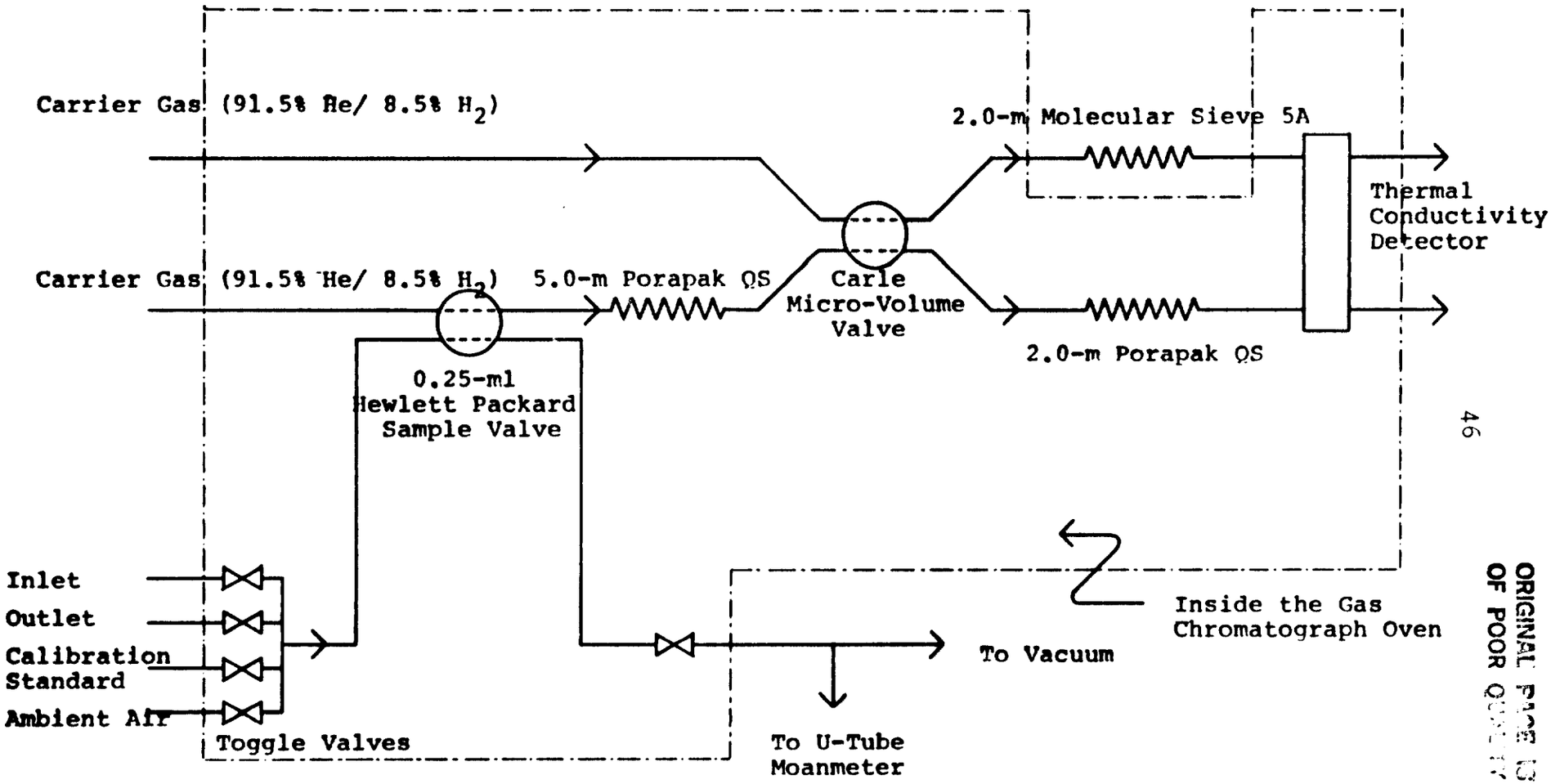


Figure 3.7 Gas Sampling and Analysis System

into the following sequence: $H_2$, CO and air, $CH_4$, $CO_2$ and $H_2O$. Separation of light gases up to methane was further accomplished at ambient temperature by the molecular sieve column housed outside the GC oven. As carbon dioxide and water were hazardous to the M5A column, a valve switching was made at an appropriate time to divert these two remaining gas components to the 2.0-m Porapak column.

To reduce the severe tailing of a water peak, Teflon-coated stainless steel tubing was used for GC columns, as suggested by Hollis and Hayes (28). The sample loops and stainless steel tubing with no Teflon coating were wrapped with heating tapes.

A major effort was put forth to obtain good gas analytical results. Optimization was made concerning gas flow rates, oven and detector temperatures, column lengths as well as integrating parameters used in an Autolab Model 6300 digital integrator. Chromatograph operating conditions are shown in Table 3.2.

The Autolab digital integrator was used in conjunction with a Honeywell chromatograph recorder to give a quantitative as well as a visual record of all samples analyzed. An external standard was used to determine response factors of the thermal conductivity detector for the five gas components. These results were then used to calculate component compositions, except for $H_2$, by the procedure described by Dal Nogare and Juvet (29). For the determination of hydrogen

Table 3.2 Gas Chromatograph Operating Conditions

| | | |
|---|---|---|
| Filaments | GOW-MAC Rhenium Tungsten Code 13.002 (wx) | |
| Sample Size | 0.25 | cc |
| Carrier Gas Flow Rate | 35 | cc/min |
| Column Operating Temperature | 418 | K |
| Detector Operating Temperature | 473 | K |
| Detector Filament Current | 200 | mA |

content, the method recommended by Purcell and Ettre (30) was applied. Direct measurement of hydrogen was made possible as the result of using a special gas mixture of 91.5% He and 8.5% $H_2$ supplied by Matheson Gas Products.

Three standards typically used in calibrating the thermal conductivity detector were: (1) pure hydrogen, (2) a certified primary gas standard containing a mixture of hydrogen, carbon monoxide, methane and carbon dioxide (see Table 3.3), and (3) a gas mixture of known water vapor content.

The raw data obtained from the GC analysis were analyzed using a modified computer program for data reduction originally developed by Manning (5).

## 3.2 Catalyst Preparation

The unsupported catalysts under investigation were ruthenium metal and Ru-Fe alloys. These were prepared by a precipitation method, wherein an aqueous metal chloride ($RuCl_3/FeCl_2$) solution of the predetermined composition was chemically reduced by sodium borohydride[1] (31). Specifically, a salt solution of 0.1-0.2 M was prepared and added to an

1. Anhydrous iron (III) chloride and sodium tetraborohydride (98%) were supplied by Alfa Products, a Ventron division. Anhydrous ruthenium (III) chloride was supplied by Strem Chemicals.

Table 3.3 Composition of Certified Primary Standard

| Gas | Mole Percent |
|---|---|
| Hydrogen | 22.10 ± 0.02 |
| Carbon Monoxide | 25.00 ± 0.02 |
| Carbon Dioxide | 25.03 ± 0.02 |
| Methane | Balance |
| Ethylene | 1.95 ± 0.02 |
| Propylene | 2.00 ± 0.02 |

excess amount of reducing $NaBH_4$ solution. The salt was instantly reduced with the formation of a black, finely divided solid. The solid precipitate was filtered, washed several times with distilled water, and air dried. The solid sample was then treated overnight at 773K under a hydrogen atmosphere, to increase crystal size and to remove traces of the chlorides.

Three types of unsupported catalysts were prepared by the method described above. They were pure ruthenium, 50Ru50Fe (atomic Ru:Fe = 1:1) and 33Ru67Fe (atomic Ru:Fe = 1:2). X-ray diffraction analysis was performed on the samples to confirm the formation of the expected alloy catalysts. The surface areas of activated samples were determined by the $BET/N^2$ method using a Quantasorb sorption system. The results are shown in Table 3.4.

## 3.3 Experimental Approach

Although represented stoichiometrically by the overall reaction (1.3), the Bosch process consists of a complex set of reactions, involving not only the gas phase reactions among the five major components -- hydrogen, carbon monoxide, methane, carbon dioxide and water -- but also the gas-solid interactions. As discussed earlier, the latter includes, for instance, oxidation of the metal as in the case of iron-catalyzed Bosch equilibrium studies and carbide formation

Table 3.4 Surface Areas of Unsupported Catalysts

| Sample | Surface Area ($m^2/g$) |
|---|---|
| Ru | 7.07 |
| 50Ru50Fe | 1.83 |
| 33Ru67Fe | 5.69 |

as in the nickel and cobalt systems. These gas-catalyst interactions have been found to account for the experimental water yield lower than predicted from the gas-graphite equilibrium. The objectives of this investigation have been to evaluate the effectiveness of Ru and Ru-Fe alloys as Bosch catalysts. This is tantamount to the determination of carbon deposition boundary lines for these proposed catalysts.

Results from previous investigations (9,10,16,17,18) have pointed out the necessity to account for the possible existence of a different form of carbon other than β-graphite in determining the carbon deposition equilibrium boundary. The approach taken in this Bosch equilibrium study was similar to the one used by Garmirian (9). $\Delta G_c$ was defined as the difference in the Gibbs energy changes involving the formation of experimental carbon and β-graphite as illustrated below.

$$\Delta G_c = \Delta G_{\text{experimental carbon}} - \Delta G_{\beta\text{-graphite}}$$

$$= -RT \ln K_{p_{\text{experimental carbon}}} + RT \ln K_{p_{\beta\text{-graphite}}} \qquad (3.2)$$

Based upon phase rule considerations, the determination of gas equilibrium compositions can be accomplished as follows. For a given temperature, pressure and gas phase O/H ratio, any three independent reactions can be chosen, one being a carbon desorption reaction. Three such reactions and their equili-

brium constants are shown below.

$$H_2 + CO_2 \rightleftarrows CO + H_2O \qquad K_{p_1} = \frac{p_{H_2O}p_{CO}}{p_{CO_2}p_{H_2}} \qquad (3.3)$$

$$3H_2 + CO \rightleftarrows CH_4 + H_2O \qquad K_{p_2} = \frac{p_{CH_4}p_{H_2O}}{p_{CO}p_{H_2}^3} \qquad (3.4)$$

$$CH_4 \rightleftarrows C + 2H_2 \qquad K_{p_3} = \frac{p_{H_2}^2}{p_{CH_4}} \qquad (3.5)$$

By allowing the equilibrium constant of reaction (3.5) to vary as

$$K_{p_3} = K_{p_{3_{\beta\text{-graphite}}}} \exp(-\Delta G_c/RT) \qquad (3.6)$$

to account for the possibility of the formation of experimental carbon other than β-graphite, equilibrium gas compositions were then determined for a given temperature, pressure and gas phase O/H ratio, thus varying the values of the parameter $\Delta G_c$ from -10.0 kcal/mole to +10.0 kcal/mole. The flow rates of each gas component were then set accordingly for desired values of $\Delta G_c$. A computer program was developed for the determination of run conditions.

# 4. Results and Discussion

## 4.1 Results

Two types of experiments were performed on the ruthenium catalyst and the two Ru-Fe alloys. The first type was carried out to see whether the powder samples catalyzed the Bosch reaction, which results in carbon deposition on the samples. The other experiments were the equilibrium studies, from which carbon deposition boundaries were determined.

### 4.1.1 Preliminary Experiments

To determine the catalytic activities of unsupported ruthenium and Ru-Fe alloys toward carbon deposition, a gas mixture of hydrogen and carbon monoxide was employed. Periodic weight measurements were made to monitor the extent of carbon deposition as a function of time. For the ruthenium catalyst, no carbon deposition was observed. In one instance, a gas mixture of equimolar $H_2$ and CO was passed over 0.19972 grams of the unsupported ruthenium catalyst at the flow rate of 20 cc/s (STP) and at the temperature of 800K for $2\ 3/4$ hours; no change in the weight of the catalyst was noted. However, in the analysis of outlet gas compositions small amounts of methane and carbon dioxide (<1.0 mole percent) were found. The detection of $CH_4$ and $CO_2$ was indicative that the ruthenium sample was catalytically active. The observation of

methane is consistent with a number of investigations carried out at lower temperatures, which have shown ruthenium as a good methanation catalyst (32,33).

Figure 4.1 shows the accumulated amount of deposited carbon as a function of time for the reactions of a 1:1 mixture of hydrogen and carbon monoxide over the 50Ru50Fe and 33Ru67Fe catalysts at 800K. While the amount of carbon deposited over long periods was a linear function of time for the 50Ru50Fe alloy, this was not the case for the 33Ru67Fe catalyst. The latter exhibited an increasing rate of carbon deposition.

### 4.1.2 Equilibrium Studies

In the equilibrium studies, the catalyst was reduced under a hydrogen flow for 2.5 - 3 hours prior to every experimental run. About 2.0 g carbon/g catalyst was then deposited from an equimolar mixture of hydrogen and carbon monoxide at the reaction temperature of an experimental run. Six or more weight measurements were normally taken at 30-minute intervals for each gas composition corresponding to the desired $\Delta G_c$. In cases where the rate of weight change was very small, experiments were run at an increased period of time to ensure accurate data acquisition. The carbon deposition boundary was determined at the point where the deposition ceased when it was approached from the carbon depositing region.

Since no detectable carbon deposition was observed on

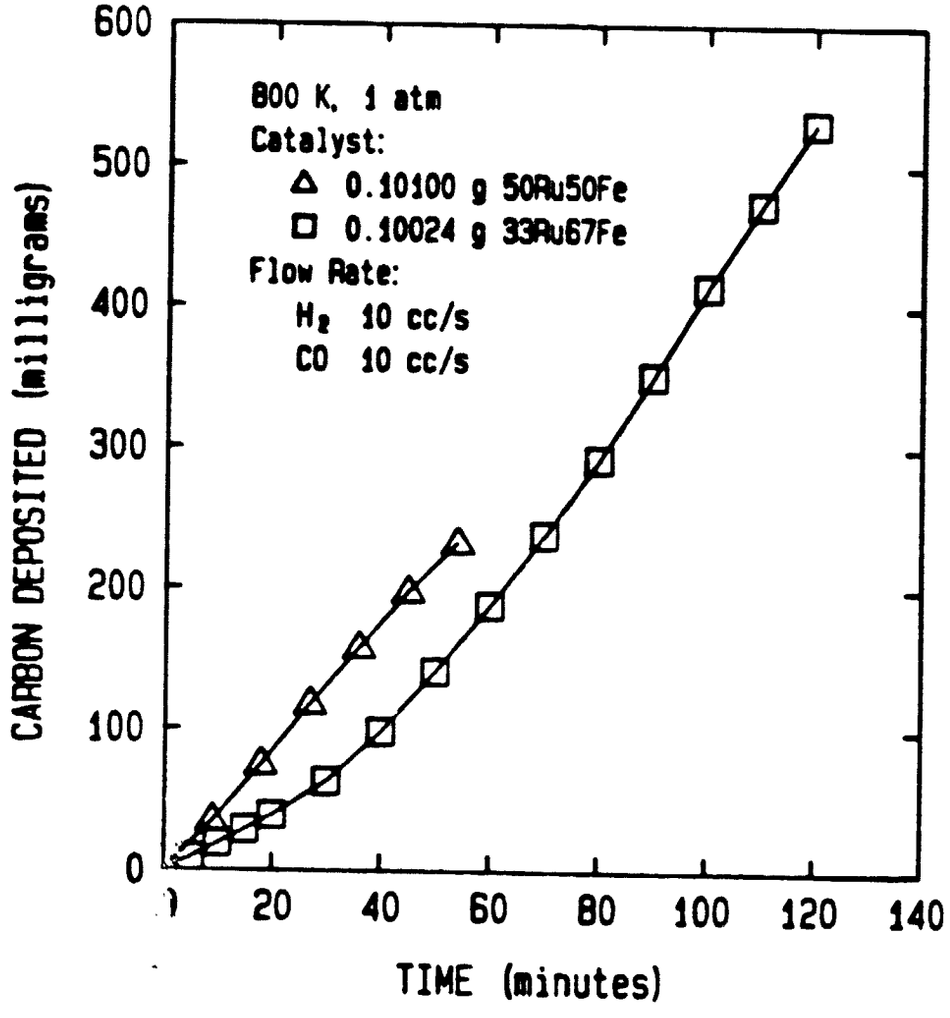


Figure 4.1 Carbon Deposition on 50Ru50Fe and 33Ru67Fe Alloy Catalysts from a $H_2$:CO (1:1) Mixture

unsupported ruthenium, as evidenced from the preliminary experiments presented earlier in Section 4.1.1, the unsupported metal was ruled out as an effective Bosch catalyst. Equilibrium studies were carried out on the two alloy catalysts, and the results are presented below.

4.1.2.1 50Ru50Fe Alloy

Shown in Figures 4.2, 4.3 and 4.4 are results from Bosch equilibrium studies at 700, 800 and 900K and a pressure of 1 atm over the 50Ru50Fe catalyst. Multicomponent gas mixtures of $H_2$, CO, $CH_4$, $CO_2$ and $H_2O$ were used with an O/H ratio of 0.5. This O/H ratio corresponds to the steady state value at which a typical Bosch reactor would be operated with a stoichiometric 2:1 feed mixture of hydrogen and carbon dioxide. The figures show experimental rates of carbon deposition plotted as a function of $\Delta G_c$, the parameter reflecting the gas phase composition in equilibrium with a carbon of the corresponding Gibbs energy. These gas phase compositions are represented in the diagrams.

Observed in this equilibrium study is a phenomenon similar to the one previously reported by Garmirian (9) and other investigators (16,17,18). The rate of carbon deposition became zero before the graphite-gas equilibrium was reached, and the deviation from the graphite equilibrium was pronounced at low temperatures. Specifically, carbon deposition ceased at an increasing value of $\Delta G_c$ as the reaction temperature was

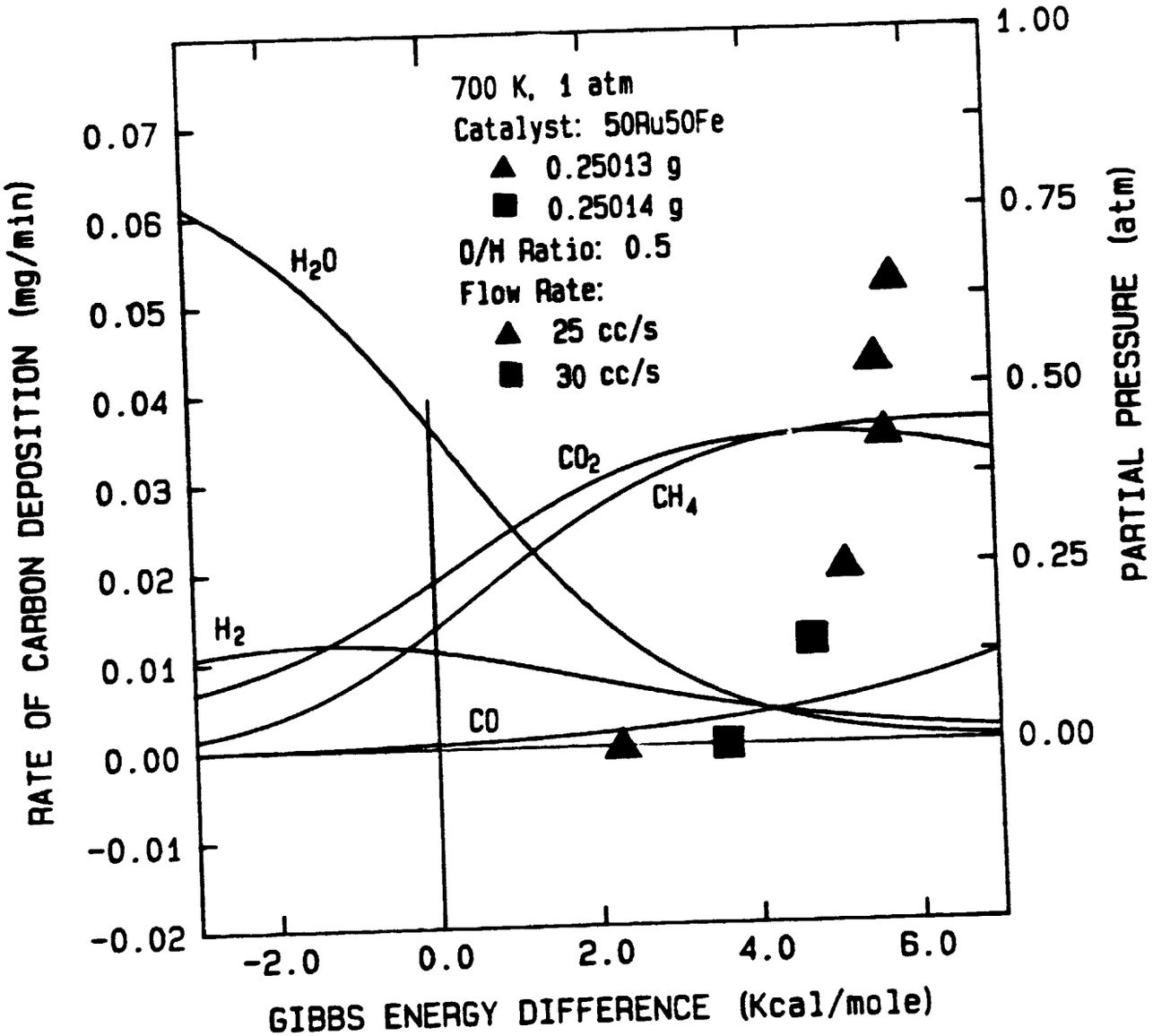


Figure 4.2 Rate of Carbon Deposition as a Function of $\Delta G_c$ for an O/H Ratio of 0.5

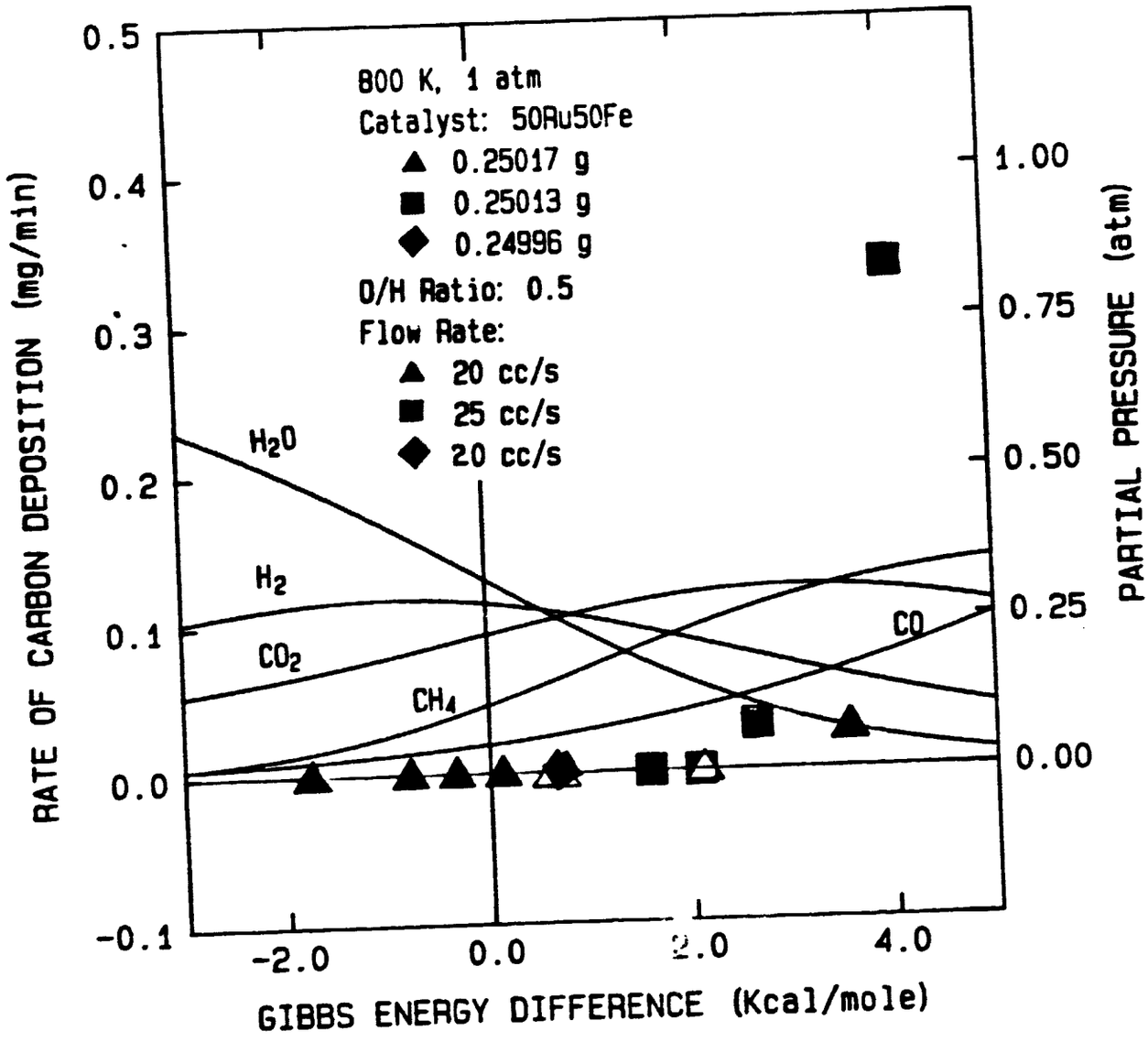


Figure 4.3 Rate of Carbon Deposition as a Function of $\Delta G_c$ for an O/H Ratio of 0.5

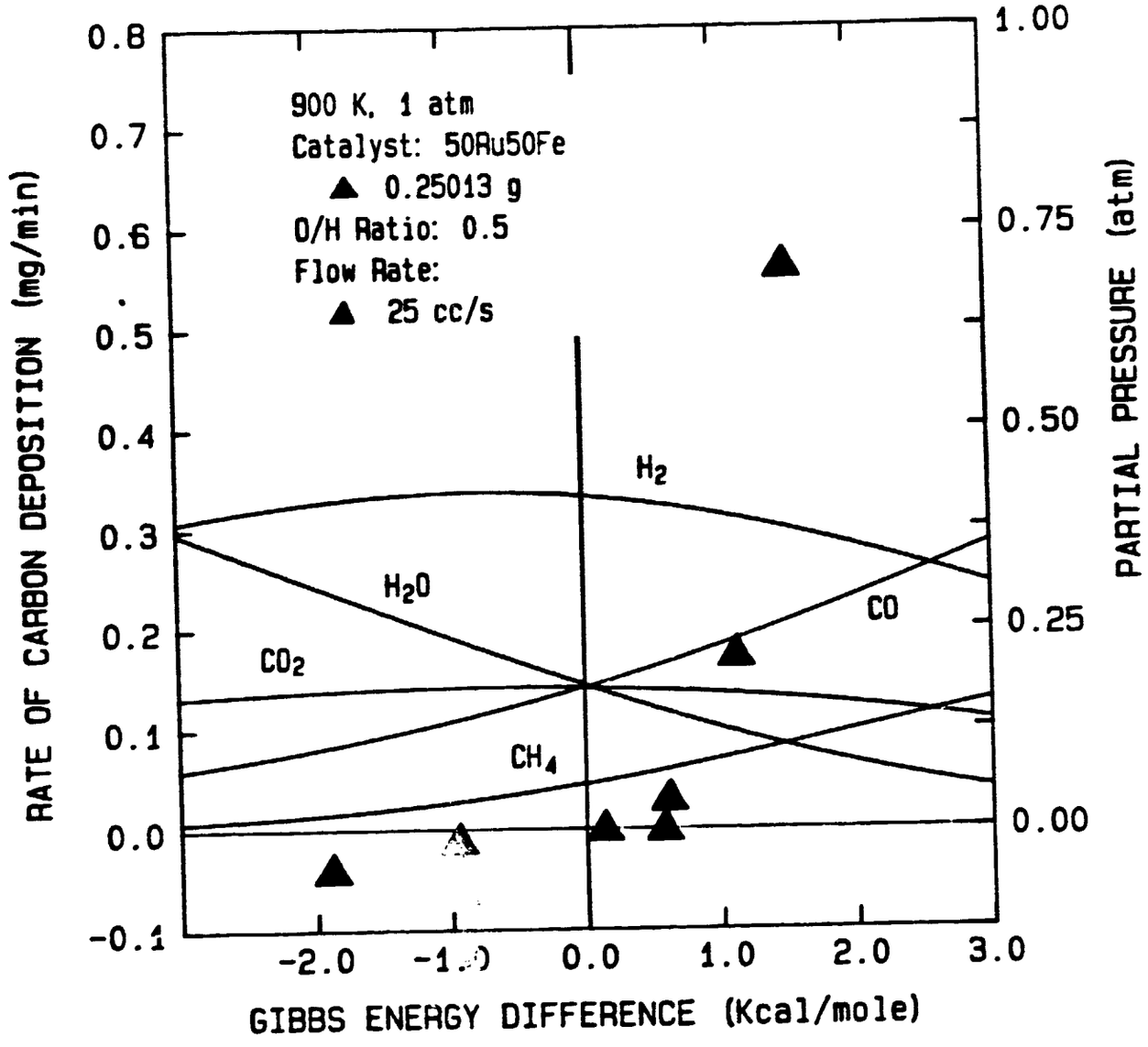


Figure 4.4 Rate of Carbon Deposition as a Function of $\Delta G_c$ for an O/H Ratio of 0.5

lowered. As can be seen in Figures 4.2, 4.3 and 4.4, carbon stopped depositing on the 50Ru50Fe catalyst at the approximate $\Delta G_c$ values of 0.6, 2.1 and 4.0 kcal/mole for the temperatures of 900, 800 and 700K, respectively. The result indicates that gas equilibrium with β-graphite over the unsupported 50Ru50Fe alloy could not be attained under the reaction conditions studied.

Another phenomenon also observed by Garmirian (9) is with regard to carbon removal. Although the data concerning carbon removal in this study are not complete, it can still be pointed out that carbon removal did not always occur right at the point where $\Delta G_c$ was less than 0.0 kcal/mole. In other words, in many cases carbon removal was not observed until gas mixtures with $\Delta G_c$ values much less than zero were passed over the catalyst. For instance, while carbon removal was recorded for the gas mixture with $\Delta G_c$ of -1.0 kcal/mole at 900K, no weight change was detected at 800K even for the $\Delta G_c$ value of -1.8 kcal/mole. The existence of region where no carbon deposition nor removal was observed possibly reflects the difference in reaction mechanisms involved in the process of carbon deposition and carbon removal.

Equilibrium studies were also performed at other O/H ratios over the 50Ru50Fe alloy. Specifically, gas mixtures with an O/H ratio of 1.5 were employed at reaction temperatures of 700, 800 and 900K. The carbon deposition equilibrium boundary was also studied at 800K using a gas mixture with an

O/H ratio of 0.17. The results are presented in Figures 4.5, 4.6, 4.7 and 4.8 in a similar fashion as those shown earlier for an O/H ratio of 0.5.

As with the O/H ratio of 0.5, the results of carbon deposition equilibrium boundary at O/H = 0.17 and 1.5 show that carbon stopped depositing before reaching the graphite equilibrium and that the deviation from the graphite equilibrium was large at low temperatures. Furthermore, the carbon deposition boundary at a given temperature was essentially independent of the O/H ratio of a gas mixture employed, as evidenced in Figure 4.9 where the value of $\Delta G_C$ at which carbon deposition started is plotted against the reaction temperature. In other words, at a given temperature, the Gibbs energy of the deposited carbon was independent of gas phase composition.

#### 4.1.2.2 33Ru67Fe Alloy

The results of Bosch equilibrium studies on the 33Ru67Fe catalyst are shown in Figures 4.10, 4.11, 4.12 and 4.13 for gas mixtures with an O/H ratio of 0.5 and at temperatures of 700, 750, 800 and 900K, respectively. This alloy catalyst showed a promising result. In contrast with the 50Ru50Fe system, the investigation on the 33Ru67Fe catalyst indicated that at 800 and 900K carbon deposition ceased as $\Delta G_C$ approached zero, which corresponded to a gas phase in equili-

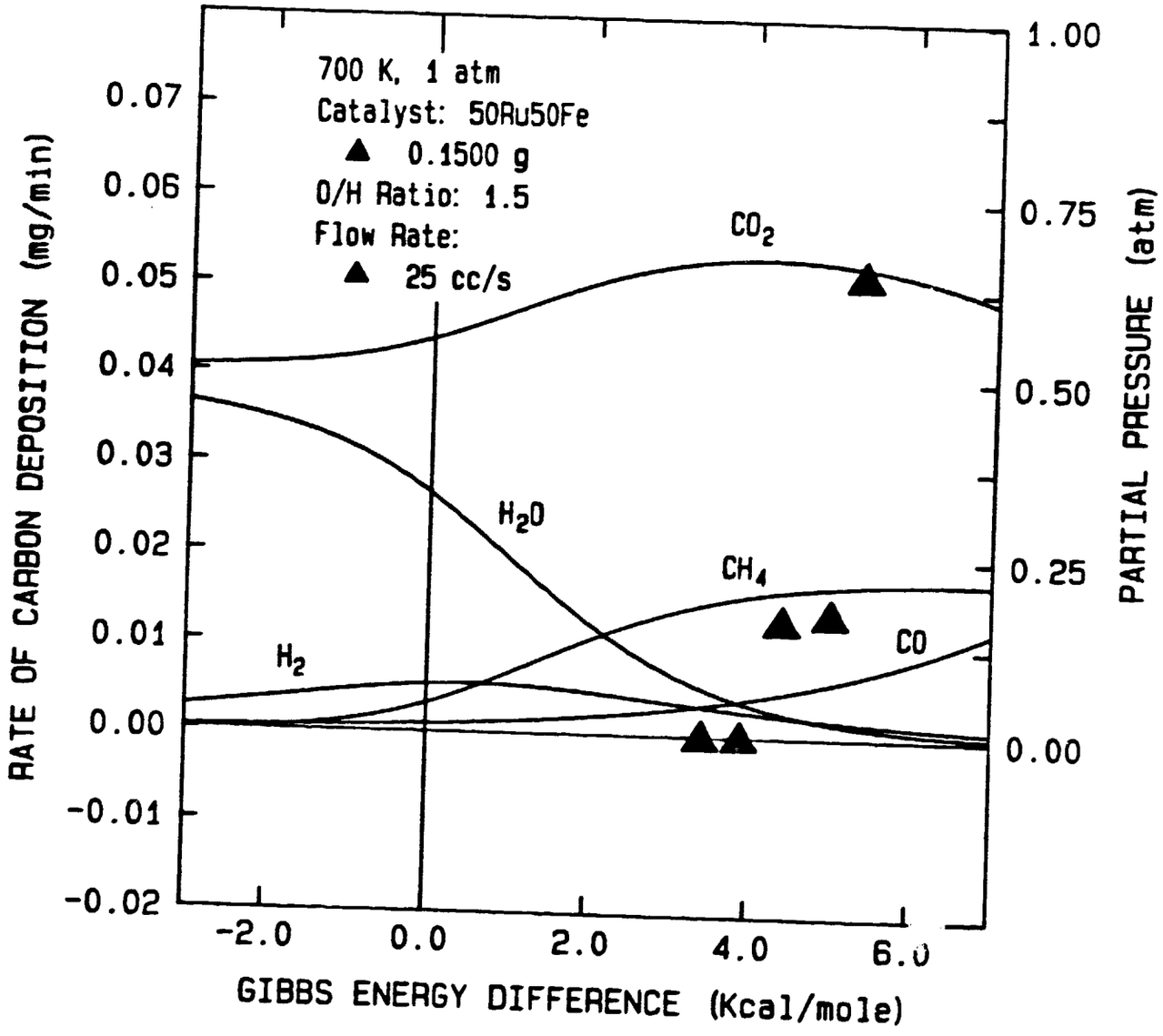


Figure 4.5 Rate of Carbon Deposition as a Function of $\Delta G_c$ for an O/H Ratio of 1.5

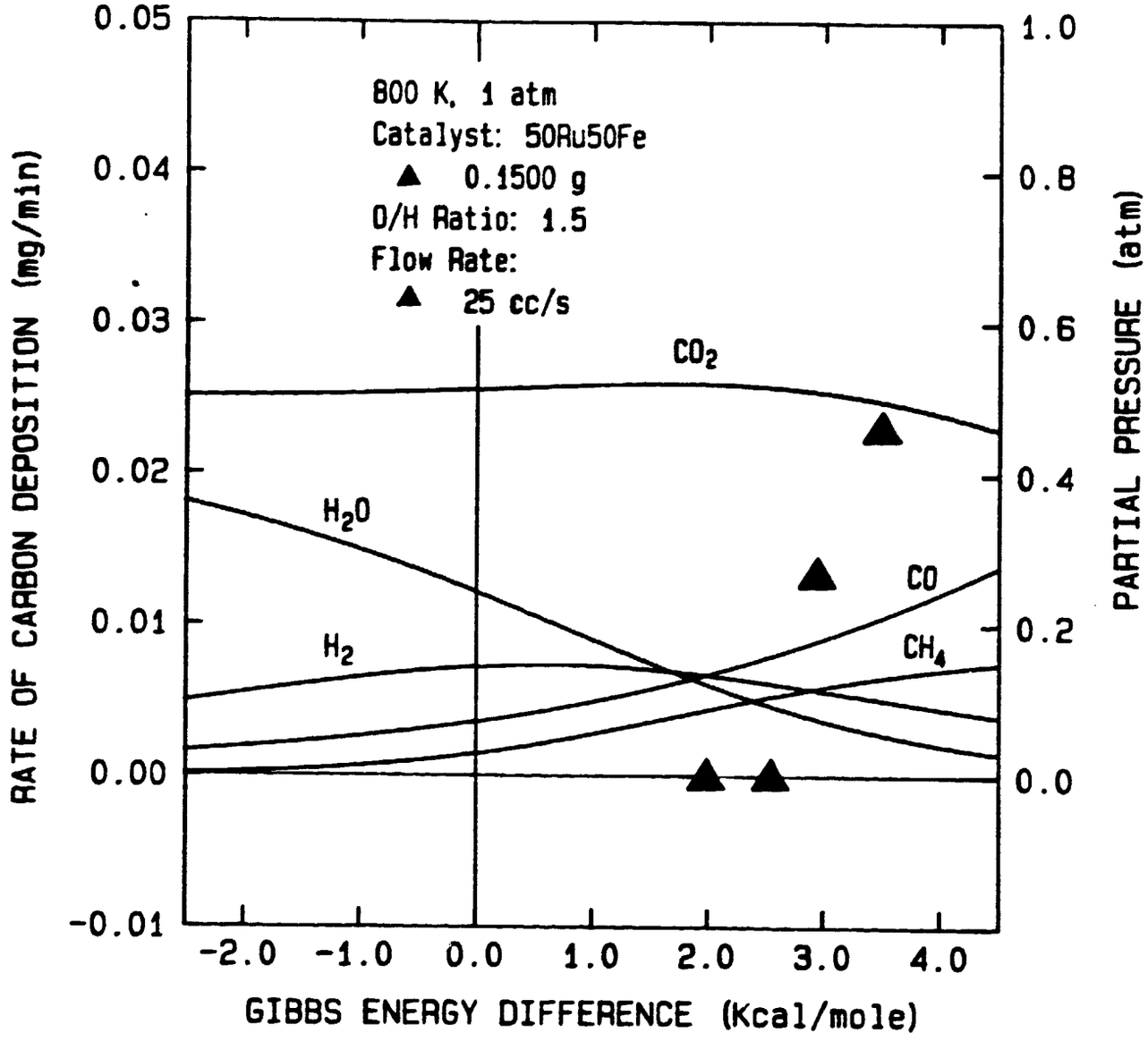


Figure 4.6 Rate of Carbon Deposition as a Function of $\Delta G_c$ for an O/H Ratio of 1.5

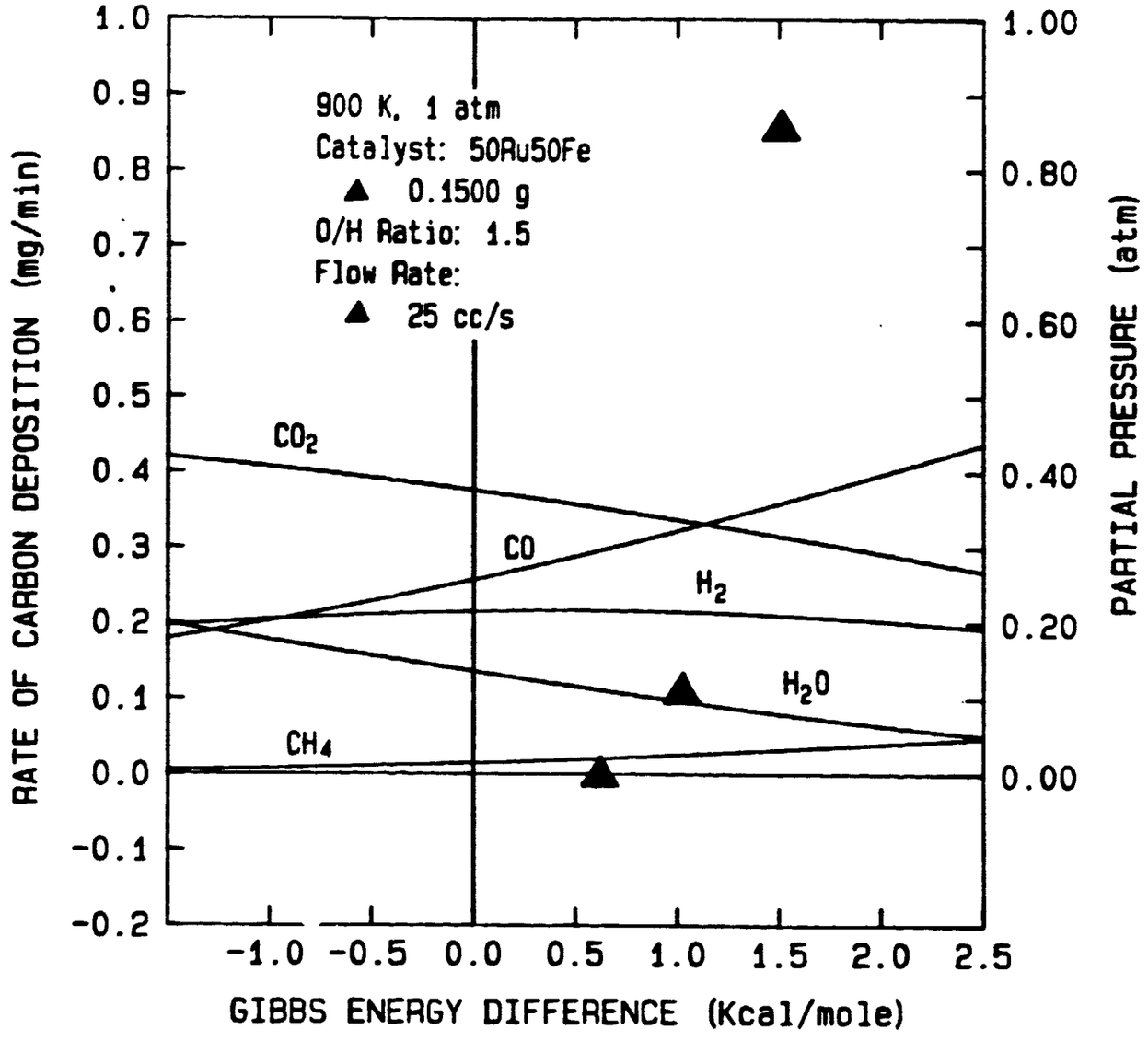


Figure 4.7 Rate of Carbon Deposition as a Function of $\Delta G_c$ for an O/H Ratio of 1.5

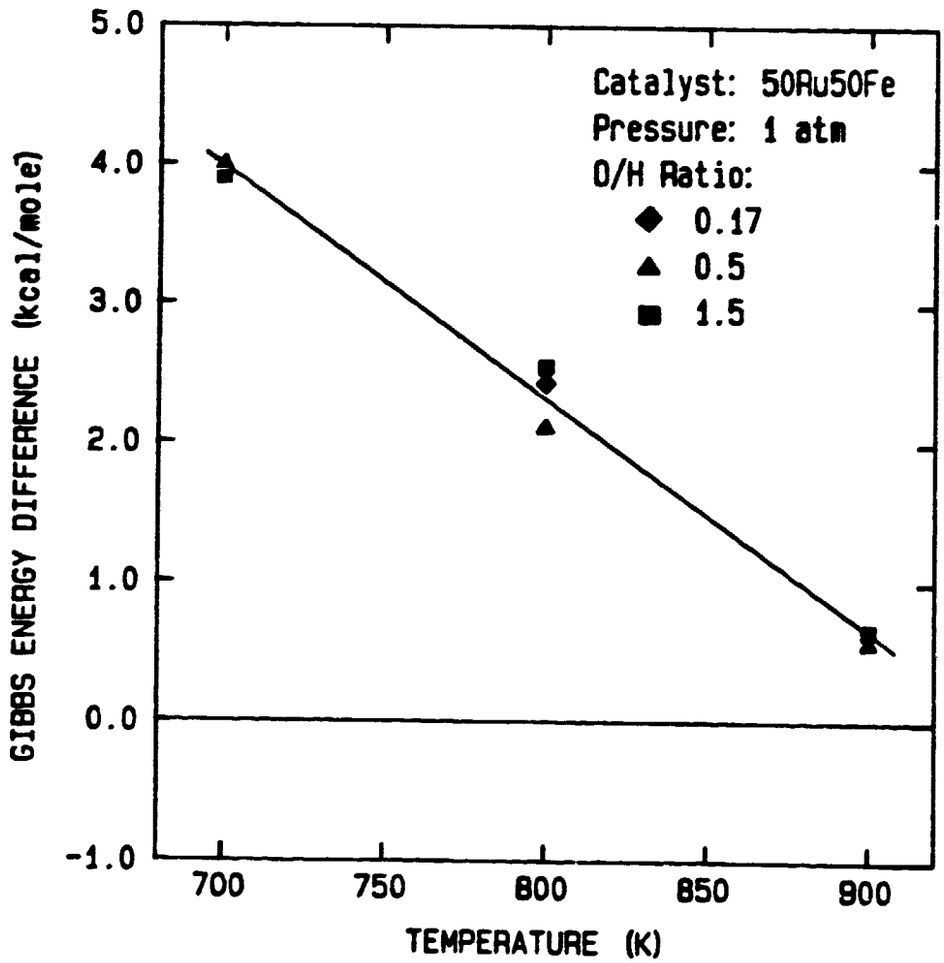


Figure 4.8 Rate of Carbon Deposition as a Function of $\Delta G_c$ for an O/H Ratio of 0.17

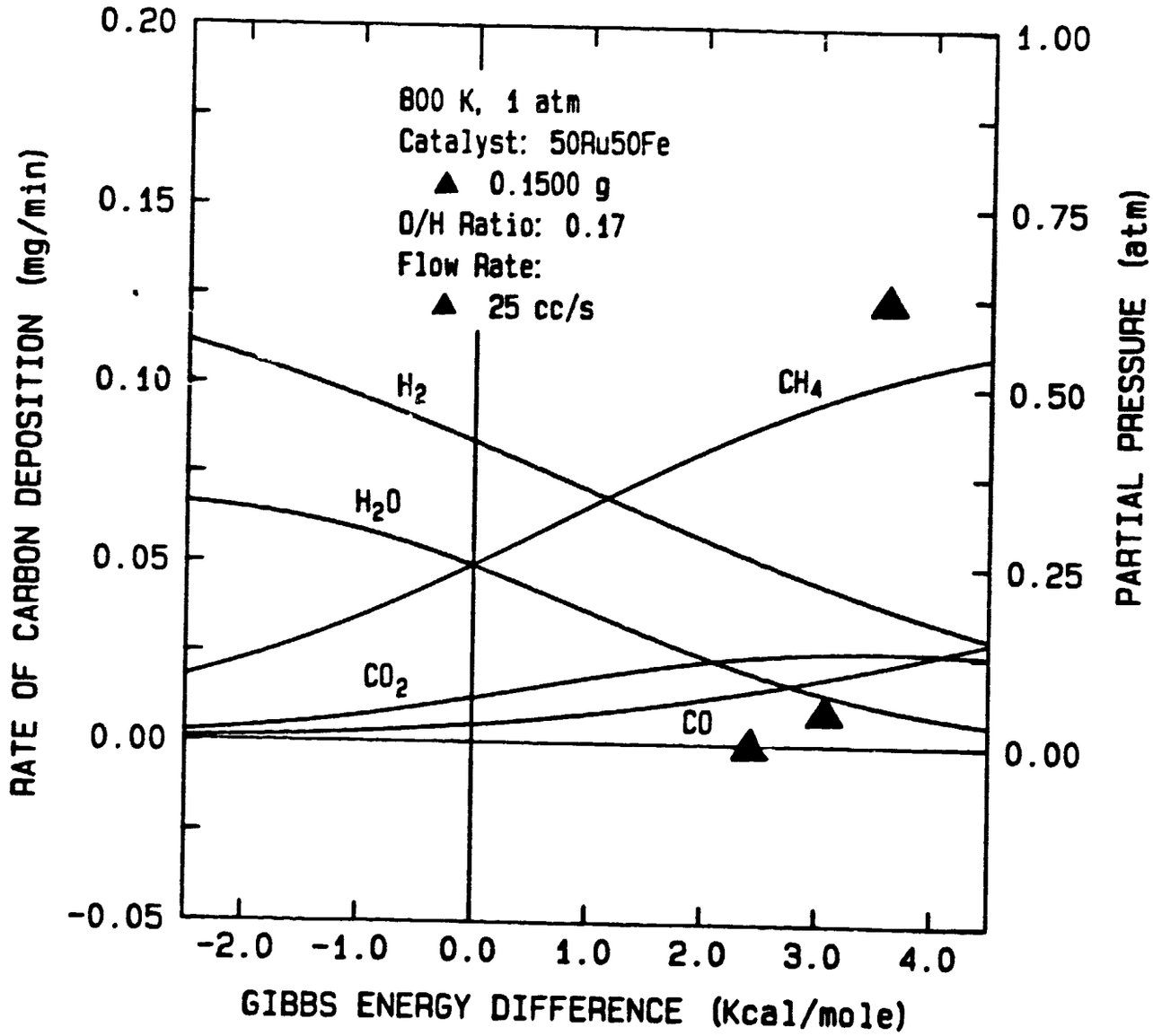


Figure 4.9 Carbon Deposition Boundary for Various O/H Ratios over 50Ru50Fe Catalyst

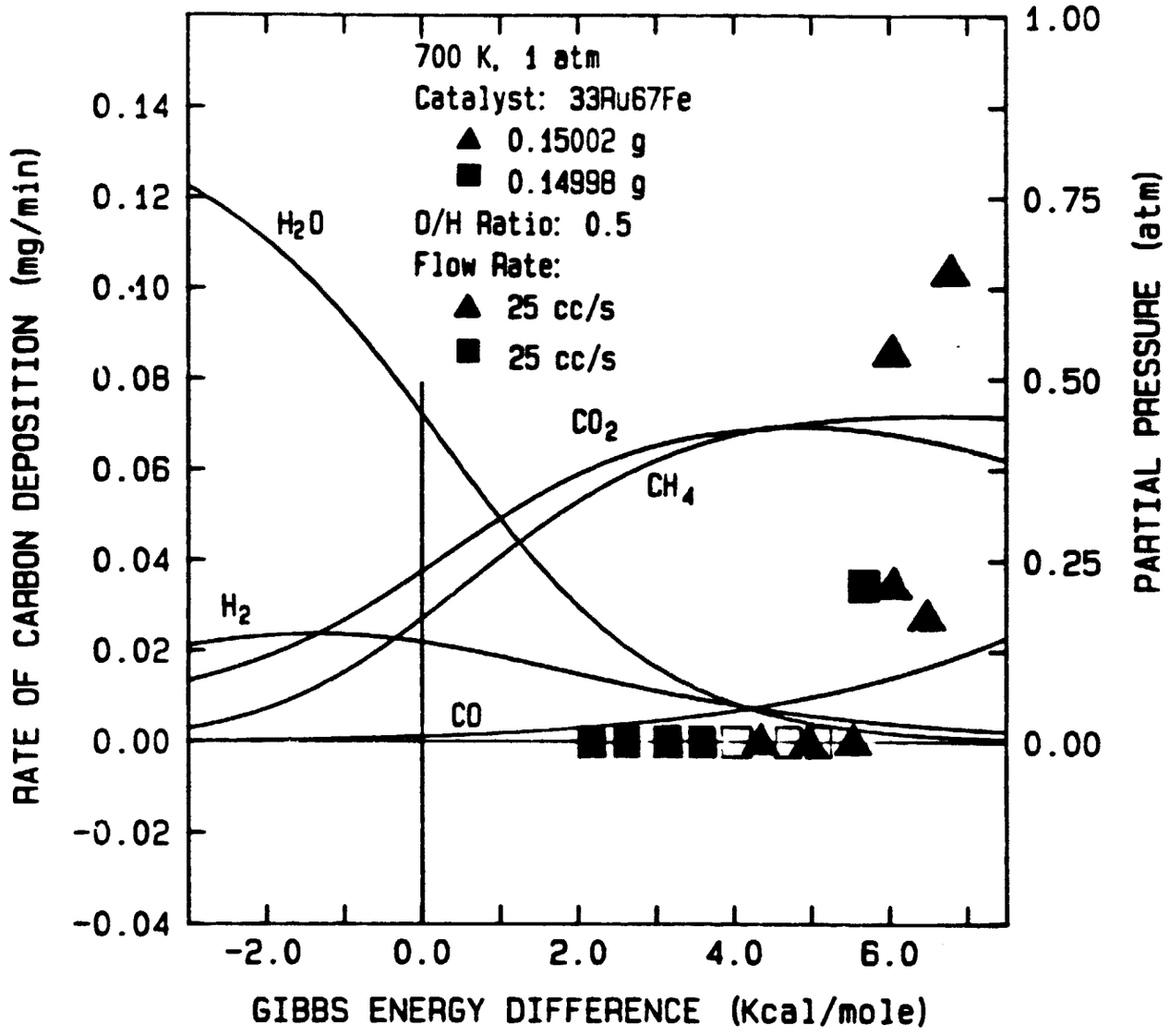


Figure 4.10 Rate of Carbon Deposition as a Function of $\Delta G_c$ for an O/H Ratio of 0.5

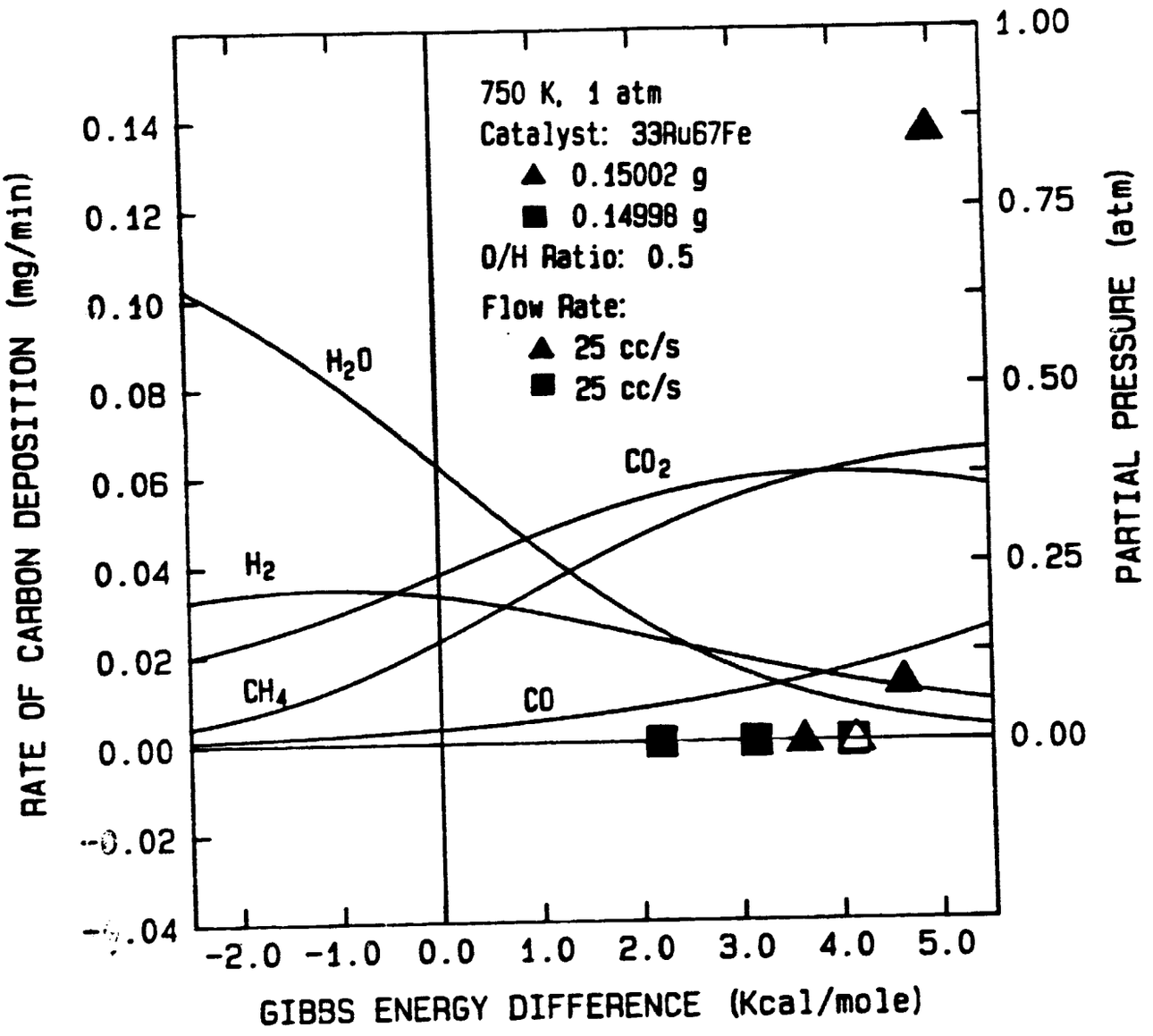


Figure 4.11 Rate of Carbon Deposition as a Function of $\Delta G_c$ for an O/H Ratio of 0.5

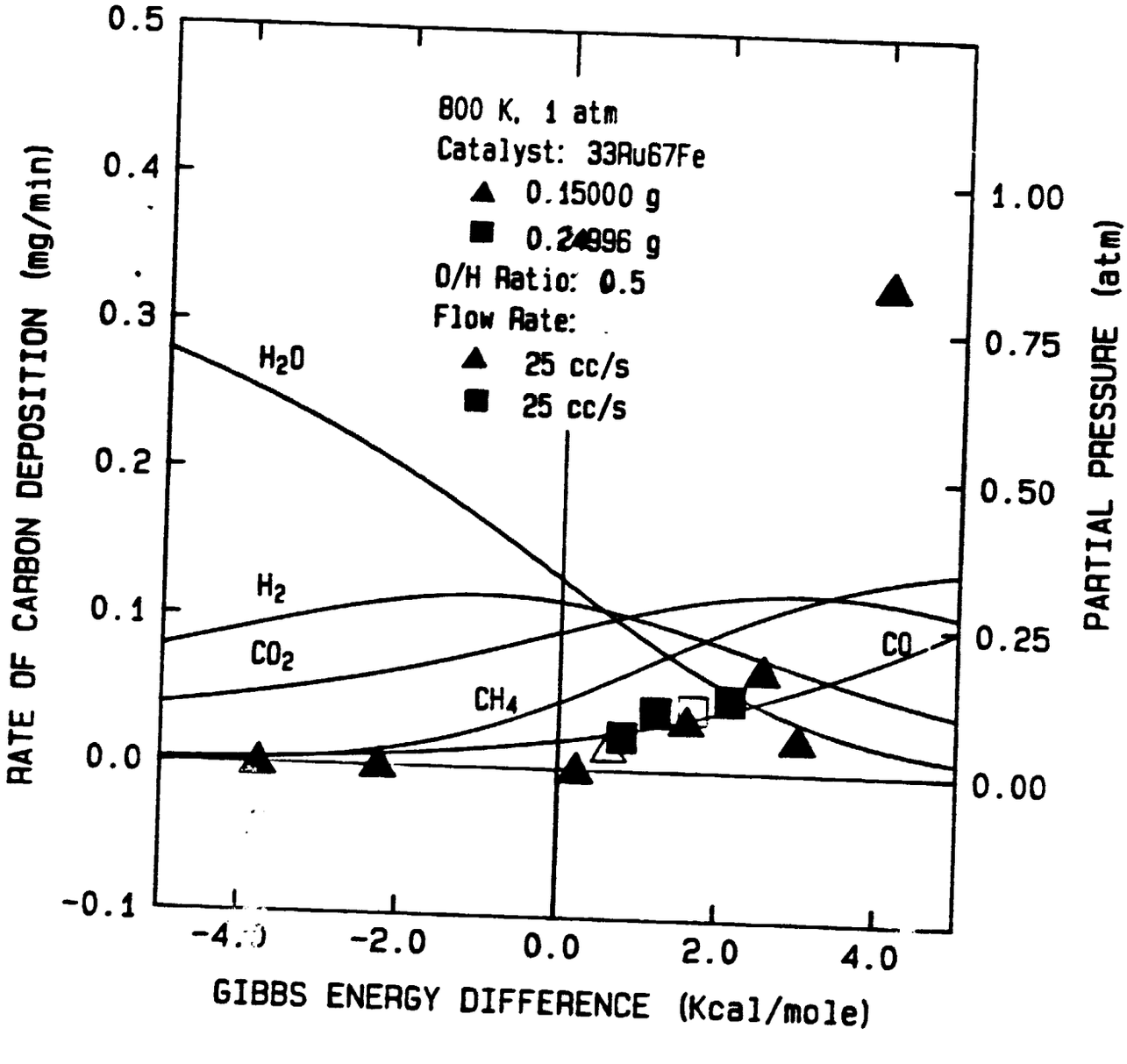


Figure 4.12 Rate of Carbon Deposition as a Function of $\Delta G_c$ for an O/H Ratio of 0.5

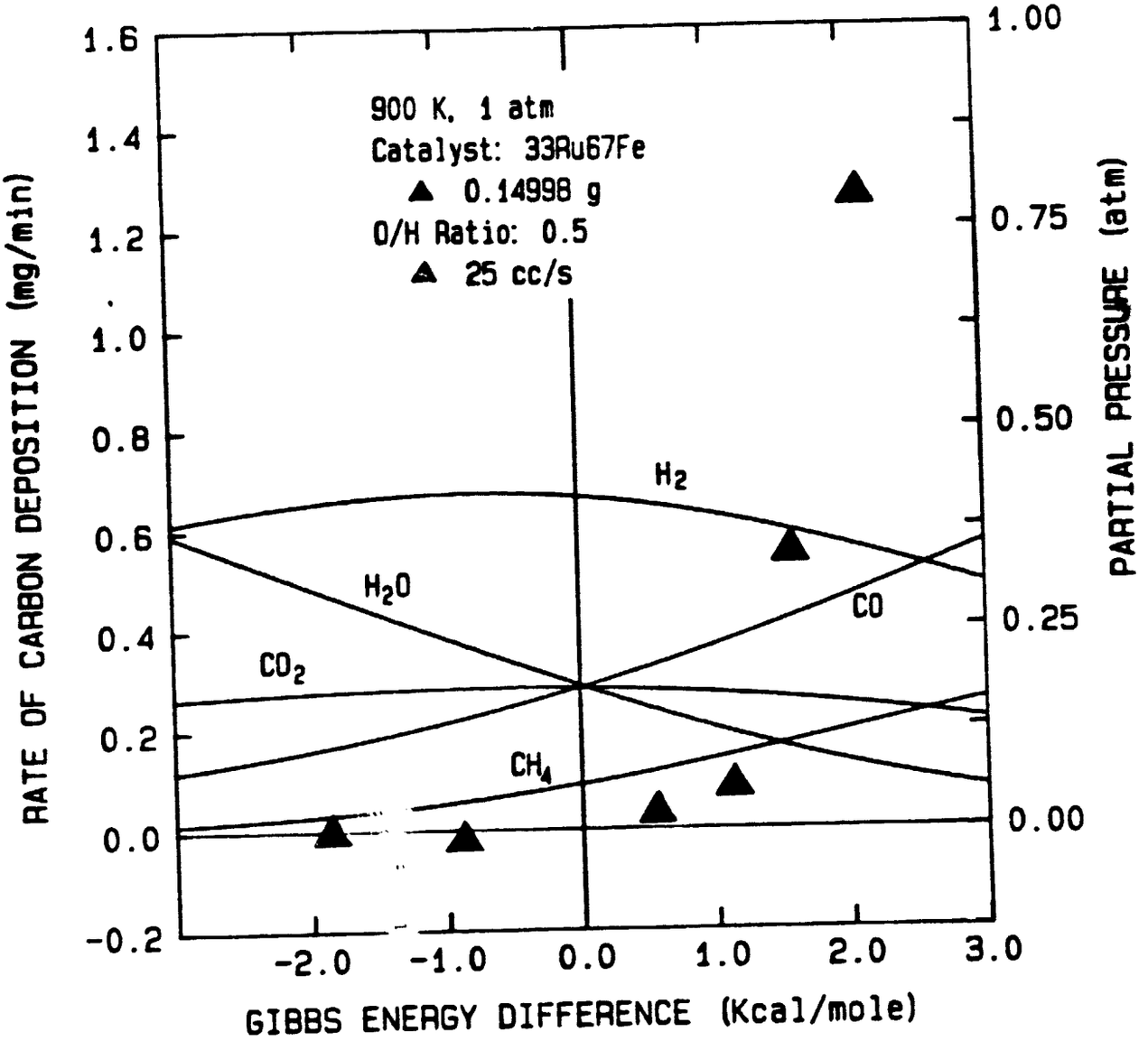


Figure 4.13 Rate of Carbon Deposition as a Function of $\Delta G_c$ for an O/H Ratio of 0.5

brium with β-graphite. However, at temperatures below 800K, the deviation from the graphite equilibrium was very pronounced. Specifically, carbon deposition stopped at the $\Delta G_c$ values of 4.1 and 5.5 kcal/mole for temperatures of 750 and and 700K, respectively. In addition, there existed a region where no carbon deposition nor removal occurred, a phenomenon similarly observed for the 50Ru50Fe catalyst

The determination of carbon deposition equilibrium boundary was also performed using gas mixtures with an O/H ratio of 1.5. The results are illustrated in Figures 4.14, 4.15 and 4.16 for temperatures of 700, 750 and 800K. Two important points can be made regarding these results. First, they confirmed the results obtained from Bosch equilibrium studies using an O/H ratio of 0.5. That is, gas equilibrium with graphite could be expected at high temperatures while carbon deposited at low temperatures appeared to have Gibbs energy higher than that of β-graphite. The second point is that, although the data obtained over the 33Ru67Fe catalyst were not as consistent as those in the 50Ru50Fe system, the carbon deposition boundary at a given temperature was again largely independent of gas mixtures. This is evidenced in Figure 4.17 which illustrates the value of $\Delta G_c$, where carbon deposition began, plotted as a function of temperatures for O/H ratios of 0.5 and 1.5. Table 4.1 tabulates the values of experimental $\Delta G_c$ at which carbon deposition began at various temperatures and O/H gas ratios for both 50Ru50Fe and 33Ru67Fe

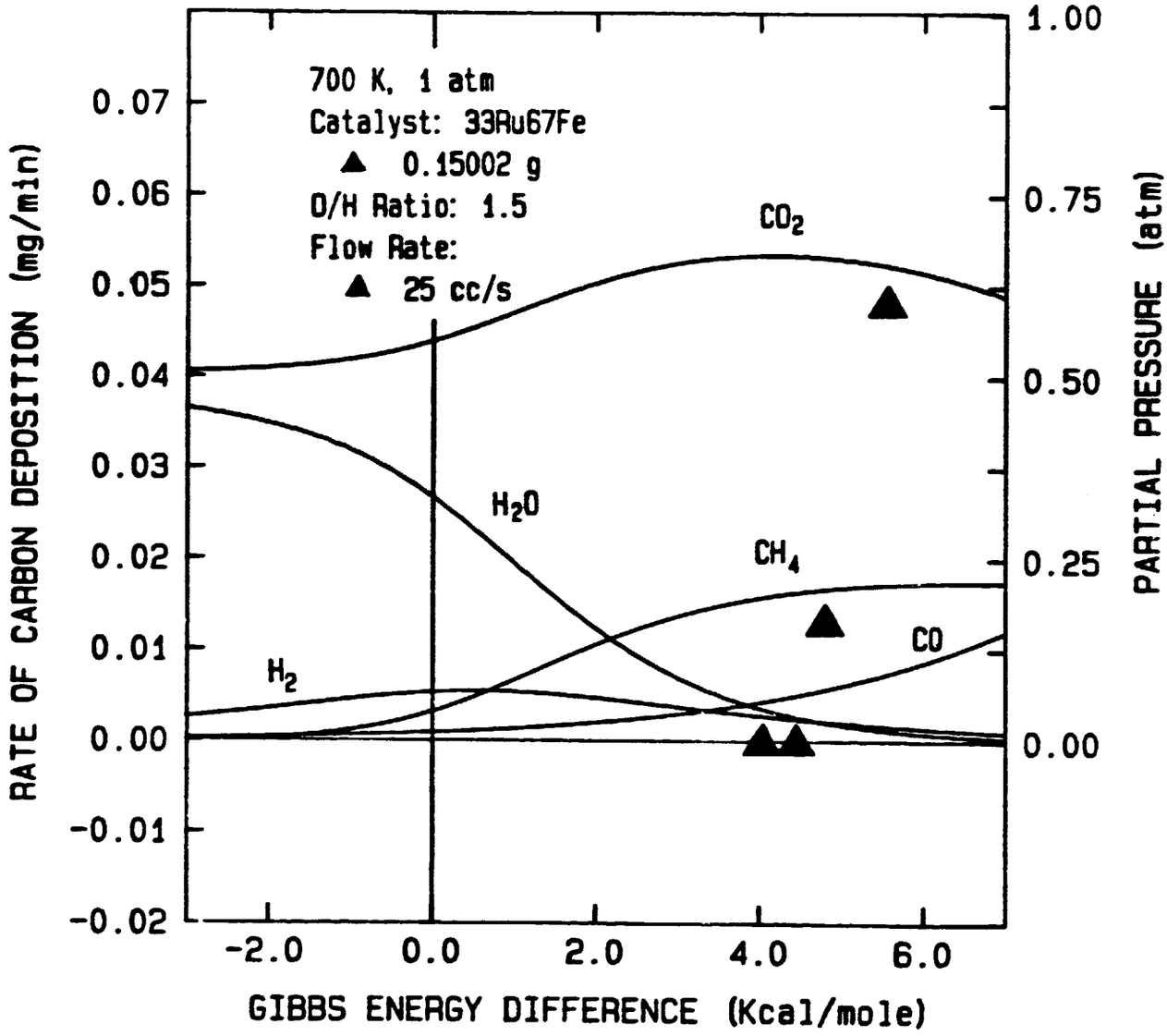


Figure 4.14 Rate of Carbon Deposition as a Function of $\Delta G_c$ for an O/H Ratio of 1.5

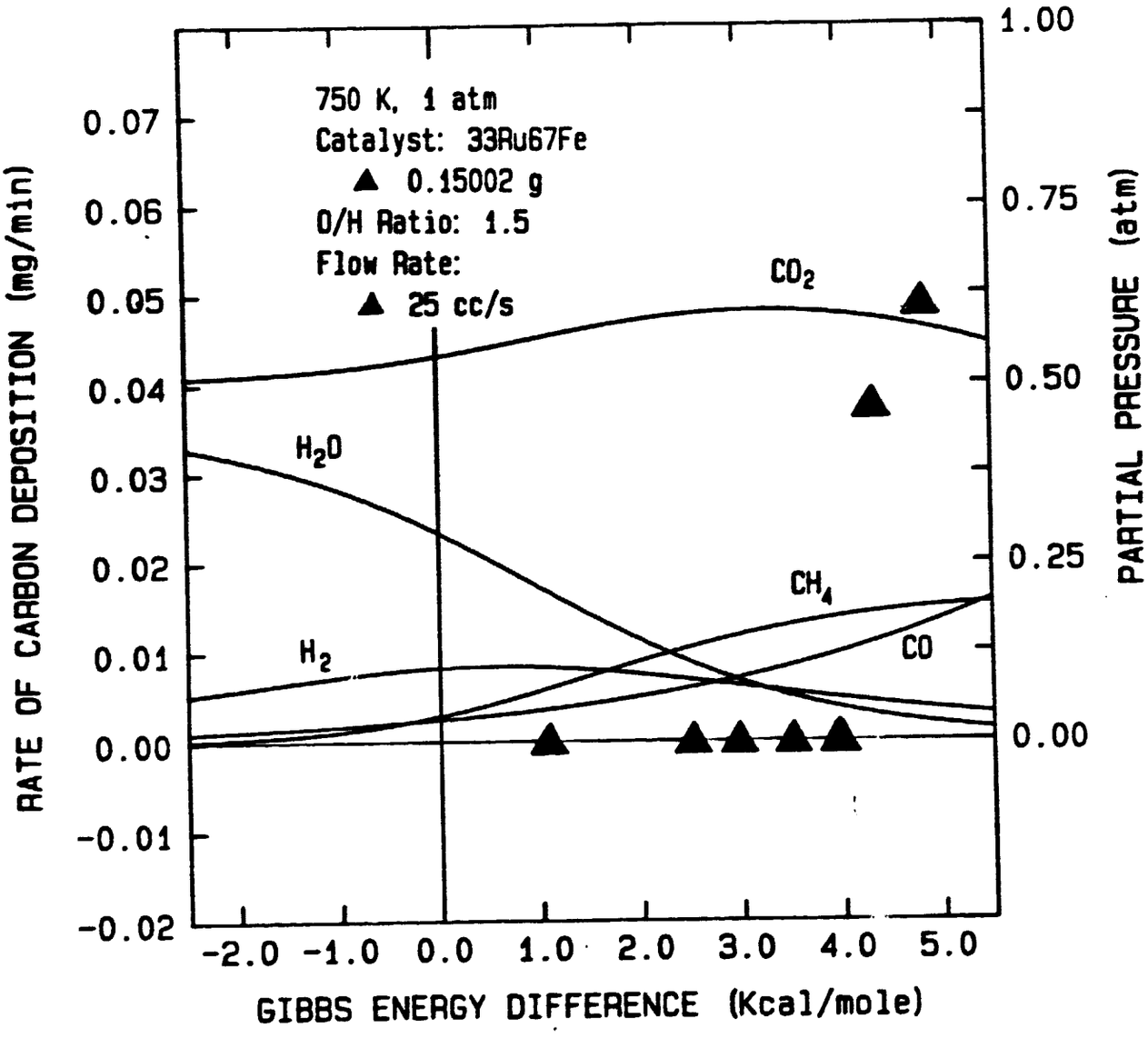


Figure 4.15 Rate of Carbon Deposition as a Function of $\Delta G_c$ for an O/H Ratio of 1.5

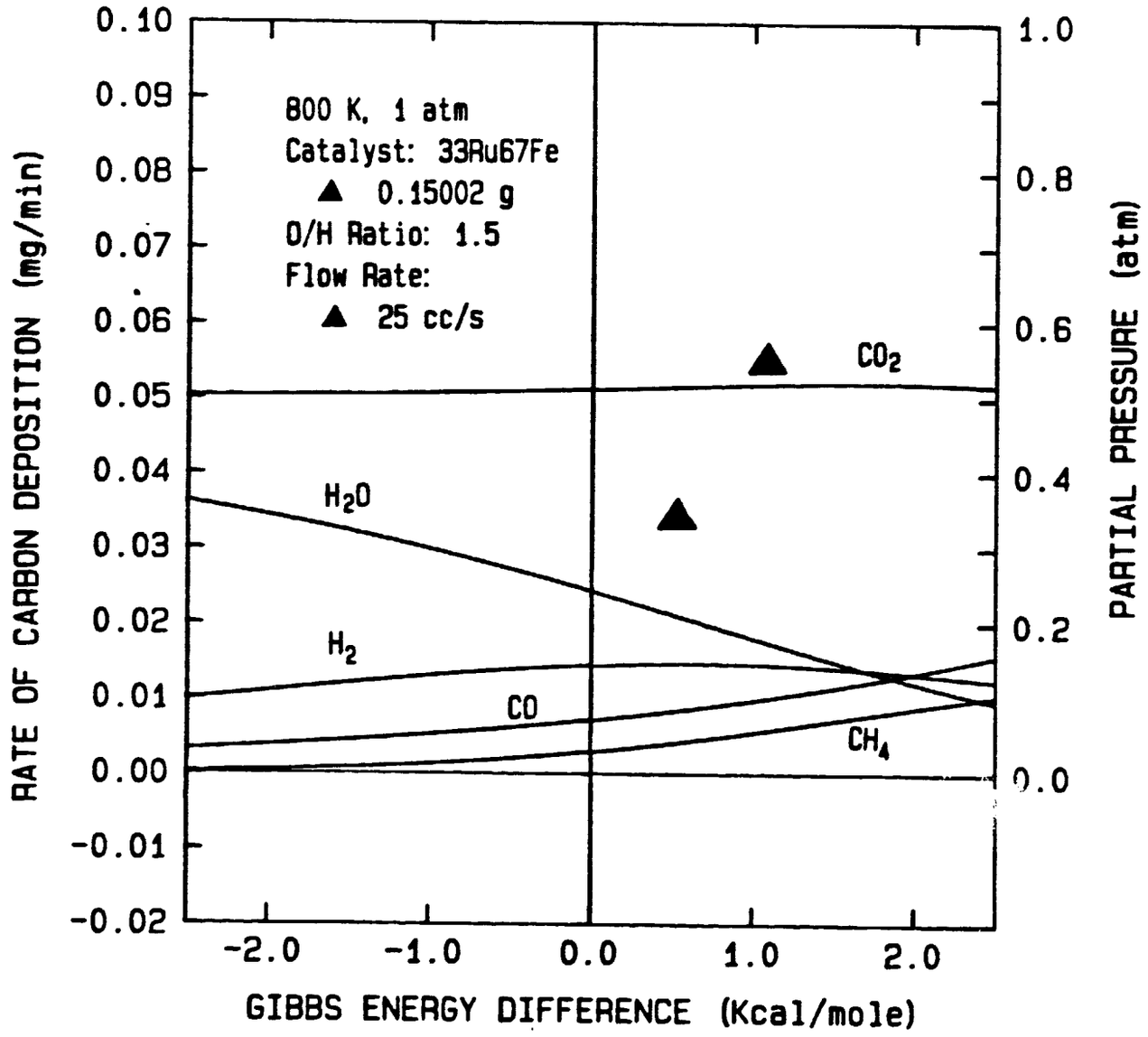


Figure 4.16 Rate of Carbon Deposition as a Function of $\Delta G_c$ for an O/H Ratio of 1.5

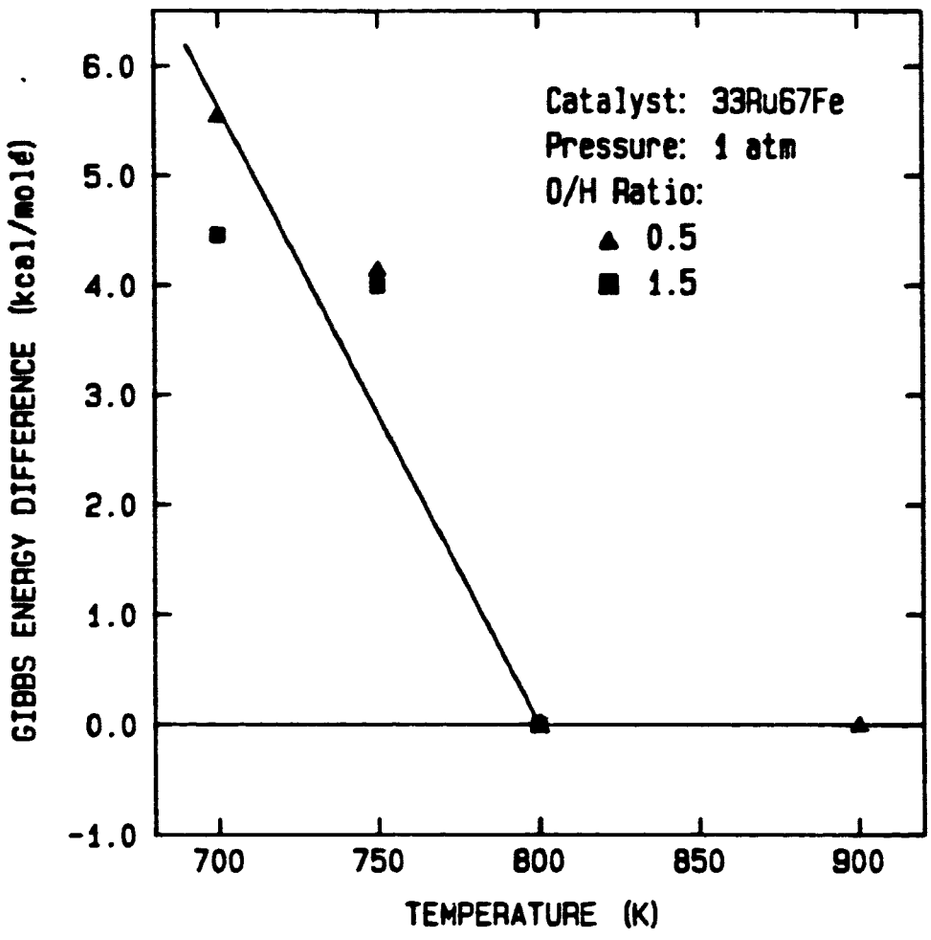


Figure 4.17 Carbon Deposition Boundary for O/H Ratios of 0.5 and 1.5 over 33Ru67Fe Catalyst

Table 4.1 $G_c$ as a Function of Temperatures and O/H Ratios for the 50Ru50Fe and 33Ru67Fe Systems

| Catalyst | Temperature (K) | O/H Ratio | $G_c$ (kcal/mole)[1] |
|---|---|---|---|
| 50Ru50Fe | 700 | 0.5 | 4.0 |
| | 800 | 0.5 | 2.2 |
| | 900 | 0.5 | 0.6 |
| | 700 | 1.5 | 3.9 |
| | 800 | 1.5 | 2.6 |
| | 900 | 1.5 | 0.6 |
| | 800 | 0.17 | 2.4 |
| 33Ru67Fe | 700 | 0.5 | 5.5 |
| | 750 | 0.5 | 4.1 |
| | 800 | 0.5 | 0.0 |
| | 900 | 0.5 | 0.0 |
| | 700 | 1.5 | 4.5 |
| | 750 | 1.5 | 4.0 |
| | 800 | 1.5 | 0.0 |

1. Experimental $\Delta G_c$ at which carbon deposition began.

catalysts.

Previous investigations by Manning (5), Sacco (7), and Garmirian (9) have shown cobalt to be the most effective Bosch catalyst among the three Group VIII metals investigated, namely iron, nickel and cobalt. For the cobalt system, gas equilibrium with ß-graphite can be attained for temperatures as low as 800K, below which deviation from the graphite equilibrium occurs. Equilibrium studies of the two unsupported ruthenium-iron alloys in this investigation indicate that while the 50Ru50Fe powder does not perform as well as cobalt, the 33Ru67Fe catalyst is as effective as cobalt for temperatures of 800K and above. At temperatures below 800K, however, deviation from the graphite equilibrium for the 33Ru67Fe system is more pronounced than that for the cobalt system.

## 4.2 Discussion

An attempt is made in this section to elucidate the behavior of ruthenium and its alloys with iron towards carbon deposition. Evidence from various sources is cited to support plausible explanations. However, further experimentation with appropriate equipment systems would be required to provide a definite substantiation.

Also presented at the end of this section is a preliminary investigation concerning the production of low molecular

weight olefins over supported ruthenium-iron alloy catalysts. This study was carried out with an anticipation that, if high production of ethylene and propylene could be achieved, an understanding of the kinetics involved in the synthesis would be beneficial for the application of a Ru-Fe catalyst in the Bosch process.

### 4.2.1 Ruthenium

As presented in Section 4.1.1, no carbon deposition on unsupported ruthenium was observed by weight measurement in this study. The result was quite different from what had originally been anticipated. As previously mentioned, favorable factors of ruthenium as a potential Bosch catalyst include the fact that the interference of ruthenium oxide formation would not occur under Bosch operating conditions. In addition, because of the very limited stability of ruthenium carbides, if they exist, carbon deposition on ruthenium would not be limited by the carbide formation, as has been the case for the nickel and cobalt systems. Furthermore, Eckerdt and Bell (26) have reported that a carbon reservoir equivalent to several monolayers was maintained on silica-supported ruthenium at 673K. CO dissociation has also been observed on alumina-supported ruthenium (25).

Results from a number of investigations have pointed to an important aspect. That is, supported and unsupported ruthenium catalysts behave differently. The support has been

suggested to alter the catalytic behavior of ruthenium through both electronic and dispersion effects (34). While CO disproportionation and carbon deposition have been shown to occur on supported ruthenium, this is not necessarily the case for the unsupported metal. Low and Bell (25), in their studies of CO desorption and reaction with $H_2$ on alumina-supported Ru, alluded to the fact that no evidence for CO dissociation had been observed on Ru single crystals, even with the high surface coverage of CO. An investigation by Delgass et al. (35,36) using x-ray photoelectron spectroscopy for surface analysis showed that less than 0.25 monolayer of carbon, if at all, was detected on the surface of unsupported Ru powder after 24 hours of Fischer-Tropsch synthesis at 573K and with a $H_2/CO$ (3:1) gas mixture. They postulated that no carbon accumulated as a result of the rich supply of adsorbed hydrogen on the ruthenium surface. Their reasoning is supported by a study at low temperatures (313-427K), in which ruthenium has been reported to have high capacity for $H_2$ adsorption in the presence of CO (32). Catalytic decomposition of carbon monoxide on single crystalline ruthenium has been studied at 823K (24); although graphite was observed, it was noted that the rate of carbon deposition was very slow.

### 4.2.2 Ruthenium-Iron Alloys

Figures 4.9 and 4.17 presented in Section 4.1.2 summarize the experimental results of equilibrium studies performed

on 50Ru50Fe and 33Ru67Fe catalysts. The results indicate that the high water concentration expected from the gas-graphite equilibrium consideration cannot be achieved in the 50Ru50Fe system at temperatures of 900K and below or in the 33Ru67Fe system at temperatures under 800K. Based upon the previous studies on the Bosch process, two possibilities are suggested to account for the low water yield. One is that some type of carbon, structurally or chemically different from β-graphite, is in equilibrium with the gas-phase composition. The other is that oxidation of the catalyst occurs and inhibits further carbon deposition, as is the case for the pure iron system.

Surface studies of unsupported Ru-Fe alloy powders have been reported in the literature (37,38). Of interest is the investigation by Ott et al. (37), employing a combination of x-ray photoelectron spectroscopy (XPS) and secondary ion mass spectroscopy (SIMS) for the study of their Ru-Fe alloy samples. The powders were reduced in $H_2$ at 573K and then passivated by exposure to 0.1-0.5 Torr of ultra-high purity of oxygen. The results of their analyses showed that the passivated surface of their samples was a Ru-Fe phase partially covered by islands of pure iron oxide. No ruthenium oxides were detected.

Their study raises the possibility of the formation of iron oxide patches on the surface of the 50Ru50Fe catalyst in this Bosch investigation. This oxide formation might, at least partially, contribute to the inhibition of further

carbon deposition. This possibility, however, is unlikely in the light of experimental results on the 33Ru67Fe catalyst at 800 and 900K for which the carbon deposition boundary appeared to coincide with that of gas-graphite equilibria. If the iron oxidation in the 50Ru50Fe catalyst did occur and were to account for the discrepancy between the carbon deposition boundaries experimentally observed and the gas-graphite equilibria, the difference should have been even more pronounced with the increase in iron content in the 33Ru67Fe system. The opposite phenomenon was observed.

Furthermore, in a subsequent study of properties of Ru-Fe alloys, Ott et al. (14) reported that the unsupported Ru-Fe samples were completely reduced under hydrogen treatment at 673K and 1 atm for 4 hours, as evidenced from XPS analysis. In a review paper on structure and catalytic properties of iron-containing bimetallic catalysts, Guczi (39) has indicated that the reduction of iron can be facilitated by introducing a second metal, such as Pt or Pd, which is highly active on hydrogenation. This phenomenon has generally been observed in the ruthenium-iron system as well. Using Mössbauer spectroscopy, Vannice et al. (40) showed that $Fe/SiO_2$ catalysts with low iron loading (~0.1 wt%) could not be reduced below the $Fe^{2+}$ state even after reduction in hydrogen at 773K. However, the addition of ruthenium to $Fe/SiO_2$ samples -- for example, 0.1 wt% Fe, 5 wt% Ru on silica support -- led to the reduction of iron from $Fe^{3+}$ to $Fe^{2+}$ upon exposure to hydrogen

even at room temperature (27). Vannice et al. (27) further reported that the supported catalyst was completely reduced at 773K and that Ru-Fe bimetallic clusters were observed by Mossbauer spectroscopy. Additionally, Good et al. (38) affirmed a complete iron reduction of an unsupported Ru-Fe sample, which was prepared from the chlorides of iron and ruthenium ($FeCl_3 \cdot xH_2O$ and $RuCl_3 \cdot 3H_2O$) and treated with hydrogen at 673K; a Mossbauer peak observed was attributed to iron in the form of a Ru-Fe alloy.

Ruthenium and iron show contrasting behaviors in their interactions with carbon. Ruthenium carbides have been reported to be unstable or of very limited stability (13). As reviewed by Shunk (23), although the observation of ruthenium carbide, RuC, was reported by one investigator, the existence could not be substantiated in two other studies. Furthermore, the solubility of carbon in ruthenium has been shown to be very small (23). On the other hand, as a result of high binding energy between carbon and iron, carbonaceous deposits are normally produced on an iron surface during the transformation of carbon-containing substances. Various iron carbides, including $Fe_2C$ and $Fe_3C$, have been widely reported in the literature (23,41,42). In addition, while CO dissociation occurs to a large degree on Fe, adsorption of $H_2$ takes place to a much lesser extent on iron than on ruthenium. Consequently, it would be expected that the tendency toward carbon deposition would rise with increasing iron content in

the Ru-Fe alloys.

In their studies of catalytic behaviors of ruthenium, iron and their alloys at 573-673K for Fischer-Tropsch synthesis, Ott et al. (14,23) and Fleisch et al. (24) carried out surface analyses of their catalyst samples using XPS and SIMS. No carbon deposition was observed on ruthenium nor on the 97Ru3Fe alloy. This phenomenon was likely a result of the large hydrogen coverage on ruthenium. Thus, hydrogen atoms were available for hydrogenation of surface carbon residues resulting from dissociative adsorption of carbon-containing species. On the other hand, with an increase in the iron content, the alloys of 75Ru25Fe and 33Ru67Fe showed a rapid carbon buildup during Fischer-Tropsch synthesis. For the case of a pure iron catalyst, a carbide formation was first noted, followed by the subsequent buildup of a carbon overlayer on top of the carbide phase. The formation rate of carbon overlayer on the pure iron catalyst was much slower than on the 75Ru25Fe and 33Ru67Fe samples. The carbon deposition rates on the two alloys were also shown to be a strong temperature dependence. Additionally, carbon deposition stopped after a certain amount of carbon had accumulated. From surface analyses and kinetic studies, Ott et al. and Fleisch et al. suggested that the buildup of carbon was nonuniform on the surface and that a fraction of metal sites remained essentially uncontaminated. High Fe surface enrichment of the Ru-Fe alloys was also reported.

An interesting observation has been made by Ekerdt and Bell (26) in their study of hydrocarbon synthesis from CO and $H_2$ over silica-supported Ru. They reported that although the catalyst maintained a reservoir of carbon equivalent to several Ru monolayers in magnitude, the surface coverage by chemisorbed CO was not affected by the accumulation of carbon. The phenomenon suggested that only a small fraction of the total carbon was present on the ruthenium surface. Ekerdt and Bell pointed to the possibility that the carbon might be present on the catalyst support or in filaments extending from the Ru surface. This speculation was not too dissimilar to the one made by Ott et al. (35) and Fleisch et al. (36). As mentioned previously, they pointed out that even though carbon equivalent to 20-30 layers had been deposited on the unsupported Ru-Fe alloys, the deposited carbon did not cover uniformly the entire surface of the catalyst. Some of the alloy surfaces were still accessible to catalyze further reactions.

The phenomena observed in this Bosch investigation can perhaps be explained in the light of the studies mentioned above. No detectable carbon deposition on the pure ruthenium catalyst reflects the characteristics of unsupported ruthenium. However, with the addition of iron to form Ru-Fe alloys, carbon deposition occurs, as has been the case for 50Ru50Fe and 33Ru67Fe. There are two hypotheses as to why carbon deposition is enhanced. One is that the introduction

of iron to ruthenium changes the electronic properties of the surface such that carbon deposition is promoted. The other is that the iron provides favored sites for the carbon to deposit; some of the carbon might be incorporated into the bulk alloy.

The enhancement of carbon deposition increases with the rise in iron content. This can be observed from the fact that while carbon deposition on the 50Ru50Fe system ceases upon reaching certain values of $\Delta G_c$, the carbon deposition equilibrium boundary in the 33Ru67Fe system approaches that of gas-graphite equilibria at 800 and 900K. However, for temperatures below 800K, the gas-graphite equilibria cannot be attained over the 33Ru67Fe catalyst, and this deviation from the desired equilibria is even more pronounced than in the 50Ru50Fe system. Left unanswered in this study is an understanding of reaction mechanisms and Ru/Fe surface interactions involved in the carbon deposition process. What limits the alloy system from approaching the gas-graphite equilibrium? Is experimental carbon formed structurally or chemically different from β-graphite?

### 4.2.3 Preliminary Study on the Synthesis of Lower Olefins[1]

An unusually high selectivity of unsupported ruthenium-iron catalysts toward ethylene and propylene has been reported in an investigation of Fischer-Tropsch synthesis by Ott *et al.* (14), as presented previously in Section 2.3.2. Their experimental data were obtained in a fixed bed reactor system operated at conversions below 3%. Of interest in this study is an understanding of kinetic effects on the production of low molecular weight olefins over alloy catalysts at various degrees of conversion. If high yields of olefinic species could actually be obtained at high conversions, such a knowledge of the kinetics involved would certainly be valuable, as it could lead to an overall improvement in the Bosch process. Specifically if ethylene and propylene could be produced at high levels, the benefits would be derived as a result of both the enhanced carbon deposition from a gas phase containing high olefin content and the low reaction temperatures used in the hydrocarbon synthesis. Highlights of this preliminary study (43,44) are presented below.

A representation of the experimental apparatus is shown in Figure 4.18. Originally used in the kinetic study of

1. Credit should be given to D. M. Borowski, B. R. Moroney, E. D. Morris, B. A. Sackett and J. C. Willard for experimental results presented in this section.

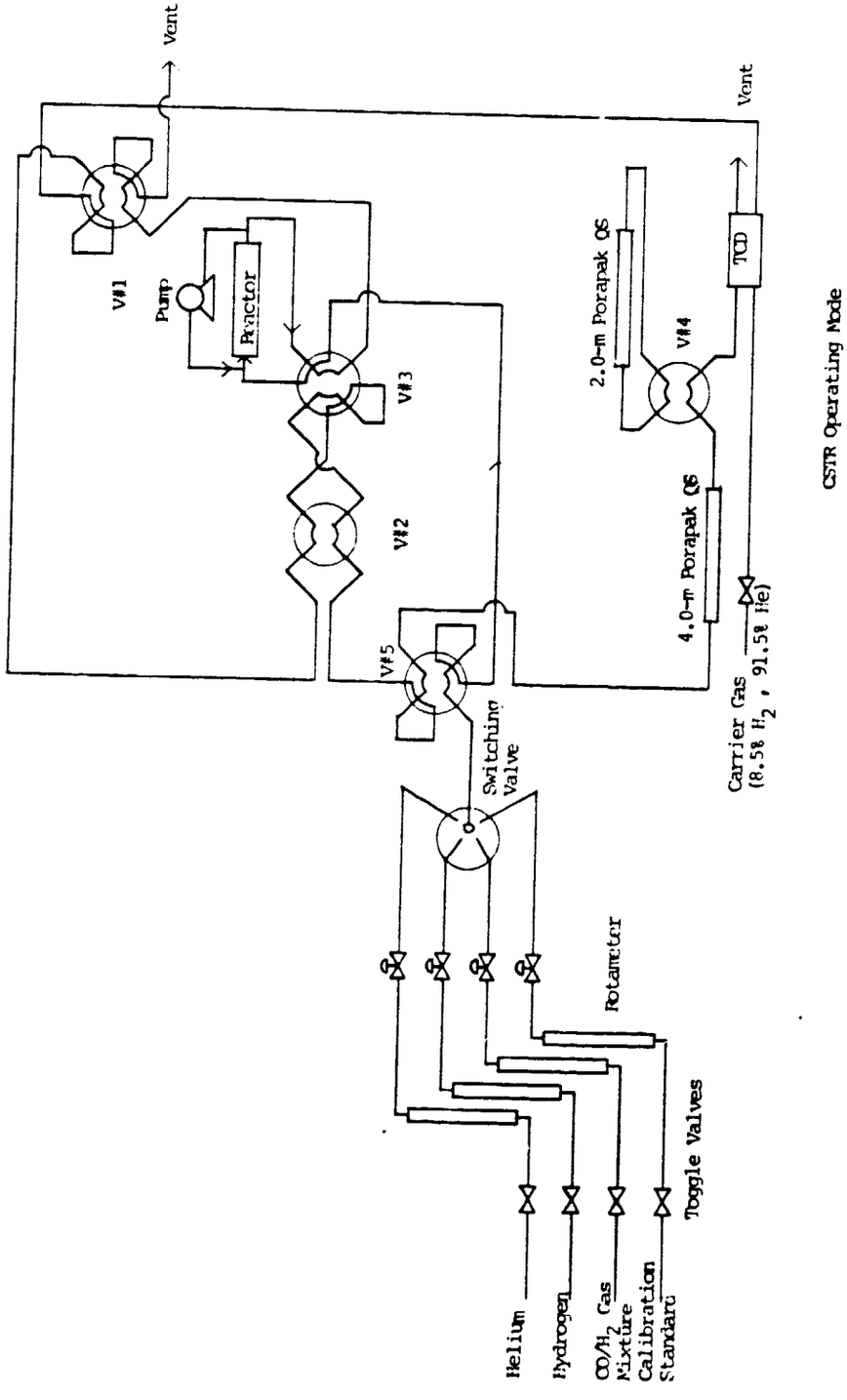


Figure 4.18 Schematic Diagram of Experimental System (CSTR Mode)

ethylene oxidation by Mahan (45), the equipment was modified and composed of three basic section: the gas feed system, the reactor, and the gas analytical system. The gas feed system included four tube rotameters equipped with mass flow regulators for the control of gas flow rates. An eight-position switching valve allowed the flow of desired gas to pass to the reactor system. Housed in a heated metal block equipped with a temperature controlling system, the reactor was made of a 1/4-inch glass-lined stainless steel tube 8 cm long. The catalyst was held in place between plugs of Pyrex wool inside the reactor. A recycle pump allowed the reactor to be operated as a CSTR. The pump could be removed from the loop and valves adjusted to form a single plug flow reactor. Through the switching of micro-volume sample valves V#5 and V#1, inlet and outlet gas samples, respectively, were introduced into the gas analytical system, which consisted of two columns of Porapak QS and a thermal conductivity detector. The gas components were separated in the following sequence: $H_2$, CO, $CH_4$, $CO_2$, $C_2H_4$, $C_2H_6$, $C_3H_6$, $C_3H_8$, and higher hydrocarbons. A pneumatic switching valve allowed the 2-m Porapak QS column to be bypassed after $CO_2$ had evolved so as to shorten the analysis time for the remaining components. A gas mixture of 91.5% He and 8.5% $H_2$ was used as a gas carrier, and the signals from the thermal conductivity detector were integrated by a Spectra Physics Minigrator. Because of the broad peak and its interference with other gas peaks, the water component was not

integrated.

Two types of catalysts were prepared by an incipient wetness technique. One type of the catalyst was a 50Ru50Fe (atomic Ru:Fe = 1:1) alloy supported on γ-alumina (20-40 mesh), having a metal loading of ~10 wt%; the other was a 97Ru3Fe (atomic Ru:Fe = 97:3) catalyst supported on 40-60 mesh γ-alumina with a 5 wt% metal loading. An aqueous metal chloride ($RuCl_3/FeCl_2$) solution of desired Ru/Fe composition and of known volume was added dropwise to the support with constant mixing so as to ensure that the solution would all be uniformly absorbed on γ-alumina. The impregnated support was air dried before being reduced in an aqueous solution of sodium borohydride. The reduced catalyst was then washed several times with distilled water, air dried and subsequently treated overnight at 773K under a hydrogen atmosphere, to remove traces of the chlorides and to presinter the catalyst before use. Determined by the BET/$N_2$ method using a Quantasorb sorption system, surface areas of the activated samples were 49.0 and 96.9 $m^2/g$ for the supported 50Ru50Fe and 97Ru3Fe, respectively.

Experiments to determine the merits of alumina-supported 50Ru50Fe and 97Ru3Fe alloys as catalysts for the synthesis of lower olefins were performed by Borowski *et al.* (43) in a recycle reactor modeled as a CSTR. Tests were done at 473, 523 and 573K with feed mixtures having the $H_2/CO$ ratio of 3:1, 2:1 and 1:1. Heat and mass transfer limitations

were shown to be negligible. Used catalysts were regenerated in hydrogen at 723K for 3 hours, and reproducible results were obtained. This is in agreement with the observation made by Ott et al. (35), who reported the restoration of the synthesis activity upon the treatment of unsupported 75Ru25Fe in hydrogen at 683K.

#### 4.2.3.1 50Ru50Fe Supported Catalyst

In their initial investigation of the supported 50Ru50Fe catalyst with CO conversions ranging from 13% to 0.4%, Borowski and coworkers reported no production of olefins and substantial deactivation of the catalyst over time. Methane was the major, and in many cases the only, hydrocarbon product. A trace of ethane was observed in some experimental runs. $CO_2$ and $H_2O$ were also formed. An example of the product distribution obtained for the 50Ru50Fe catalyst is presented in Figure 4.19. Figure 4.20 illustrates the characteristic deactivations of the catalyst, which was observed for $CH_4$ and $CO_2$ in all of the runs. The drop in catalytic activity was sharp initially and leveled off over a period of time. Borowski et al. noted that similar trends probably existed for any undetectable hydrocarbons, as, for instance, a trace of ethane was detected initially in some runs but unobserved at a later stage with increasing catalyst deactivation.

The results obtained by Borowski et al. (43) are not

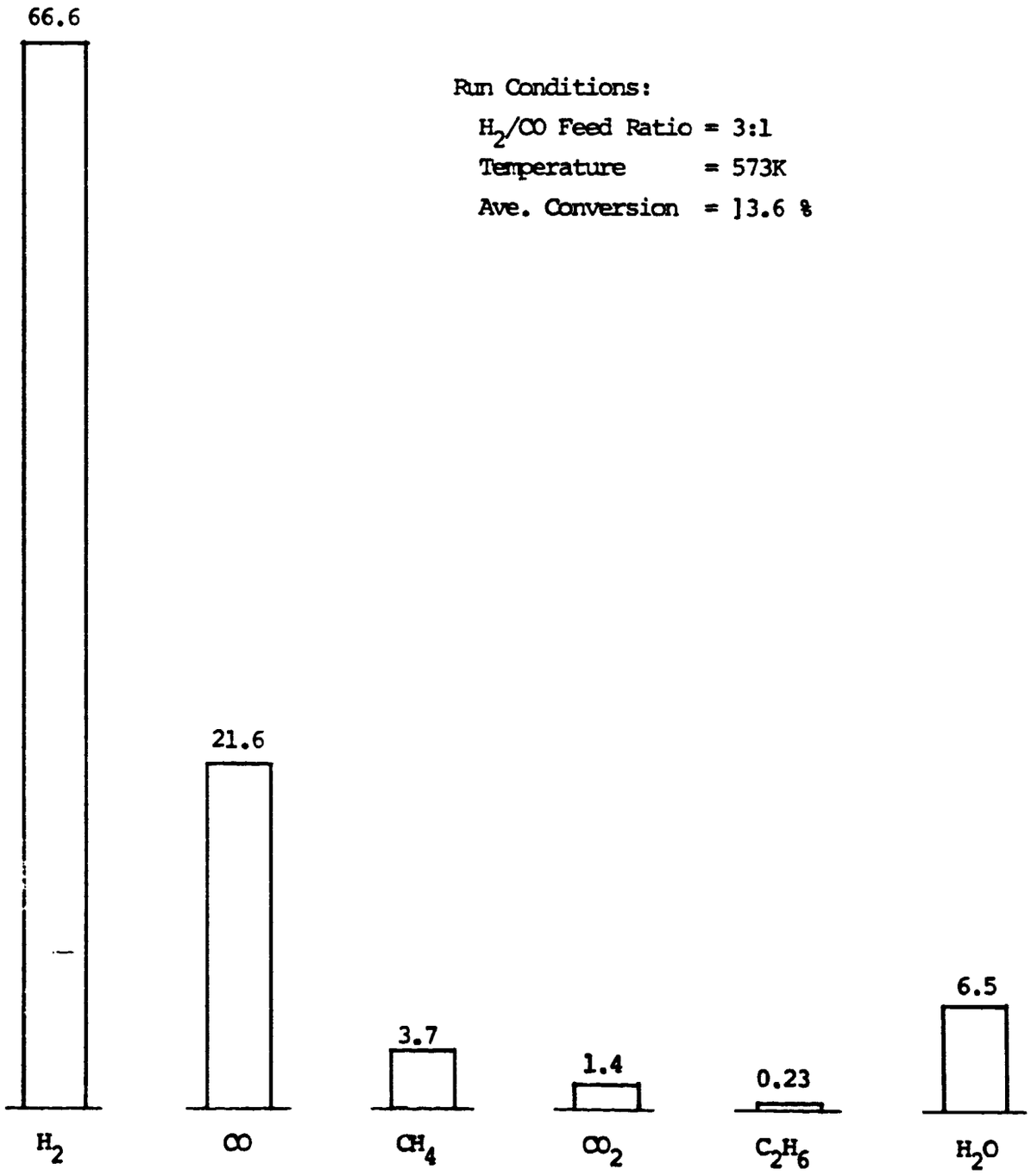


Figure 4.19 Product Distribution for 50Ru50Fe Catalyst (43)

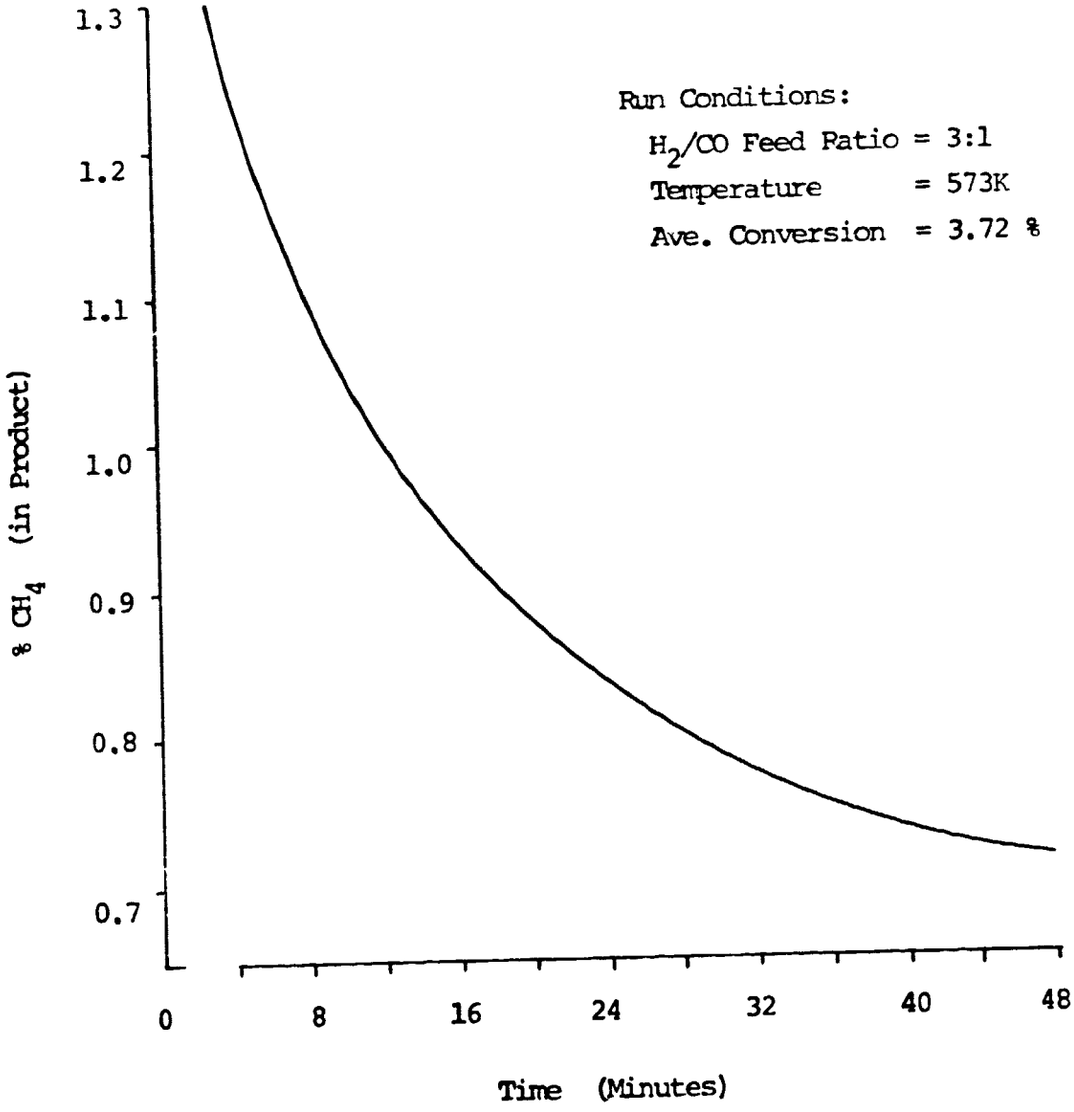


Figure 4.20 Catalyst Deactivation for 50Ru50Fe Catalyst (43)

too dissimilar from those reported by Ott et al. (14,35). In their study of Fischer-Tropsch synthesis over unsupported Ru-Fe alloys using a gas mixture of 3.3 $H_2/CO$, Ott et al. indicated a rapid carbon buildup on both the 33Ru67Fe and 75 Ru25Fe catalysts, resulting in a significant drop of the catalytic activity as active sites on the surface decreased. More importantly, the selectivity of the catalyst shifted sharply towards methane and carbon dioxide as the carbon buildup proceeded. A decrease in ethylene selectivity was also observed; as pointed out by Ott et al. (35), this change is significant in that a low conversion usually leads to an increase in olefinic to paraffinic ratios. The shift in selectivity is indicative of large metal ensembles required for the production of higher hydrocarbons.

While catalyst deactivation was observed by both Borowski et al. (43) and Ott et al. (14,35), a major difference was that the deactivation occurred at a much faster rate in the case of Borowski and coworkers than in the other study. A combination of factors might contribute to this difference. It might be accounted for by the influence of metal-support interaction and metal particle size of the alumina-supported catalyst. In addition, in contrast with the differential conversion performed by Ott et al., Borowski et al. carried out their investigation normally at a relatively high conversion, which would result in a rapid carbon buildup on the catalyst. The rapid coverage of catalyst surface with

carbon would lead to a sharp decline in large metal ensembles necessary for the production of higher hydrocarbons. Consequently, only traces of ethane were observed at an initial stage of the experiments. Secondary reactions, including hydrogenation, hydrogenolysis and cracking, could also be enhanced, as hydrocarbon intermediate species, if formed, were recycled back in a CSTR-simulated recycle reactor. The last hypothesis on secondary reactions has been tested on another alumina-supported catalyst, 97Ru3Fe, in a pulse reactor, and the results are presented in a later section.

4.2.3.2 97Ru3Fe Supported Catalyst

Ott et al. (14,35) have shown that an unsupported 97Ru3Fe alloy, contrary to 33Ru67Fe and 75Ru25Fe catalysts, exhibited constant selectivity towards hydrocarbon formation over time, as a result of essentially no carbon buildup on the alloy. When corrected for an increase in particle size during the course of reactions, the overall catalytic activity also remained unchanged. Consequently, as the 50Ru50Fe catalyst experienced heavy carbon deposition, an alumina-supported 97Ru3Fe catalyst was chosen by Borowski et al. (43) as an alternative choice for further investigation of the merits of Ru-Fe alloys in the synthesis of lower olefins. CO conversions were in the range of 10-25% in most cases, although conversions above 30% were occasionally experienced -- for instance, at 573K with $H_2/CO$ feed ratios of 2:1 and 3:1.

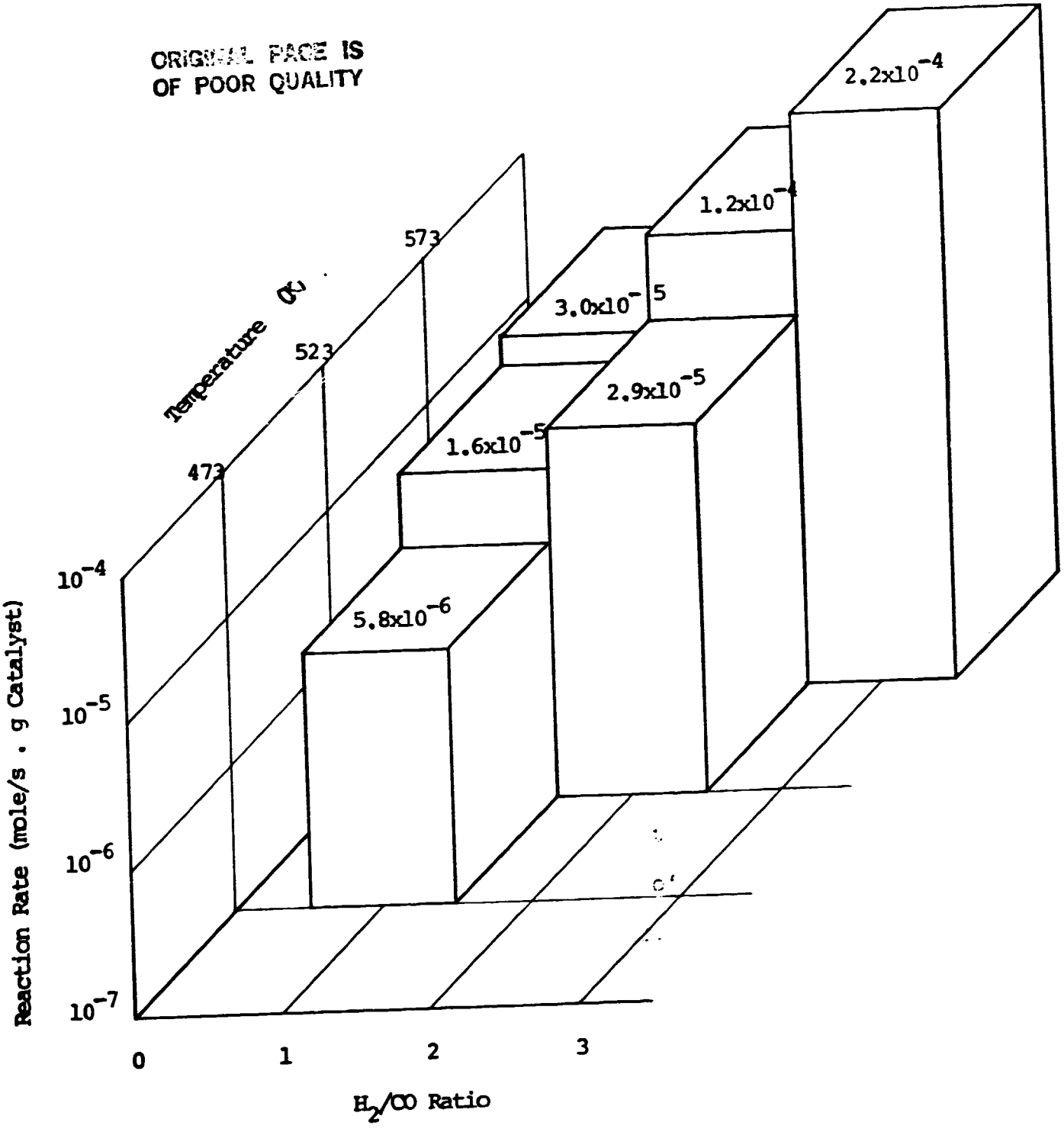


Figure 4.21 Overall Reaction Rates of 97Ru3Fe Catalyst at Various Temperatures and $H_2/CO$ Feed Ratios (43)

C - 2

Shown in Figure 4.21 are overall reaction rates of the supported 97Ru3Fe catalyst in a recycle reactor at various temperatures and $H_2/CO$ feed ratios. As expected, the rate of reaction increased with temperature. In addition, an increase in the $H_2/CO$ feed ratio led to a rise in reaction rate, possibly as a result of additional hydrogen available to hydrogenate adsorbed species and keep the catalyst surface clean. Product distributions obtained from the recycle reactor under the same operating conditions and at 573K are compared in Figure 4.22 for feed gas mixtures with the $H_2/CO$ ratios of 1:1, 2:1 and 3:1. As mentioned earlier, the overall conversion increased with the $H_2/CO$ feed ratio. Small amounts of ethane and propane were observed for the 1:1 $H_2/CO$ feed, which also corresponded to a low conversion. However, as the $H_2$ content in the feed stream increased, the product distribution shifted strongly toward the formation of methane. Borowski et al. pointed to the importance of the water-gas shift reaction in shifting the distribution of water and carbon dioxide as the feed ratio of $H_2/CO$ varied.

Borowski and coworkers also noted that an increase in the flow rate of the fresh gas feed to the recycle loop resulted in a decline in conversion and generally led to a rise in selectivity towards higher hydrocarbons. Figure 4.23 compares the selectivity towards $C_2$ and $C_3$ hydrocarbons for $H_2/CO$ feed ratios of 1:1 and 1:2 and at temperatures of 523

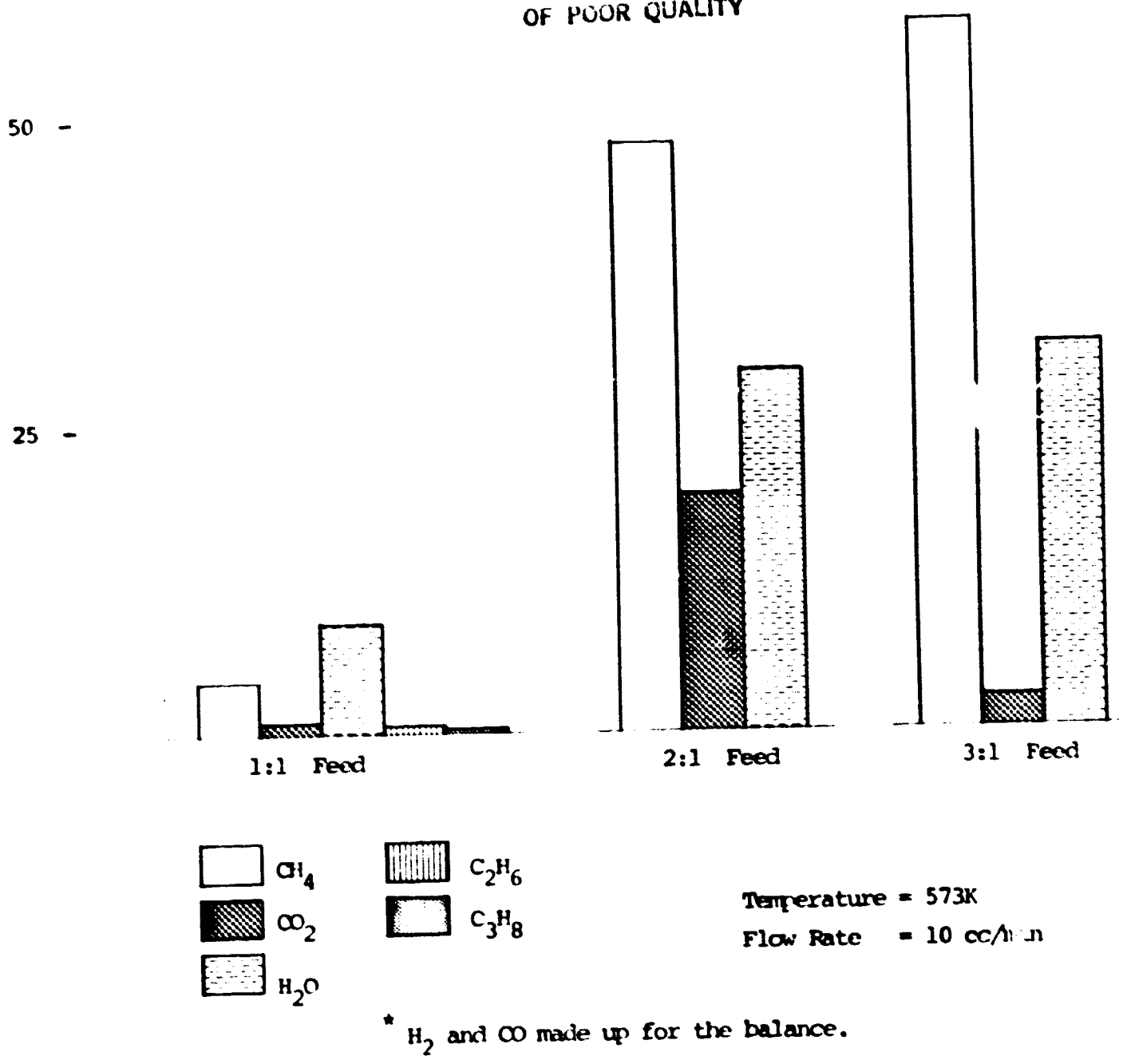


Figure 4.22 Product Distributions over 97Ru3Fe Catalyst at Varying Feed Gas Ratios (43)

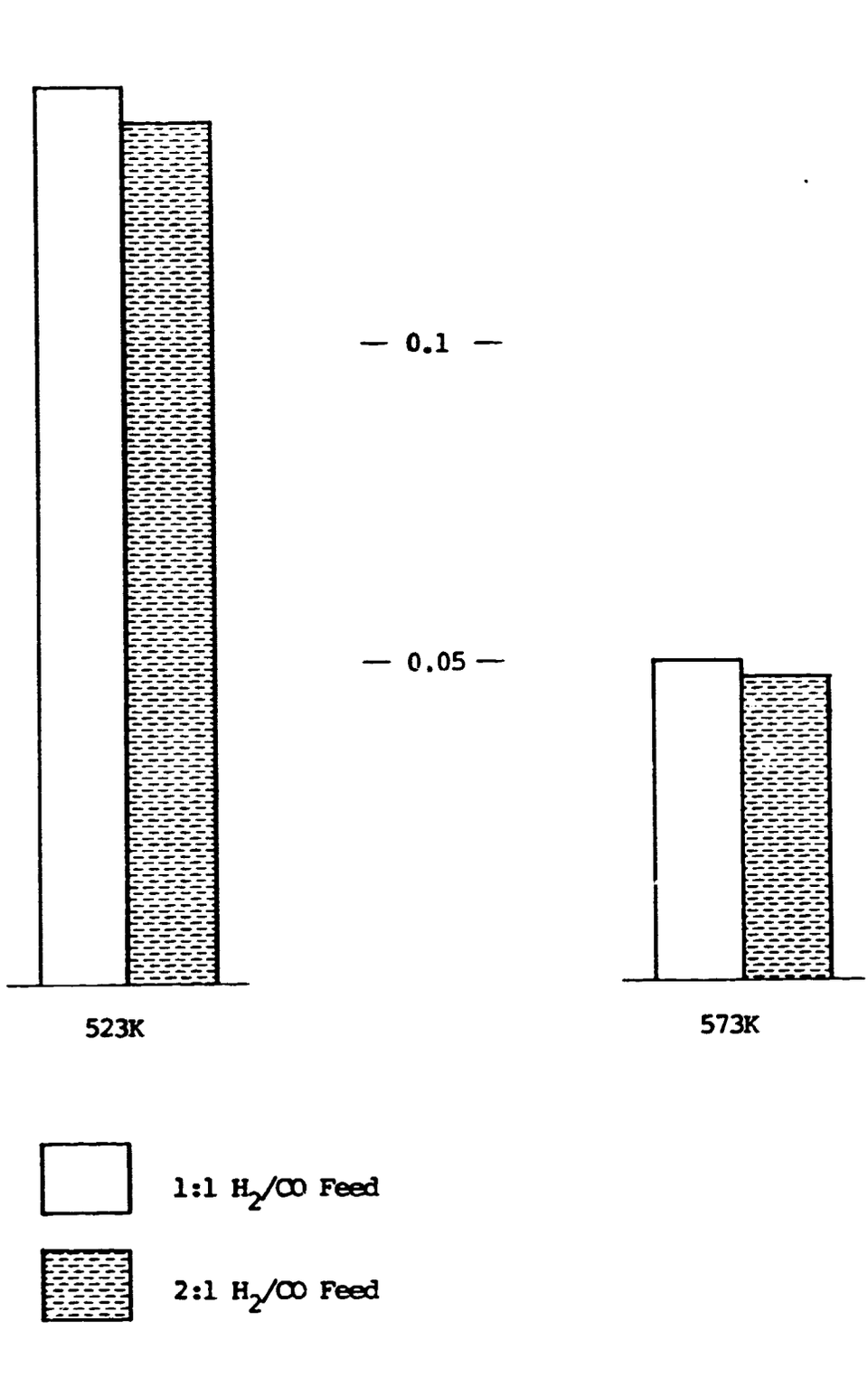
0.1
0.05
523K
573K
1:1 $H_2/CO$ Feed
2:1 $H_2/CO$ Feed

and 573K. As can be seen from the diagram, the selectivity towards higher hydrocarbons at 523K was much greater than at 573K. A small amount of ethylene, the only olefin ovserved in this investigation, was observed at 523K with a $H_2/CO$ feed ratio of 1:1.

Although, for all experiments carried out by Borowski et al. (43), conditions at 523K and $H_2/CO$ feed ratios of 1:1 and 2:1 showed the most promising result in terms of the production of $C_2$ and $C_3$ hydrocarbons, the selectivity towards higher hydrocarbons at these conditions was still at an unacceptably low level. In addition, no olefins were detected in most cases. The results of this alumina- supported catalyst are in marked contrast with those of unsupported 97Ru3Fe, for which an unusually high selectivity towards ethylene and propylene has been noted. One possible factor accounting for this difference in performance is the high CO conversion level employed in the Borowski investigation. This notion, however, attributes only partially to the difference in catalytic activities, as has been substantiated in a subsequent study by Sackett and Willard (44). Using the same experimental apparatus as Borowski et al. (43) but operated in a plug flow reactor (PFR) mode with the recycle loop removed, Sackett and Willard performed experiments over the supported 97Ru3Fe catalyst with a $H_2/CO$ feed ratio of 3:1 at varying flow rates and temperatures. These experiments were intended to simulate the differential conversion as carried out by Ott et al. (14)

over their unsupported catalyst at 573K with a 3.3 $H_2/CO$ gas mixture. However, no hydrocarbon product except methane was observed.

The above study by Sackett and Willard indicates an important point: a difference between supported and unsupported catalysts as well as a difference even among catalysts of various supports, as has been reported in a number of studies (34,39,46). Vannice et al. (27) have also obtained high olefin yields over silica- supported Ru-Fe alloys, but the selectivity is lower than that observed by Ott et al. (14). The metal-support interaction, metal particle size, and degree of metal dispersion are among possible factors to be considered. In addition, the expected alloy formation on the alumina support used in the studies by Borowski et al. (43) and Sackett and Willard (44) might not have occurred as had been anticipated. Furthermore, the catalyst might not be completely reduced to its ground state as a result of the influence of the support, as evidenced in many observations made in the case of well dispersed iron supported catalysts (39).

Since an unusually high selectivity towards ethylene and propylene has been observed in a differential reactor using an unsupported 97Ru3Fe catalyst, it would be interesting to see whether the same highly selective result could be obtained when the reactor is operated at high conversions.

4.2.3.3 Secondary Reactions

A number of investigations (47,48) have provided evidence that, except for methane, the primary products from synthesis gas are olefins. When operated in a recycle mode or at a high conversion, reaction products formed could be subject to secondary reactions, including hydrogenation, hydrogenolysis and cracking. These secondary reactions could account for, at least partially, the low production of higher hydrocarbons, and specifically olefinic compounds, observed in the Borowski study.

The postulate of secondary reactions taking place in the CSTR- simulated recycle reactor has been confirmed in a study by Sackett and Willard (44). The reactor was operated in a PFR mode. Feed mixtures composed of $H_2$, CO and $C_{24}$ at various compositions ($H_2$:CO = 3:1; $C_2H_4$ ~ 25-40%) passed through supported 97Ru3Fe catalysts at temperatures of 473, 523 and 573K. The following were generally observed in most cases. Over 50 percent of ethylene was hydrogenated to ethane initially; the percentage dropped with increasing time on stream while the fraction of unreacted ethylene increased, the phenomenon indicative of catalyst deactivation possibly as a result of surface coverage with carbon and adsorbed species. Small amounts of methane and propylene were observed, and so were traces of propane which, interestingly, appeared in a smaller quantity than propylene. These products also declined as reaction time increased. The results are consistent with a

general observation that hydrogenation of olefins occurs more rapidly than the cracking activity (49). Furthermore, the presence of ethylene enhanced the incorporation of additional carbon, resulting in the formation of propane and propylene.

A blank run was also carried out to determine whether secondary reactions would occur over the support. A gas mixture of 25% ethylene and 75% $H_2/CO$ (3:1) was passed over γ-alumina with no metal loading at 523K. Only traces of methane and ethane were observed, thus indicating virtually no direct influence of the support on secondary reactions. This conclusion does not, however, exclude the metal-support interaction which alters catalytic properties of supported catalysts from unsupported ones.

Sackett and Willard (44) further investigated the influence of supported 97Ru3Fe on secondary reactions, specifically cracking, using a pulse reactor shown schematically in Figure 4.24. Helium was used as a carrier gas and was constantly passed over the catalyst. A pulse of a desired gas component, 0.10 $cm^3$ in volume, was injected into the reactor through the switching valve V#1. The effluent stream was analyzed by the on-line gas analytical system described earlier.

The catalyst, 0.30 gram, was pulsed with ethane, ethylene and propane at 523k. In the case of ethane, cracking occurred to a large extent, resulting in the formation of methane. No ethane was observed initially. After ten pulses,

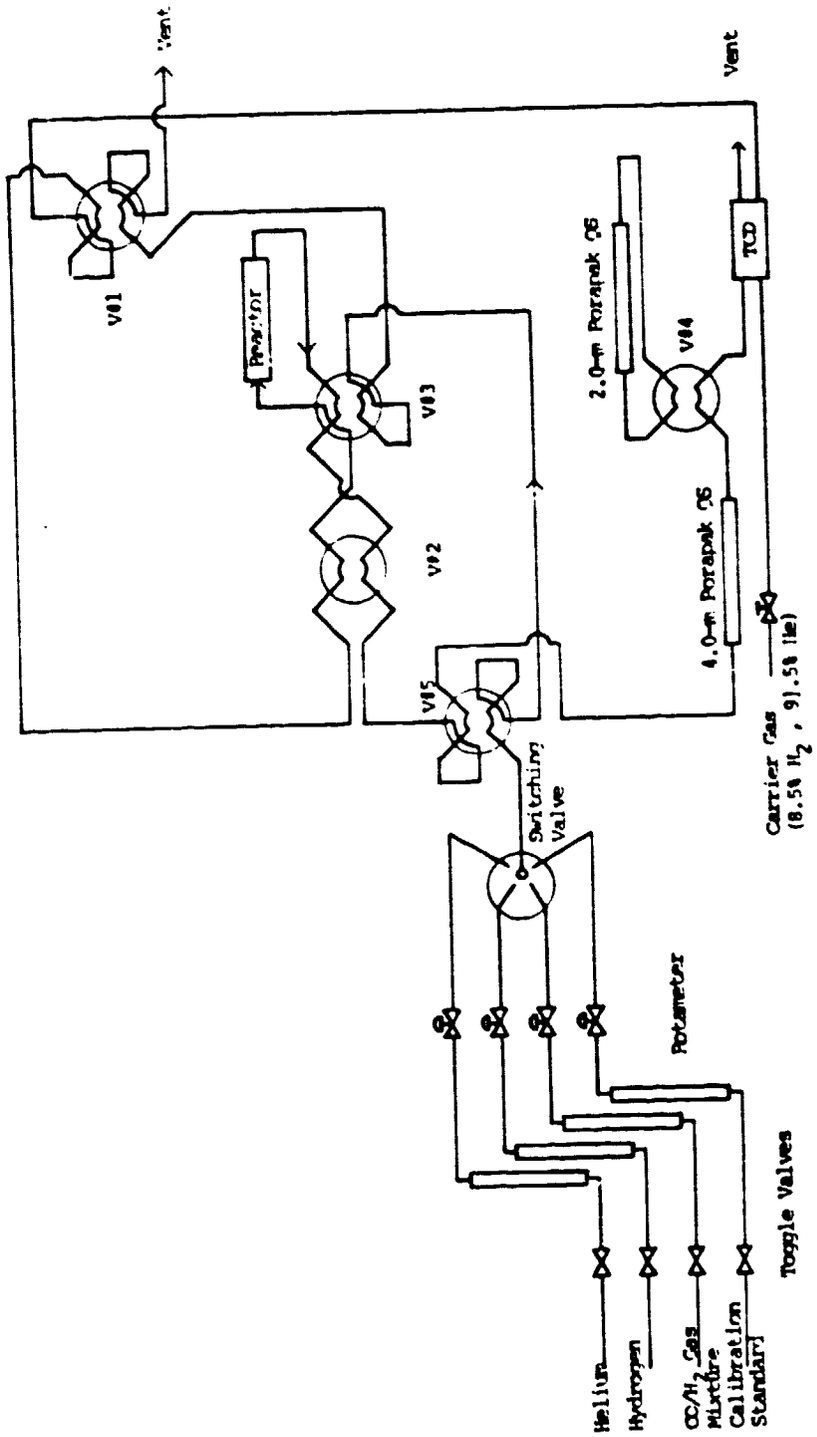


Figure 4.24 Schematic Diagram of Experimental System (Pulse Mode)

however, ethane started appearing and its content increased with an increasing number of pulsing while the fraction of methane declined. A small amount of hydrogen was observed throughout the run. For the pulsing experiment with ethylene, methane was the only hydrocarbon product observed initially. A small amount of ethane was observed after seven pulses, and ethylene appeared at the eighth pulsing. The formation of methane dropped dramatically in subsequent pulses; meanwhile, ethane reached its peak, after which it declined rapidly and ethylene became the dominant species. Again, hydrogen was detected throughout the experiment.

The saturated hydrocarbons methane, ethane and propane were observed throughout the pulsing study with propane. At an early stage, methane was the dominant product. However, with an increase in the number of pulsing, the fraction of propane rose while the methane content decreased substantially. Ethane remained at a low level throughout the run. In all three pulse experiments, the catalyst was pulsed with hydrogen after the pulsing with hydrocarbons was completed. A substantial amount of methane was detected in all cases, indicative of active surface carbon on the catalyst.

The results from the pulse experiments clearly show that the Ru-Fe catalyst enhances the cracking activity. Furthermore, mass balance and a drop in activity indicate some of the products were strongly adsorbed on, and thus poisoned,

the catalyst surface. Both the PFR study and the pulse experiments by Sackett and Willard (44) substantiate the activity of hydrogenation and cracking over the 97Ru3Fe supported catalyst. Consequently, for a successful production of low molecular weight olefins as primary products, not only is the development of a highly selective catalyst required, but the suppression of secondary reactions is also necessary to minimize the desired olefins converted to unwanted products.

## 5. Application of the Results

Ruthenium and its unsupported alloys with iron -- 50Ru50Fe and 33Ru67Fe -- have been investigated in this study in a continuing process to develop an efficient catalyst for the Bosch process. An efficient Bosch catalyst is defined as the one which can yield the maximum water concentration thermodynamically allowable at moderate temperatures (700-800K). This yield corresponds to the water concentration in equilibrium with the β-graphite phase. The extent of water conversion is a major consideration in designing a recycle equilibrium Bosch process as remaining gas components are to be recycled to the reactor. The higher the water conversion per pass is, the lower the recycle ratio is required.

Shown in Figure 5.1 are equilibrium water concentrations as a function of temperature for the β-graphite and various catalyst systems for an O/H ratio of 0.5. Inhibited by the formation of oxides, the iron system exhibits the maximum water concentration at 915K, the temperature at which the iron-iron oxide-gas equilibrium and the graphite-gas equilibrium intersect at an O/H ratio of 0.5 (5,7). For nickel and cobalt catalysts, the water concentration is determined by the carbide equilibrium at low temperatures and the graphite equilibrium at high temperatures. The maximum water concentration for the cobalt and nickel systems occurs at 800 and 825K, respectively (9). It should be noted that

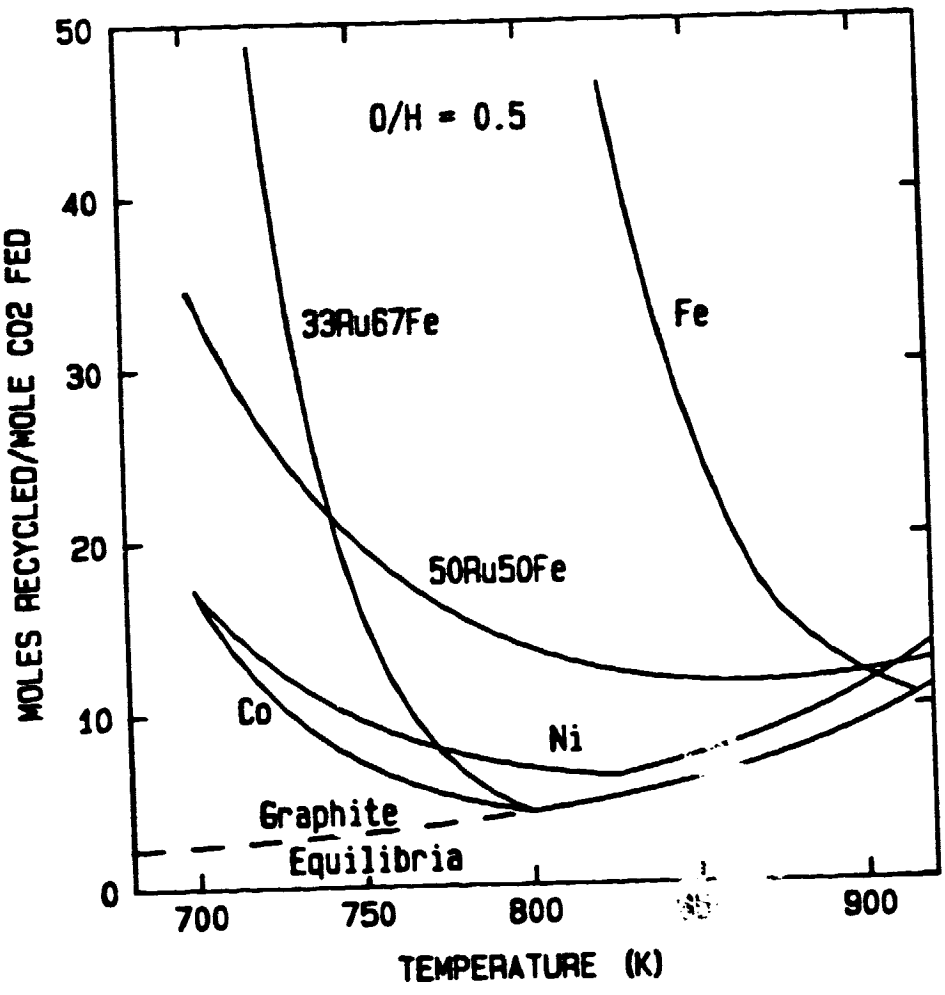


Figure 5.1 Equilibrium Water Concentration of a Bosch Reactor for Various Catalyst System

the maximum water yield for the nickel system does not correspond to the temperature where the carbide-gas equilibrium coincides with the graphite-gas equilibrium, as is the case for cobalt. Garmirian (9) reported the graphite-gas equilibrium for the nickel catalyst not attainable even at 900K. Similar results have been observed in this study for the unsupported 50Ru50Fe system, in which $\Delta G_c$ was 0.6 kcal/mole at 900K. The maximum water concentration for the 50Ru50Fe alloy takes place at 865K. Figure 5.1 also shows the water mole fraction as a function of temperature for the 33Ru67Fe system, having the maximum water content at 800K. The water concentrations of the Ru-Fe alloy systems were determined from the values of $\Delta G_c$ of the carbon deposition boundaries linearly interpolated about experimental points, as shown in Figures 4.9 and 4.17. The maximum water concentrations attainable for different Bosch catalysts are tabulated in Table 5.1 with their corresponding temperatures.

A Bosch recycle reactor is shown schematically in Figure 5.2. For every two moles of $H_2$ and one mole of $CO_2$ fed to the reactor, two moles of water are produced. In a simplified calculation with the assumption that the removal of water by condensation from the reactor effluent stream is 100%, the number of moles of recycled gases ($H_2$, CO, $CH_4$ and $CO_2$) per mole of $CO_2$ fed is

$$r = 2\left[\frac{1}{x_{H_2O,equilbrium}}\right] - 1 \qquad (5.1)$$

Table 5.1 Maximum Water Concentrations and Minimum Recycle Ratios for Various Bosch Catalysts

| Catalyst | Temperature (K) | Maximum Water | Minimum Recycle |
|---|---|---|---|
| Fe | 915 | 15.8 | 10.6 |
| Ni | 825 | 24.5 | 6.2 |
| Cc | 800 | 32.3 | 4.2 |
| 50Ru50Fe | 865 | 14.8 | 11.5 |
| 33Ru67Fe | 800 | 32.3 | 4.2 |

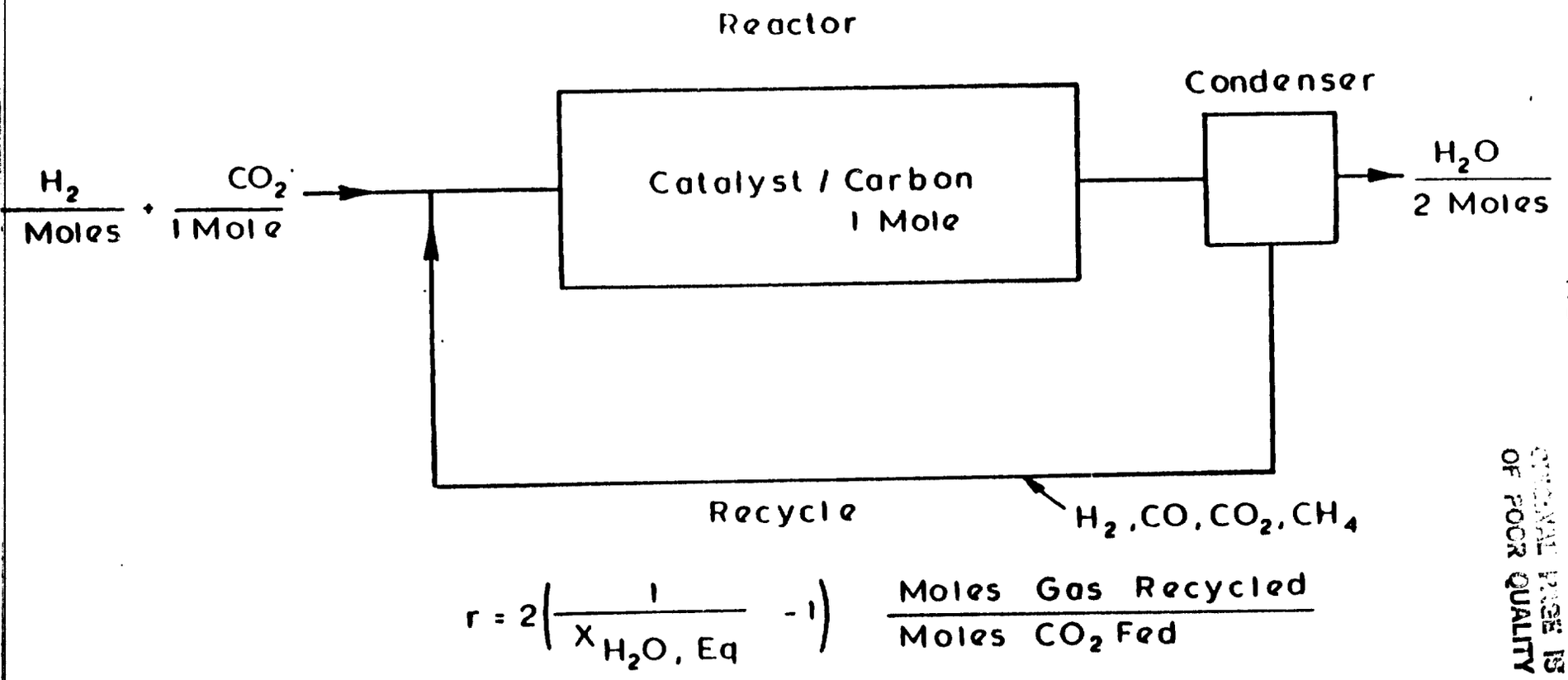


Figure 5.2 Bosch Recycle Reactor (9)

where $x_{H_2O,equil}$ is the equilibrium mole fraction of water.

Figure 5.3 shows the recycle ratios as a function of temperatures for various catalysts. The minimum recycle ratios for iron, cobalt, nickel, 50Ru50Fe and 33Ru67Fe are 10.6, 4.2, 6.2, 11.5 and 4.2, respectively. A substantial reduction in recycle ratio can be achieved by the addition of a reverse water-gas shift reaction before the gas mixture is sent to the Bosch reactor; details of improved versions of the Bosch process can be found in Manning (5), Sacco (7) and Garmirian (9).

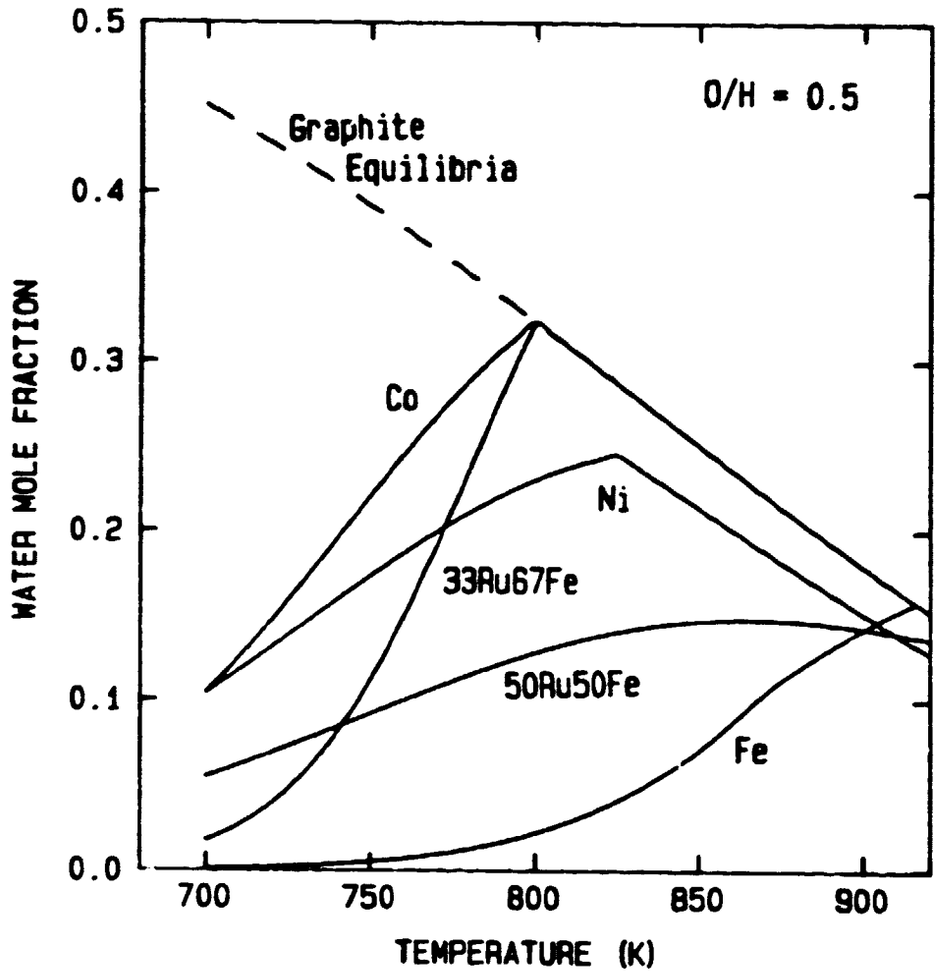


Figure 5.3 Gas Recycle Ratio for a Bosch Recycle Equilibrium Reactor

## 6. Conclusions

No detectable carbon deposition by weight measurement has been observed for unsupported ruthenium powders, thus ruling out the possibility of this unsupported metal being a good Bosch catalyst. The result is in marked contrast with that of supported ruthenium, for which carbon deposition has been observed in a number of studies. Furthermore, experimental results indicate that the 50Ru50Fe alloy is not superior to the two previously investigated cobalt and nickel catalysts. On the other hand, results from the 33Ru67Fe system are promising. At temperatures of 800K and beyond, maximum water concentrations in equilibrium with $\beta$-graphite can be attained in the 33Ru67Fe system, as has also been the case for the cobalt catalyst. However, the deviation from graphite-gas equilibria in the 33Ru67Fe system at 700 and 750K is more pronounced than that observed with the cobalt catalyst or even the 50Ru50Fe alloy. Definite explanations for reaction mechanisms and the influence of ruthenium/iron content on the carbon deposition process are unavailable from this study. Such an understanding of surface behaviors of alloy catalysts could lead to the development of an improved Bosch catalyst.

In the investigation of synthesis of low molecular weight olefins, methane was the dominant hydrocarbon product for both 50Ru50Fe and 97Ru3Fe catalysts supported on

γ-alumina. Most experiments were conducted at CO conversions of 10-30% in the temperature range of 473-573K using $H_2/CO$ gas mixtures of various compositions. For the 50Ru50Fe supported catalyst, ethane was the only higher hydrocarbon observed and appeared in a small amount in the initial stage of experiments. Catalyst deactivation occurred very rapidly. On the other hand, the 97Ru3Fe supported catalyst showed higher catalytic activity, better selectivity towards $C_2$ and $C_3$ hydrocarbons and longer catalyst life than the 50Ru50Fe catalyst. However, the selectivity towards higher hydrocarbons, and specifically towards olefins, was still at an unacceptably low level. Experiments on the 97Ru3Fe catalyst have also shown secondary reactions, namely, hydrogenation and cracking, to take place under synthesis conditions.

The results from the study of hydrocarbon synthesis over the supported catalysts have proved to be quite different from those originally anticipated. The unusually high selectivity towards ethylene and propylene, as reported by Ott *et al.* (14) using a differential reactor with unsupported Ru-Fe alloys, has not been observed in this study. The selection of γ-alumina as a support is perhaps an unwise choice as a result of metal-support interactions. It would be interesting to determine whether the high selectivity of unsupported Ru-Fe alloys towards ethylene and propylene would still be maintained when the catalysts are operated at high conversions.

## References

1. R. C. Reid, "University Role in Astronaut Life Support Systems: Atmosphere". NASA CR-1552, May 1970.

2. R. F. Holmes, E. F. Keller and C. D. King, "A Carbon Dioxide Reduction Unit Using Bosch Reaction and Expendable Catalyst Cartridge". NASA CR-1682, November 1970.

3. R. F. Holmes, E. F. Keller and C. D. King, "Bosch $CO_2$ Reduction System Development". CASD-NAS-76-020, April 1976.

4. D. B. Heppner, T. M. Hallick, D. C. Clark and P. D. Quattrone, "Bosch: An Alternate $CO_2$ Reduction Technology". ASME Paper No. 79-ENAS-32, July 1979.

5. M. P. Manning, "An Investigation of the Bosch Process". Sc.D. Thesis, Massachusetts Institute of Technology, 1976.

6. M. P. Manning and R. C. Reid, "Carbon Dioxide Reduction by Bosch Process". ASME Paper No. 75-ENAS-22, July 1975.

7. A. Sacco, "An Investigation of the Reactions of Carbon Dioxide, Carbon Monoxide, Methane, Hydrogen and Water over Iron, Iron Carbides, and Iron Oxides". Ph.D. thesis, Massachusetts Institute of Technology, 1977.

8. A. Sacco and R. C. Reid, "Limitations on Water Production in the Iron-Catalyzed Bosch Process". ASME Paper No. 78-ENAS-4, July 1978.

9. J. E. Garmirian, "Carbon Deposition in a Bosch Process Using a Carbon and Nickel Catalyst", Ph.D. thesis, Massachusetts Institute of Technology, 1980.

10. J. E. Garmirian, M. P. Manning and R. C. Reid, "The Use of Nickel and Cobalt Catalysts in a Bosch Reactor". ASME Paper No. 80-ENAS-15, July 1980.

11. J. A. Rabo, A. P. Reisch and M. L. Poutsma, "Reactions of Carbon Monoxide and Hydrogen on Co, Ni, Ru and Pd Metals", J. Catalysis, 53, 295, 1978.

12. W. E. Bell and M. Tagami, "High-Temperature Chemistry of the Ruthenium-Oxygen System", J. Phys. Chem., 67, 2432, 1963.

13. R. B. Levy, "Properties of Carbides, Nitrides and Borides: Implications for Catalysts". Chapter 4 in "Advanced Materials in Catalysis". New York, Academic Press, 1977.

14. G. L. Ott, T. Fleisch and W. N. Delgass, "Fischer-Tropsch Synthesis over Freshly Reduced Iron-Ruthenium Alloy", J. Catalysis, 60, 394, 1979.

15. R. T. K. Baker, "The Formation of Filamentous Carbon". Chapter 2 in "Chemistry and Physics of Carbon", 14, 1979.

16. J. F. Dent, L. A. Moignard, W. H. Blackgraun and D. Herbden, "An Investigation into the Catalytic Synthesis of Methane by Town Gas Manufacturing", 49th Report of the Joint Research Committee of the Gas Research Board of the University of Leeds, GRB 20, 1945.

17. J. R. Rostrup-Nielsen, "Equilibrium of Decomposition Reactions of Carbon Monoxide and Methane over Nickel Catalysts", J. Catalysis, 27, 343, 1972.

18. L. C. Browning and P. H. Emmett, "Equilibrium Measurements in the $Ni_3C$-Ni-$CH_4$-$H_2$ and $Co_2C$-Co-$CH_4$-$H_2$ Systems", J. Am. Chem. Soc., 74, 1680, 1952.

19. L. J. E. Hofer, E. M. Cohn and W. C. Peebles, "Isothermal Decomposition of the Carbides in a Carburized Cobalt Fischer-Tropsch Catalyst", J. Phys. Col. Chem., 53, 661, 1949.

20. L. J. E. Hofer, E. M. Cohn and W. C. Peebles, Isothermal Decomposition of Nickel Carbide", J. Phys. Col. Chem., 54, 1161, 1950.

21. S. Nagakura, "Study of Metallic Carbides by Electron Diffraction: Part I. Formation and Decomposition of Nickel

Carbide", J. Phys. Soc. of Japan, 12(5), 482, 1957.

22. S. Nagakura, "Study of Metallic Carbides by Electron Diffraction: Part IV. Cobalt Carbides", J. Phys. Soc. of Japan, 16(6), 1213, 1961.

23. F. A. Shunk, "Constitution of Binary Alloys, Second Supplement". New York, McGraw-Hill, 1969.

24. K. J. Singh and H. E. Grenga, "Catalytic Decomposition of Carbon Monoxide on Single Crystalline Ruthenium", J. Catalysis, 47, 328, 1977.

25. G. G. Low and A. Bell, "Studies of CO Deposition and Reaction with $H_2$ on Alumina-Supported Ru", J. Catalysis, 57, 397, 1979.

26. J. G. Ekerdt and A. Bell, "Synthesis of Hydrocarbons from CO and $H_2$ over Silica-Supported Ru: Reaction Rate Measurements and Infrared Spectra of Adsorbed Species", J. Catalysis, 57, 397, 1979.

27. M. A. Vannice, Y. L. Lam and R. L. Garten, "Carbon Monoxide Hydrogenation over Well-Characterized Ruthenium-Iron Alloys", in "Hydrocarbon Synthesis from Carbon Monoxide and Hydrogen", edited by American Chemical Society, Washington, DC, 25, 1979.

28. O. L. Hollis and M. V. Hayes, "Water Analysis by Gas Chromatography Using Porous Polymer Columns", J. Gas Chromatography, 4, 235, 1966.

29. S. Dal Nogare and R. S. Juvet, "Gas-Liquid Chromatography, Theory and Practice". New York: Wiley, pp. 257-264, 1962.

30. J. E. Purcell and L. S. Ettre, "Analysis of Hydrogen with Thermal Conductivity Detectors", J. Gas Chromatography, 3, 69, 1965.

31. H. C. Brown and C. A. Brown, "New Highly Active Metal Catalysts for the Hydrolysis of Borohydride", J. of the

American Chemical Society, 84, 1493, 1962.

32. D. W. McKee, "Interaction of Hydrogen and Carbon Monoxide on Platinum Group Metals", J. Catalysis, 8, 240, 1967.

33. G. A. Mills and F. W. Steffgen, "Catalytic Methanation", Catalysis Reviews, 8(2), 159, 1973.

34. D. L. King, "A Fischer-Tropsch Study of Supported Ruthenium Catalysts", J. Catalysis, 51, 386, 1978.

35. G. L. Ott, T. Fleisch and W.N. Delgass, "Carbon Deposition and Activity Changes over FeRu Alloys during Fischer-Tropsch Synthesis", J. Catalysis, 65, 253, 1980.

36. T. Fleisch, W. N. Delgass and N. Winograd, "Secondary Ion Mass Spectroscopy/X-Ray Photoelectron Spectroscopy Study of CO Adsorption on Ni and of Fischer-Tropsch Synthesis on FeRu Alloys", Surface and Interface Analysis, 3(1), 23, 1981.

37. G. L. Ott, W. N. Delgass, N. Winograd and W. E. Baitinger, "X-Ray Photoelectron Spectroscopy/Secondary Ion Mass Spectrometry of FeRu Alloy Catalysts", J. Catalysis, 56, 174, 1979.

38. M. L. Good, M. Akbarnejad, M. D. [illegible]til and J. T. Donner, "Utility of the Mössbauer Effect in the assessment of Chemical Transformations in Unsupported Catalyst Systems as a Function of the Metal Salt", in "Nuclear and El[illegible]ron Resonance Spectroscopies Applied to Materials Scienc[illegible], edited by Kaufmann and Shenoy. New York: Elsevier North Holland, 271, 1981.

39. L. Guczi, "Structure and Catalytic Properties of Iron-Containing Bimetallic Catalysts", Catal. Rev.- Sci. Eng., 23(3), 329, 1981.

40. R. L. Garten, "Mössbauer Effect Methodology", vol. 10. New York: Plenum, 69, 1976.

41. M. Hansen, "Constitution of binary Alloys". New York: McGraw-Hill, 1958.

42. R. P. Elliott, "Constitution of Binary Alloys, First Supplements". New York: McGraw-Hill, 1965.

43. D. M. Borowski, B. R. Moroney, E. D. Morris, B. A. Sackett and J. C. Willard, "Determination of Olefin Selectivity of Fe/Ru Alloy Catalysts in Fischer-Tropsch Reactions", a report of the course Chemical Engineering Laboratory (10.26), Massachusetts Institute of Technology, December 1981.

44. B. A. Sackett and J. C. Willard, "Determination of Usefulness of Fe/Ru Alloy Catalysts for Olefin Production", 10.91 Project Report, Massachusetts Institute of Technology, May 1982.

45. M. W. Mahan, "The Kinetics of Ethylene Oxidation over a Supported Silver Catalysts", S. M. Thesis, Massachusetts Institute of Technology, 1980.

46. M. A. Vannice and R. L. Garten, "The Influence of the Support on the Catalytic Behavior of Ruthenium in $CO/H_2$ Synthesis Reactions", J. Catalysis, 63, 255, 1980.

47. B. A. Xexton and G. A. Somorjai, "The Hydrogenation of CO and $CO_2$ over Polycrystalline Rhodium: Correlation of Surface Composition, Kinetics and Product Distributions", J. Catalysis, 46, 167, 1977.

48. L. L. Lauderback, "Fischer-Tropsch Synthes s over $SiO_2$ Supported Iron- Ruthenium Based Bimetallic Catal sts", M. S. Thesis, Purdue University, 1977.

END

DATE

FILMED

AUG 30 1983